Between Seismic Speed and Glacial Pace: Cryoseismic Observation of Intermediate-Scale Processes at Lemon Creek Glacier, Alaska

Thesis by
Celeste Ritter Labedz

In Partial Fulfillment of the Requirements for
the Degree of Doctor of Philosophy

Caltech

CALIFORNIA INSTITUTE OF TECHNOLOGY
Pasadena, California

2022
(Defended 12 May 2022)

© 2022

Celeste Ritter Labedz
ORCID: 0000-0001-7339-2170

ACKNOWLEDGEMENTS

This thesis is dedicated to Dorothy Ritter. The last six years have been a lot of work to put Dr. in front of Celeste Ritter Labedz. None of it would have been possible without D.R. behind Celeste Ritter Labedz from day one.

Thank you to all.

To family. To my parents, Cynthia Ritter and Thomas Labedz, and my brother, Spencer Labedz, for building me, loving me, and being my home even when I am away. To the Ritter side, especially Janice and Karla, who show me how to make every moment special. To the Labedz side, especially Marie, who shows me that attitude is everything. To those that didn't make it to today, who I know are proud of me.

To my partner. To Preston Cosslett Kemeny, who is my home, too. I'll take your hand and walk through the rain to the edge of the world any day, but maybe we can also just relax on the couch with the dog sometimes.

To friends. To Shelby, Sam, Jenn, Savanna, Carol, and Liz, who helped me grow into myself, however awkwardly. To Nikita and Jane, who go to strange new worlds with me. To Madison, Cullen, Lily, and Ameera, who were a delight to come home to. To the GPS crew my year, who check all the boxes. To the GPS crew a year below me, who let me into their fun. To ballroom and swing dance clubs, who remind me to connect.

To peers. To the whole Seismo Fam, especially Rachel, Chris, Ethan, Tobi, and Jimmy in 358, who go on the best tangents with me. To the WinG women, especially Leah, Usha, Alex, and Clare, who make me want to be a leader. To all of the GPS graduate students, who were a big reason why I came to Caltech and an even bigger reason why I stayed.

To advisors and teachers. To Mike Gurnis and Jennifer Jackson, who see that sometimes the best help is simply not giving up. To Zhongwen Zhan, Rob Clayton, and Mark Simons, who offered perspective. To the rest of the GPS faculty, who always had something interesting to share. To my collaborators, especially Tim Bartholomaus, who made me feel smarter after every conversation than I felt before. To Shireen Adenwalla, who is a role model. To Mark Shearer, who suggested geophysics.

To support. To Kim, Donna, Rosemary, Priscilla, and Sarah in the Seismo Lab office, and to Julie, Julia, Leticia, Jen, and the rest of the GPS administrative team, who can make anything happen. To Cruz the custodian, who always says hello. To Kitty and the rest of the CTLO staff, and to Erin-Kate and the rest of the CCID staff, who remind me to look both inward and outward to grow. To the Juneau Icefield Research Program, who made field work possible, safe, and successful. To science Twitter, who are my network.

To Earth. To the ice, who we are lucky to have and should do our best to keep. To the noise and the signals, who we are lucky to sense and should do our best to listen to.

To even more than I could fill pages and pages with.

Thank you to all.

ABSTRACT

In this thesis, I present three studies in environmental seismology. First, I present an analysis of seismic tremor generated from subglacial water flow during the rapid drainage of an ice-marginal supraglacial lake, collected by an on-ice nodal seismic array. I find that seismic tremor indicates a partial pressurization of the subglacial hydrologic system that was not accompanied by the expected change in glacier surface velocity, suggesting that factors like glacier geometry play a significant role in whether pressurization necessarily leads to velocity change. Using seismometers in this way allows remote observation of active subglacial hydrologic systems as they vary over space and time, a vital parameter for understanding how liquid water affects glacier motion, melting, fracture, and hazards. Second, I present observations of glacier surface crevasse development over space and time, as detected by a dense array of seismometers atop the glacier. I find that icequakes associated with surface crevassing have a magnitude distribution that is swarm-like, rather than aftershock-like, and that the spatiotemporal distribution of events indicates that crevasses regularly widen, deepen, reactivate, and trigger activity at nearby crevasses through cryoseismicity. Understanding surface crevassing activity is valuable for constraining the degree to which glacier surface velocity measurements represent ice flow as a whole, and for interpreting how glacier flow responds to changes in forcing over time. Third, I present an investigation of changes in anthropogenic urban seismic noise in Los Angeles associated with changes in community behavior. I find that changes in human activity from the scale of hours to the scale of months create distinguishable differences in ambient seismic noise power that correlate well with other measures of community behavior. Characterizing anthropogenic seismic noise is beneficial for accurately interpreting measurements of transient seismic wave data collected in urban areas toward goals such as hazard mapping.

PUBLISHED CONTENT AND CONTRIBUTIONS

Chapter 2 is reformatted (integrating supplemental figures into the main text) from this published work for which C.R.L. was the lead author, performed field work, processed and analyzed data, and wrote the manuscript:

Labedz, C. R., Bartholomaus, T. C., Amundson, J. M., Gimbert, F., Karplus, M. S., Tsai, V. C., & Veitch, S. A. (2022). Seismic mapping of subglacial hydrology reveals previously undetected pressurization event. Journal of Geophysical Research: Earth Surface, 127, e2021JF006406. https://doi.org/10.1029/2021JF006406

Chapter 4 contains data also included as a small part of this publication, on which C.R.L. was a co-author, processed data for some cities, and provided contributions to manuscript editing:

Lecocq, T., Hicks, S. P., Van Noten, K., Van Wijk, K., Koelemeijer, P., De Plaen, R. S., ... & Xiao, H. (2020). Global quieting of high-frequency seismic noise due to COVID-19 pandemic lockdown measures. Science, 369(6509), 1338-1343. https://doi.org/10.1126/science.abd2438

TABLE OF CONTENTS

LIST OF ILLUSTRATIONS AND TABLES

C h a p t e r   1

INTRODUCTION

Accurate and reliable field observations of glaciers are necessary not only for the general pursuit of knowledge about the cryosphere and its role in geological, hydrological, and environmental processes, but also for the pressing human need of adapting to rapidly shifting resources and hazards due to anthropogenic climate change. Millions of people around the world rely on glacial melt as a freshwater source, and millions face the hazards of sea level rise on coastlines or glacial lake outburst floods downstream of glaciers. Supporting communities to prepare themselves for the changing future of resources and hazards will require observation and analysis of glaciers with many geophysical tools that operate across a range of spatial and temporal scales. Seismology is a uniquely valuable yet currently underutilized tool for monitoring glacier behavior, particularly for processes operating on time scales of hours to days, and the integration of seismology into glaciological study will advance glacier science and real-world monitoring.

Many physical processes in glaciers generate seismic waves, such as iceberg calving (e.g. Qamar & St. Lawrence 1983; Nettles and Ekström 2010), basal stick-slip motion (e.g. Anandakrishnan & Alley 1994; Helmstetter et al. 2015a), surface crevassing (e.g. Roux et al. 2010; Mikesell et al 2012), englacial and basal fracture (e.g. Walter et al. 2013; Helmstetter et al. 2015b), ice shelf rifting (e.g. Chen et al. 2011; Olinger et al. 2019), subglacial water flow (e.g. Winberry et al. 2009; Bartholomaus et al. 2015), moulin tremor (e.g. Röösli et al. 2014, 2016), and more (Podolskiy & Walter 2016). The aspects of these processes that generate readily detectable seismic waves operate necessarily on short time scales, e.g. individual icequakes with sub-second rupture times (Water et al. 2013) and water turbulence with sub-second characteristic times (Gimbert et al. 2014), with an upper limit of glacial earthquakes (large iceberg calving events) with source durations of a few 10s of

minutes (Qamar & St. Lawrence 1983). Individual short time scale events may not be of wide utility for glacier observation in isolation, but the patterns and trends that many individual events make over time can reveal information about processes on longer time scales. For example, water turbulence noise can change amplitude on the scale of hours as an outburst flood passes through (Gimbert et al. 2016), sequences of icequakes can follow the progression of an ice shelf rift on the scale of days to months (Olinger et al. 2019), and glacial earthquakes can reveal the rate of large mass loss events at tidewater glaciers across seasons and years (Nettles and Ekström 2010). Many glacier processes at these longest time scales are already well-captured by other forms of glaciological observation, such as on-ice GPS motion data that provides reliable velocities starting at the scale of days, satellite imagery with repeat cycles of days to weeks, or annual field campaigns to record properties like snow accumulation. Seismology is posed to make the most unique contributions to glacier observation and analysis for processes on the scale of hours to days, between the scales of individual sub-second events (which have limited utility on their own) and longer months-to-years changes (where other observational methods can operate more efficiently).

Seismology also offers benefits to glacier observation through the spatially flexible nature of its recordings. Many glaciological tools, like borehole water pressure gauges and GPS receivers, can only directly record local behavior, while seismometers can record seismic waves generated in the region surrounding them. Seismic deployments can be designed at vastly different scales depending on the processes of interest, from a few hundred meters to observe small local activity on alpine glaciers (e.g. Walter et al. 2013) or several tens or hundreds of kilometers to observe regional activity on large ice streams (e.g. Pratt et al. 2014). The spatial flexibility of seismology is particularly useful for observations of subglacial processes where the exact location of activity of interest may not be easily determinable from surface observations and may even migrate over time, such as basal icequakes (e.g. Walter et al. 2013) or subglacial conduit migration (e.g. Vore et al. 2019).

In this thesis, I use seismic data from Lemon Creek Glacier, an isolated mountain glacier situated on local diorite and gabbro bedrock (Thiel et al. 1957) at the southern tip of the

Juneau Icefield on Tlingit lands in Alaska (Thornton 2012), to observe two glacial processes that take place in the intermediate temporal scale where seismic observations are uniquely useful. To collect this data, I co-led a field expedition in June to July of 2017 to Lemon Creek Glacier to deploy 55 nodal seismometers in surface snow, two GPS receivers on ice-mounted poles, a stage gauge in the ice-marginal lake, and a rain gauge on the marginal ridge with a team of collaborators and field assistants. After deployment, I remained at the glacier for the duration of the seismometers' battery life to record via notes and photographs the local weather conditions, glacier surface conditions, lake drainage progression, and human activity on the glacier from the Juneau Icefield Research Program with data interference potential. Shortly after the battery life of the seismometers had passed, a second field team joined me to retrieve all 55 seismometers. Another field team returned to the glacier in late August 2017 to retrieve the GPS receivers and hydrologic gauges.

First, in Chapter 2 (published as Labedz et al., 2022), I observe seismic tremor generated by turbulent water flow in the subglacial hydrologic system. I observe that the changing relationship between seismic tremor power levels and subglacial water flux indicate the pressurization state of the subglacial hydrologic system. Over the course of the 36-hour drainage event of an ice-marginal lake at the head of the glacier, I find that the subglacial hydrologic system undergoes partial pressurization: during rising water flux, pressurization occurs under the upper portion of the glacier only. This pressurization event was surprisingly not accompanied by a noticeable increase in glacier velocity, indicating that it would have been difficult to observe at all without the contribution of the glaciohydraulic tremor data, highlighting the importance of diverse data types when validating or challenging assumptions about the connections between glacier hydrology and velocity.

Then, in Chapter 3, I observe discrete icequake events occurring at the surface of the glacier. The spatial patterns of these events relative to the known surface stress state of the glacier, as well as the angular distribution of the polarization and amplitude of the emitted Rayleigh waves, indicate that these events are generated by the opening of surface crevasses on the glacier. These icequakes reveal the lengthwise propagation of crevasses, the reactivation of

crevasses after quiescent periods of hours to days, and the influence that crevasse behaviors have on their neighboring crevasses. The icequakes comprising these crevassing events have a swarm-like magnitude distribution, as opposed to the classic mainshock-aftershock magnitude distribution more typical of tectonic earthquakes.

In addition to the cryoseismology work in this thesis, I explore another avenue of environmental seismology in Chapter 4: anthropogenic seismic noise. In this study, I explore statistical choices toward optimizing noise amplitude analysis for the urban anthropogenic noise environment, and apply the analysis toward observations of changing urban noise in Los Angeles at long time scales with COVID-19-related lockdowns and at short time scales with the 2022 Super Bowl.

Interest in seismic signals from glacier processes has grown rapidly in the last decade among environmental seismologists (Podolskiy & Walter 2016), but cryoseismology is still in the early stages of being applied regularly as a tool for glaciology research, or implemented for applications like real-time flood hazard monitoring. Building the future of glacier science in a way that advances knowledge and supports communities will require geophysical tools that provide information across the full range of relevant spatial and temporal scales. Seismology will be a valuable asset to that goal, particularly for observing phenomena at the scale of hours to days, such as those presented in this thesis.

References

Anandakrishnan, S., & Alley, R. B. (1994). Ice Stream C, Antarctica, sticky spots detected by microearthquake monitoring. Annals of Glaciology, 20, 183-186. https://doi.org/10.3189/1994AoG20-1-183-186

Bartholomaus, T. C., Amundson, J. M., Walter, J. I., O'Neel, S., West, M. E., & Larsen, C. F. (2015). Subglacial discharge at tidewater glaciers revealed by seismic tremor. Geophysical Research Letters, 42, 6391–6398. https://doi.org/10.1002/2015GL064590

Chen, X., Shearer, P. M., Walter, F., & Fricker, H. A. (2011). Seventeen Antarctic seismic events detected by global surface waves and a possible link to calving events from satellite images. Journal of Geophysical Research: Solid Earth, 116(B6). https://doi.org/10.1029/2011JB008262

Gimbert, F., Tsai, V. C., & Lamb, M. P. (2014). A physical model for seismic noise generation by turbulent flow in rivers. Journal of Geophysical Research: Earth Surface, 119, 2209–2238. https://doi.org/10.1002/2014JF003201

Gimbert, F., Tsai, V. C., Amundson, J. M., Bartholomaus, T. C., & Walter, J. I. (2016). Subseasonal changes observed in subglacial channel pressure, size, and sediment transport. Geophysical Research Letters, 43, 3786–3794. https://doi.org/10.1002/2016GL068337

Helmstetter, A., Nicolas, B., Comon, P., & Gay, M. (2015a). Basal icequakes recorded beneath an Alpine glacier (Glacier d'Argentière, Mont Blanc, France): Evidence for stick-slip motion?. Journal of Geophysical Research: Earth Surface, 120(3), 379-401. https://doi.org/10.1002/2014JF003288

Helmstetter, A., Moreau, L., Nicolas, B., Comon, P., & Gay, M. (2015b). Intermediate-depth icequakes and harmonic tremor in an Alpine glacier (Glacier d'Argentière, France): Evidence for hydraulic fracturing?. Journal of Geophysical Research: Earth Surface, 120(3), 402-416. https://doi.org/10.1002/2014JF003289

Labedz, C. R., Bartholomaus, T. C., Amundson, J. M., Gimbert, F., Karplus, M. S., Tsai, V. C., & Veitch, S. A. (2022). Seismic mapping of subglacial hydrology reveals previously undetected pressurization event. Journal of Geophysical Research: Earth Surface, 127(3), e2021JF006406. https://doi.org/10.1029/2021JF006406

Mikesell, T. D., van Wijk, K., Haney, M. M., Bradford, J. H., Marshall, H. P., & Harper, J. T. (2012). Monitoring glacier surface seismicity in time and space using Rayleigh

waves. Journal of Geophysical Research: Earth Surface, 117(F2). https://doi.org/10.1029/2011JF002259

Nettles, M., & Ekström, G. (2010). Glacial earthquakes in Greenland and Antarctica. Annual Review of Earth and Planetary Sciences, 38, 467-491. https://doi.org/10.1146/annurev-earth-040809-152414

Olinger, S. D., Lipovsky, B. P., Wiens, D. A., Aster, R. C., Bromirski, P. D., Chen, Z., ... & Stephen, R. A. (2019). Tidal and thermal stresses drive seismicity along a major Ross Ice Shelf rift. Geophysical Research Letters, 46(12), 6644-6652. https://doi.org/10.1029/2019GL082842

Pratt, M. J., Winberry, J. P., Wiens, D. A., Anandakrishnan, S., & Alley, R. B. (2014). Seismic and geodetic evidence for grounding-line control of Whillans Ice Stream stick-slip events. Journal of Geophysical Research: Earth Surface, 119(2), 333-348. https://doi.org/10.1002/2013JF002842

Podolskiy, E. A., & Walter, F. (2016). Cryoseismology. Reviews of geophysics, 54(4), 708-758. https://doi.org/10.1002/2016RG000526

Qamar, A., & Lawrence, W. F. S. (1983). An investigation of icequakes on the Greenland icesheet near Jakobshavn icestream. University of Colorado, World Data Center A for Glaciology.

Röösli, C., Walter, F., Ampuero, J. P., & Kissling, E. (2016). Seismic moulin tremor. Journal of Geophysical Research: Solid Earth, 121(8), 5838–5858. https://doi.org/10.1002/2015JB012786

Röösli, C., Walter, F., Husen, S., Andrews, L. C., Lüthi, M. P., Catania, G. A., & Kissling, E. (2014). Sustained seismic tremors and icequakes detected in the ablation zone of the Greenland ice sheet. Journal of Glaciology, 60(221), 563–575. https://doi.org/10.3189/2014JoG13J210

Roux, P. F., Walter, F., Riesen, P., Sugiyama, S., & Funk, M. (2010). Observation of surface seismic activity changes of an Alpine glacier during a glacier-dammed lake outburst. Journal of Geophysical Research: Earth Surface, 115(F3). https://doi.org/10.1029/2009JF001535

Thornton, T. F. (2012). Haa Léelk'w has Aaní Saax': Our grandparents' names on the land. Sealaska Heritage Institute and University of Washington Press.

Vore, M. E., Bartholomaus, T. C., Winberry, J. P., Walter, J. I., & Amundson, J. M. (2019). Seismic tremor reveals spatial organization and temporal changes of subglacial water system. Journal of Geophysical Research: Earth Surface, 124(2), 427-446. https://doi.org/10.1029/2018JF004819

Walter, F., Dalban Canassy, P., Husen, S., & Clinton, J. F. (2013). Deep icequakes: What happens at the base of Alpine glaciers?. Journal of Geophysical Research: Earth Surface, 118(3), 1720-1728. https://doi.org/10.1002/jgrf.20124

Winberry, J. P., Anandakrishnan, S., & Alley, R. B. (2009). Seismic observations of transient subglacial water-flow beneath MacAyeal Ice Stream, West Antarctica. Geophysical Research Letters, 36(11). https://doi.org/10.1029/2009GL037730

C h a p t e r   2

SEISMIC MAPPING OF SUBGLACIAL HYDROLOGY REVEALS PREVIOUSLY UNDETECTED PRESSURIZATION EVENT

Abstract

Understanding the dynamic response of glaciers to climate change is vital for assessing water resources and hazards, and subglacial hydrology is a key player in glacier systems. Traditional observations of subglacial hydrology are spatially and temporally limited, but recent seismic deployments on and around glaciers show the potential for comprehensive observation of glacial hydrologic systems. We present results from a high-density seismic deployment spanning the surface of Lemon Creek Glacier, Alaska. Our study coincided with a marginal lake drainage event, which served as a natural experiment for seismic detection of changes in subglacial hydrology. We observed glaciohydraulic tremor across the surface of the glacier that was generated by the subglacial hydrologic system. During the lake drainage, the relative changes in seismic tremor power and water flux are consistent with pressurization of the subglacial system of only the upper part of the glacier. This event was not accompanied by a significant increase in glacier velocity; either some threshold necessary for rapid basal motion was not attained, or, plausibly, the geometry of Lemon Creek Glacier inhibited speedup. This pressurization event would have likely gone undetected without seismic observations, demonstrating the power of cryoseismology in testing assumptions about and mapping the spatial extent of subglacial pressurization.

1. Introduction

Glacier behavior is strongly influenced by subglacial hydrology, which affects processes such as basal motion, melting, fracture, erosion, sediment and nutrient export, ice-ocean interactions, and more (Bartholomaus et al., 2011; Iken & Truffer, 1997; Lydersen et al., 2014; Motyka et al., 2006; Schoof, 2005; Slater et al., 2015). However, observations of subglacial hydrologic systems are spatially and temporally limited by the nature of traditional glaciological observations; in situ methods via boreholes sample only single locations (e.g., Hubbard et al., 1995), while methods like ice-penetrating radar sample only single points in time (e.g., Moore et al., 1999). Expanding observational scales of subglacial hydrology is vital to predicting how glacial systems will impact humanity through changes in water resources, flood hazards, and sea level.

Measurement of glaciohydraulic tremor, the continuous seismic signal generated by turbulent water flow in a glacier, can improve the spatial and temporal scales of subglacial hydrological observations. By adapting theoretical descriptions of tremor generation from fluvial seismology (Burtin et al., 2008, 2011; Gimbert et al., 2014; Schmandt et al., 2013; Tsai et al., 2012), glaciohydraulic tremor has already been shown to reveal properties of subglacial hydrologic systems such as water flux (Bartholomaus et al., 2015; Winberry et al., 2009), sediment transport (Gimbert et al., 2016), water pressurization (Gimbert et al., 2016; Lindner et al., 2020; Nanni et al., 2020), water flow source location (Nanni et al., 2021; Vore et al., 2019), and flood front propagation (Eibl et al., 2020). In addition, analysis of tremor signals at glaciers can also be interpreted to locate and describe other glaciohydraulic sources such as moulin activity (Aso et al., 2017; Lindner et al., 2020; Röösli et al., 2014, 2016) and crack waves in the basal water layer (Gräff et al., 2019). These studies demonstrate the potential power of glaciohydraulic tremor as an observational tool, and the need to explore its utility in a range of contexts and scales in order to best apply it to studies of glacier systems.

In this study, we observe glaciohydraulic tremor at Lemon Creek Glacier, Alaska with a dense array of seismometers (Section 2.1) in order to expand the spatial scale and detail in which subglacial hydrologic properties can be observed continuously in time, and compare it with hydrologic data collected at the glacier (Section 2.2). We process this data to preserve continuous signals (Section 2.3) and compare the observed signal with theoretical models of tremor generation (Section 2.4). We observe different relationships between seismic tremor and water flux across the surface of the glacier and over time during the course of a lake drainage (Section 3). We interpret these observations as glaciohydraulic tremor reflecting the pressurization state of the subglacial system, and conclude that the upper portion of the glacier pressurized during an increase in water flux from the drainage of an ice-marginal lake, but that this pressurization was not accompanied by a significant increase in glacier velocity (Section 4).

2. Field Instrumentation and Data Analysis Methodology

2.1. Field Site and Instrumentation

In this study, we observe seismic signals at Lemon Creek Glacier, Alaska (Figure 1), an isolated mountain glacier at the southern tip of the Juneau Icefield, on Tlingit lands (Thornton, 2012). Lemon Creek Glacier is approximately 6.5 km long and 1.5 km wide, has a 3–7° surface slope, and flows northward at 20–40 m/yr (Pelto et al., 2013; Thiel et al., 1957; Veitch et al., 2021). The glacier is approximately 350 m thick at its thickest point (located at approximately the same area as the southern GPS receiver in Figure 1) and has a shallow reverse bed slope over the next ~600 m downglacier, as determined by an active seismic reflection survey in Veitch et al. 2021. The glacier is situated on local gabbro and diorite bedrock (Thiel et al. 1957). The glacier resides at the headwaters of the Lemon Creek drainage. At the head of the glacier, an ice-marginal lake, Lake Linda, fills with melt and rain water in the early summer (2017 volume was approximately 570,000 m^3, see Section

2.2), before rapidly draining directly into the subglacial hydrologic system. Lake drainages have been observed annually since at least 1967 (Post & Mayo, 1971).
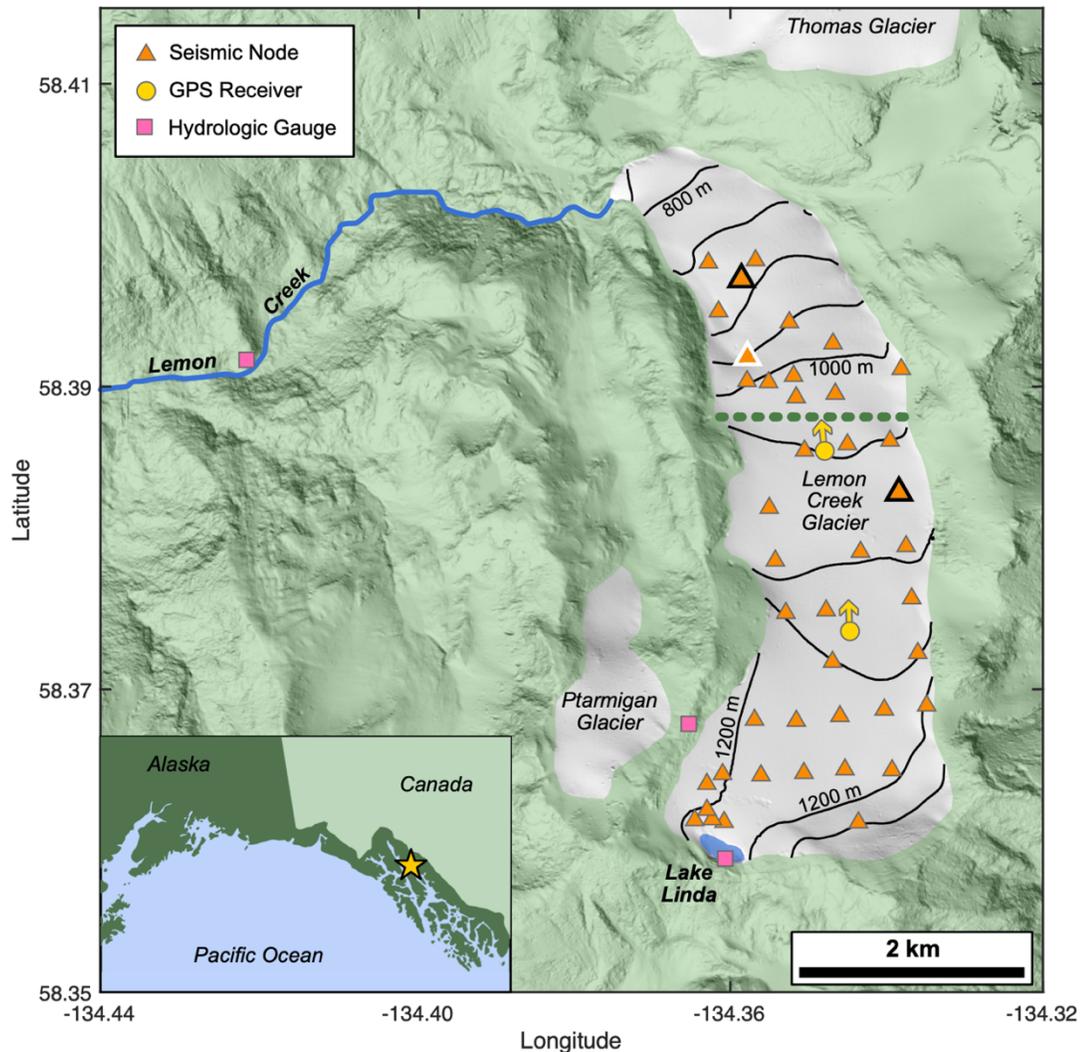
Figure 1. Map of Lemon Creek Glacier, showing glacier surfaces (white), Lake Linda and Lemon Creek (blue), locations of geophysical instrumentation used in this study (seismometers – orange triangles, GPS receivers – yellow circles, hydrologic gauges – pink squares), topography of Lemon Creek Glacier (black lines at 50 m intervals from 750 to 1,250 m), and approximate location of surface slope break (dotted green line). Arrows on GPS receiver icons indicate flow direction. Bold-outlined seismometer icons denote stations used for data displayed in Figure 5 (white outline) and Figure 6 (black outline). Hydrologic gauges are a lake stage gauge (in Lake Linda), rain gauge (west rim of glacier), and USGS stream gauge (on Lemon Creek). Hillshade from ArcticDEM by Polar Geospatial Center (Porter et al., 2018). Inset shows location of Lemon Creek Glacier in Southeast Alaska.

We use continuous seismic data from 42 single-component FairfieldNodal (now Magseis Fairfield) ZLand nodal seismometers that were buried in surface snow across the glacier from 28 June to 13 July 2017. These and other instrumentation are shown in Figure 1. We deployed 55 nodes sampling at 250 Hz in an array with 300–400 m spacing, however some gaps appear in the final data due to malfunctioned sensors. We also deployed two Trimble NetRS GPS receivers attached to poles bored approximately 10 m into the ice. GPS data points every 15 s were processed against the UNAVCO Mendenhall AB50 base station using *track*, which is part of the GAMIT-GLOBK processing software (Chen, 1998).

2.2. Discharge Measurements and Modeling

During our 2017 experiment, we recorded the initial onset of Lake Linda drainage on July 4 with a stage gauge deployed in the lake. This gauge malfunctioned shortly after the drainage began, so the progression of the drainage was then monitored through time-stamped photographs recorded by our field team (Figures 2 and 3). The lake drainage rate increased sharply by mid-day on July 5, and the lake reached its minimum water level by mid-morning on July 7 (Figure 2). The drained volume was approximately 570,000 m^3, calculated with a digital elevation model of the emptied lake basin collected by drone photogrammetry on July 8, after the drainage was complete (personal communication, Matt Beedle, 2018). This volume of water is equivalent to approximately 6 cm of rain across the entire surface of the glacier.

Lemon Creek is monitored by a USGS streamflow gauge approximately 3 km downstream from the toe of the glacier (USGS, 2017). This gauge also receives outflow from the smaller Ptarmigan and Thomas glaciers to the west and north of Lemon Creek Glacier, respectively. The volume of the Ptarmigan and Thomas glaciers are likely each an order of magnitude smaller than that of Lemon Creek Glacier based on their relative surface areas (McNeil, 2016), so the outflow Q measured by the streamflow gauge is dominated by the outflow of

Lemon Creek Glacier, especially during times of low precipitation and after seasonal snowpack has melted from the lower reaches of the basin.
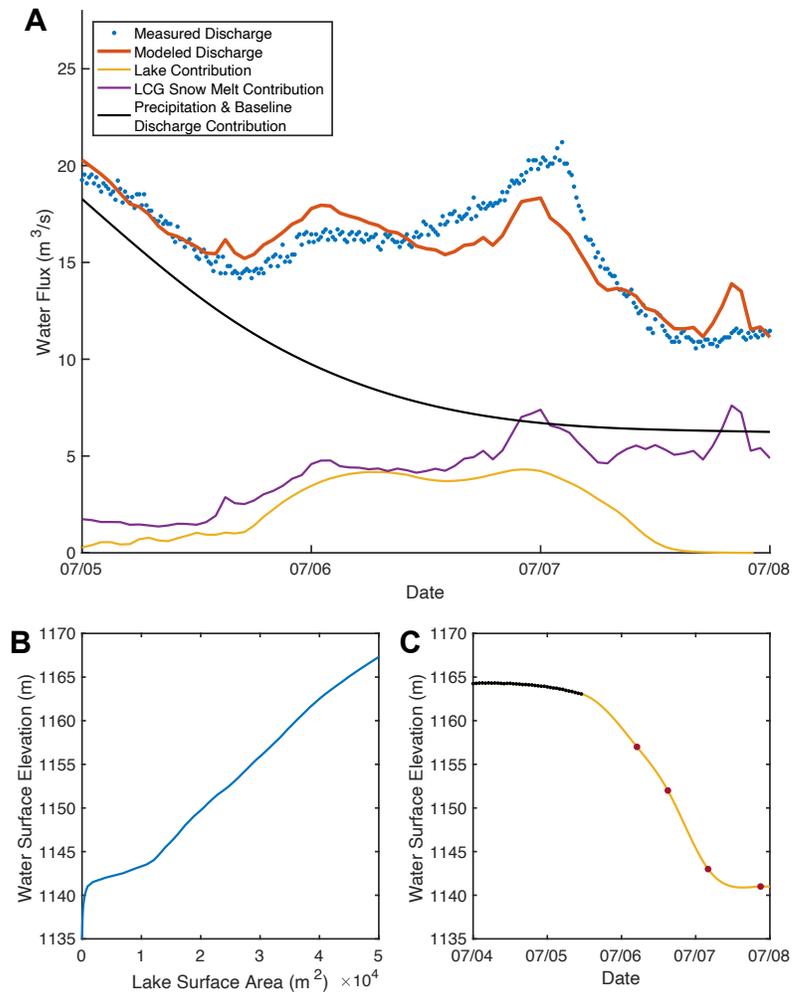
Figure 2. [a] Hydrologic budget for water flux measured at the USGS stream gauge at the time of interest for this study. Blue dots: stream flux as measured by USGS gauge. Yellow line: outflow from Lake Linda during drainage, calculated from hypsometry in [b] and observed water levels in [c]. Purple line: Contribution of snow melt to total discharge at the terminus of Lemon Creek Glacier, modeled using the degree day approach. Black line: Estimated runoff decay from July 1-5 rain event back to baseline level. Red line: sum of fluxes from lake drainage, melting, and baseline. [b] Lake Linda hypsometry, calculated from a digital elevation model from drone photogrammetry on July 8 (personal communication, Matt Beedle, 2018). [c] Black dots: observed water level in Lake Linda from stage gauge before malfunction. Red dots: observed water level in Lake Linda from field photographs. Yellow line: cubic smoothing spline fit of observations.
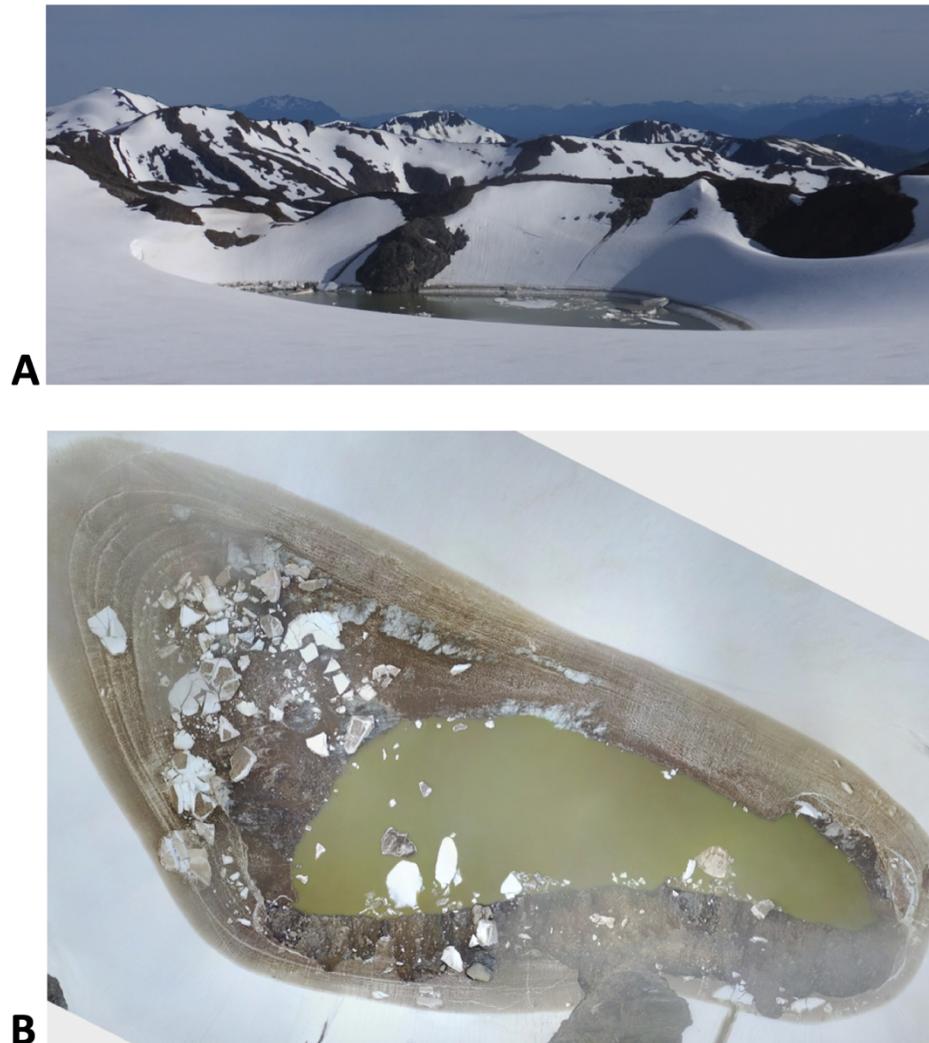
Figure 3. [a] Photograph of Lake Linda taken at UTM 2017-07-06 01:48, an example of images used to track lake level over time via "bathtub ring" features after stage gauge malfunction. [b] Drone image of the emptied Lake Linda from the image set used to make the digital elevation model, with "bathtub ring" features visible, courtesy Matt Beedle.

In order to confirm the reliability of water flux Q recorded at the streamflow gauge as a measure of Lemon Creek Glacier's outflow, we modeled sources of water outflow from the glacier. During our experiment, nearly the entirety of Lemon Creek Glacier was snow covered. To determine the contribution to outflow of snowmelt, we modeled snowmelt from the surface using a degree-day approach (Hock, 2003) driven by air temperatures recorded at a Juneau Icefield Research Program camp, located at 1,280 m near the head of Lemon

Creek Glacier. We distributed temperatures over an ArcticDEM tile (Porter et al., 2018) using a −0.006°C/m lapse rate, and then modeled melt using a 4.5 mm/d/°C degree day factor appropriate for snow in maritime climates (Hock, 2003). During July 3-4, 6 cm of rain fell at the camp, and the runoff from this event contributes to the flux of Lemon Creek, decreasing over time after the rain ceases. We estimate the decreasing rain runoff contribution to Lemon Creek after this rain event by extrapolating the decrease in water flux at the stream gauge between the end of the rain event and the start of the lake drainage event into a smooth decay to the baseline stream flux observed after the lake drainage event and before the next precipitation event using a cubic smoothing spline fit. At the location of the USGS gauge, measured and modeled cumulative runoff are within 5% of each other (Figure 2).

2.3. Seismic Signal Processing

We quantify glaciohydraulic tremor from the ambient seismic field at each station by calculating a median power spectral density (PSD), as described in Bartholomaus et al., 2015. In this method, we calculate the PSD (units $(m/s)^2/Hz$) of all consecutive short-duration (30 s) waveforms within a long-duration (30 min) time window. At a given frequency, we find the median of all power values among the short-duration PSDs. The long-duration median PSD is composed of these individual medians at each frequency value in the spectrum. Because the median PSD method removes the contribution from discrete short-term events as outliers while preserving the contribution from continuous signals, there is no need for prior removal of data segments containing earthquakes, icequakes, or other events. See Figure 4 for an example of median PSD processing on a segment of data. We discuss the interpretation of median PSD signals in Section 4. The median PSD of an example station is shown in Figure 5a. Some stations experienced intermittent data quality issues on July 8-10; these data segments clearly contain significant non-natural contributions, which we manually removed after median PSD calculation. These issues occurred around the time that stations were melting out from their burial surface snow, but no causal relationship between the issues and melt-out is clear. In order to determine tremor amplitude (shown in Figure 5c) from the

median PSDs, we integrate over a given frequency range to determine the median absolute ground velocity in that range (Press et al., 1988), which is the square root of the signal power as integrated over that range.
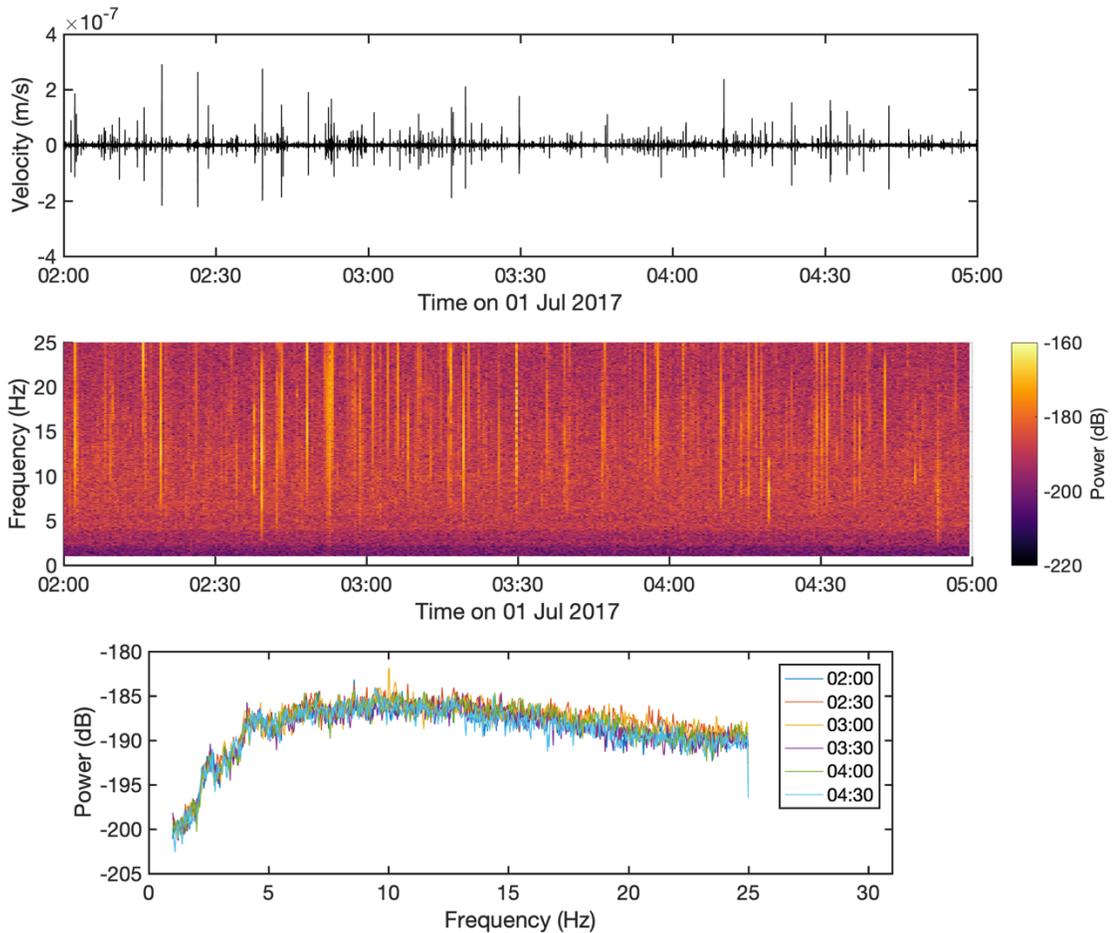
Figure 4. Top: A 3-hour segment of raw velocity data from a seismic station on the surface Lemon Creek Glacier. Middle: Power spectral densities for 30-second waveforms within the 3- hour segment. Bottom: Median power spectral densities (as described in main text section 2.3) for 30-minute windows within the 3-hour segment, colored by the start time of the window.
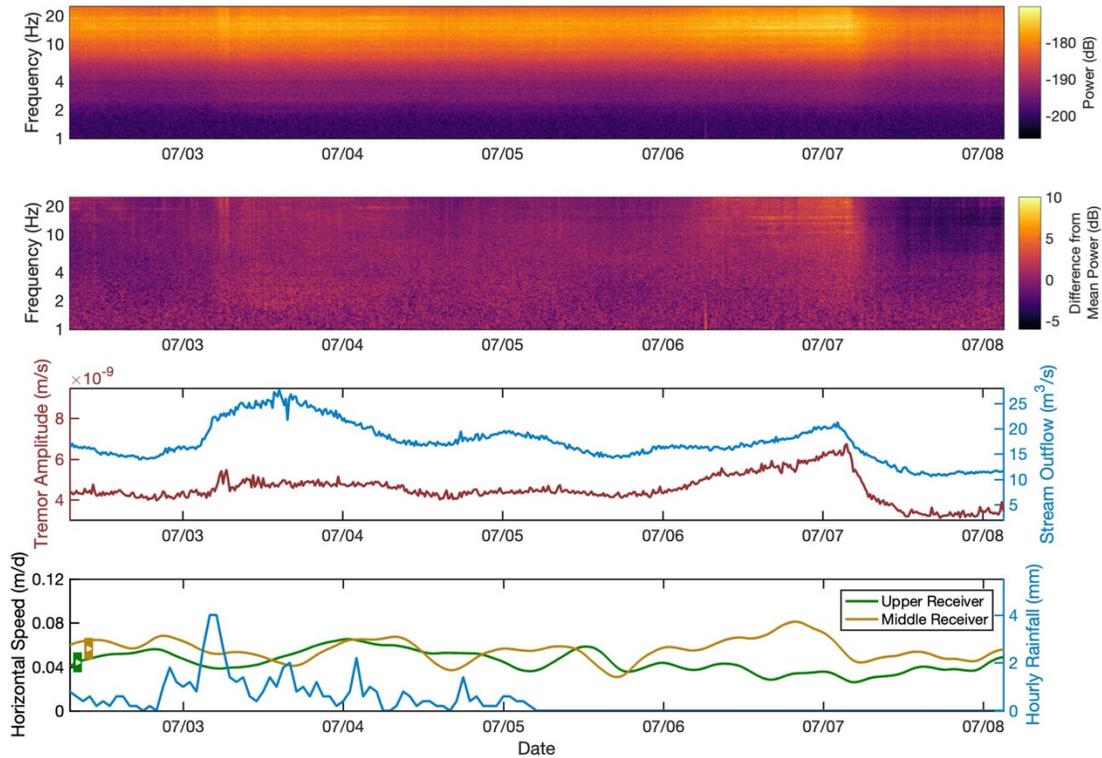
Figure 5. (A) Spectrogram of median power spectral density (PSD) over a logarithmic frequency axis from 1 to 25 Hz recorded by one seismometer deployed at Lemon Creek Glacier (outlined in white in Figure 1) during 3–8 July 2017. (B) Deviation from the mean median PSD from the same station over the same time period. (C) Median tremor amplitude (red) for the 1.5–25 Hz range for the same seismometer as in [a], and water flux (blue) recorded at the stream gauge on Lemon Creek. (D) Hourly rainfall (blue) and horizontal speeds of the two GPS receivers deployed on the glacier (green and gold). Vertical bars at left show one standard deviation above and below the mean speed (white triangle).

2.4. Source Theory

Environmental seismic noise has various sources (Larose et al., 2015), but the portion of the ambient seismic field that is attributable to glaciohydraulic tremor in a glacier system can be predicted by adapting theories of tremor generation originally developed for fluvial systems (Gimbert et al., 2014; Tsai et al., 2012). One major source of glaciohydraulic tremor is

turbulent water flow. As derived in Gimbert et al., 2016, seismic tremor power P produced by a channel of constant geometry is modeled to increase as a power law with water volume flux Q, with the exponent depending on hydraulic regime, as described below. For a channel where changes in Q are driven by changes in hydraulic radius (the cross-sectional area of the flow divided by the wetted perimeter) while hydraulic pressure gradient remains constant, Gimbert et al., 2016 predicts

$$P \propto Q^{5/4} . \qquad (1)$$

For example, this scenario describes a semi-filled channel or a channel freely growing or shrinking to completely accommodate flux changes, Alternatively, for a filled channel where changes in Q are driven by changes in hydraulic pressure gradient, while hydraulic radius remains constant, Gimbert et al., 2016 predicts

$$P \propto Q^{14/3} . \qquad (2)$$

Thus, the strength of the scaling between seismic power and water outflow is predicted to depend on the pressurization state; power scales more weakly with flux for a channel with constant pressure gradient and variable hydraulic radius, and it scales more strongly with flux for a channel with constant hydraulic radius and variable pressure gradient. Refer to Figure 6a for a diagram, and see Gimbert et al., 2016 for full, detailed derivation. These end-member scenarios are theoretical and do not describe every possible source of changing seismic power in a complex environment (e.g., tremor generated during significant co-evolution of both pressure gradient and hydraulic radius), but multiple seismic studies of real glacier systems have observed tremor consistent with these models (Bartholomaus et al., 2015; Gimbert et al., 2016; Lindner et al., 2020; Nanni et al., 2020; Vore et al., 2019).

In order to determine which hydraulic regime appears to dominate the generation of glaciohydraulic tremor detected at any particular station, we compare the water flux Q to the median seismic tremor power P at that station. We use the 1.5–25 Hz frequency range, where glaciohydraulic tremor is expected to appear when the source-receiver distances are only a

few hundred meters (Bartholomaus et al., 2015; Gimbert et al., 2014; Lindner et al., 2020; Nanni et al., 2020). We plot scaled power (P/P_{ref}) against scaled discharge ($\log(Q/Q_{ref})$), setting the lowest value in the time period of interest as the scaling reference value (as shown in Figures 6b and 6c), and then use a linear least squares regression to find the best-fitting slope b, representing the exponent in a power-law relationship between tremor and discharge:

$$P \propto Q^{b}. \qquad (3)$$
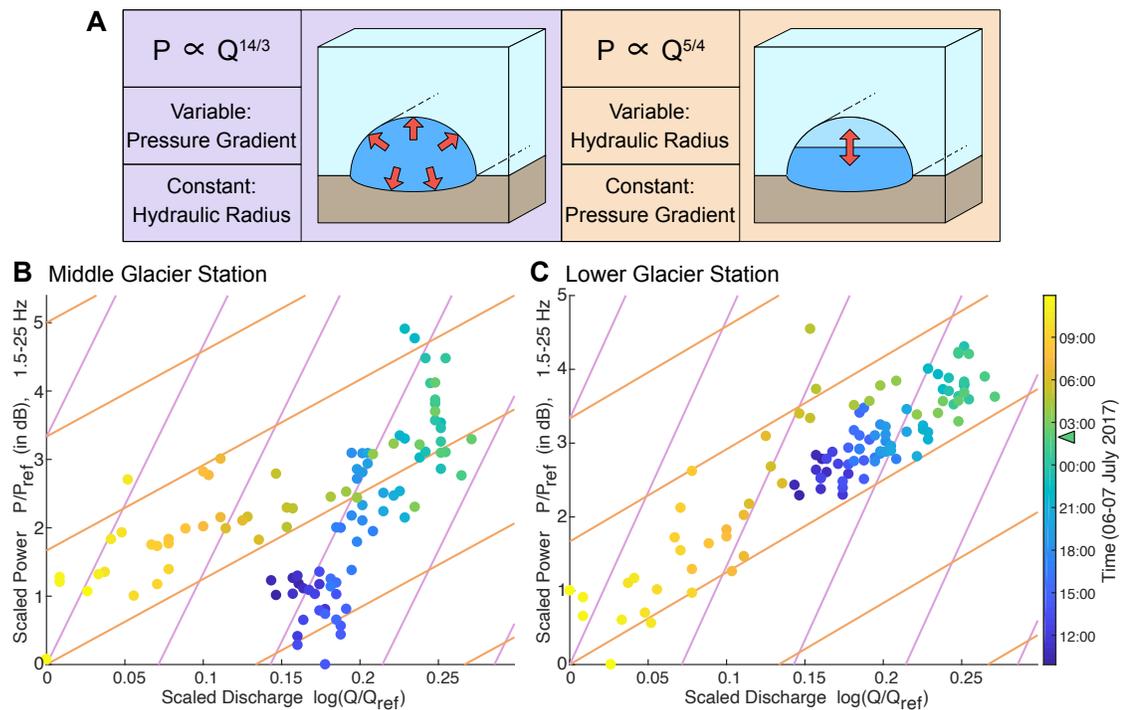
Figure 6. (a) Diagram showing two possible relationships between seismic power and water flux: in purple, a channel with variable pressure gradient and constant hydraulic radius and in orange, a channel with variable hydraulic radius and constant pressure gradient. (b and c) Examples of the relationship between seismic tremor power and water flux over the course of the drainage of Lake Linda for two seismometers (one near the middle of the glacier and one at lower altitude nearer the toe of the glacier, outlined in black in Figure 1). Peak outflow time (02:00 on July 7) is highlighted with the triangle icon on the color bar. Purple lines indicate the slope of a variable pressure gradient system, and orange lines indicate the slope of a variable hydraulic radius system.

We then compare the fitted *b* value to the theoretically predicted relationships (Equation 1 and Equation 2) for each subglacial hydrologic regime. Values of *b* near 5/4 imply variations in tremor generation dominated by changes in hydraulic radius, while values of *b* near 14/3 imply variations in tremor generation dominated by changes in pressure gradient.

3. Results

Hydrologic activity varied over the course of the seismic deployment; rain fell during 2–4 July, and Lake Linda drained during 5–7 July (see Figure 7 for full season precipitation data). We find that the amplitude of ambient seismic tremor in the 1.5–25 Hz range at seismic nodes also varied over this period, correlating positively with the water flux measured at the USGS gauge, as shown in Figure 5. Seismic tremor power for all stations can be seen in Figure 8.
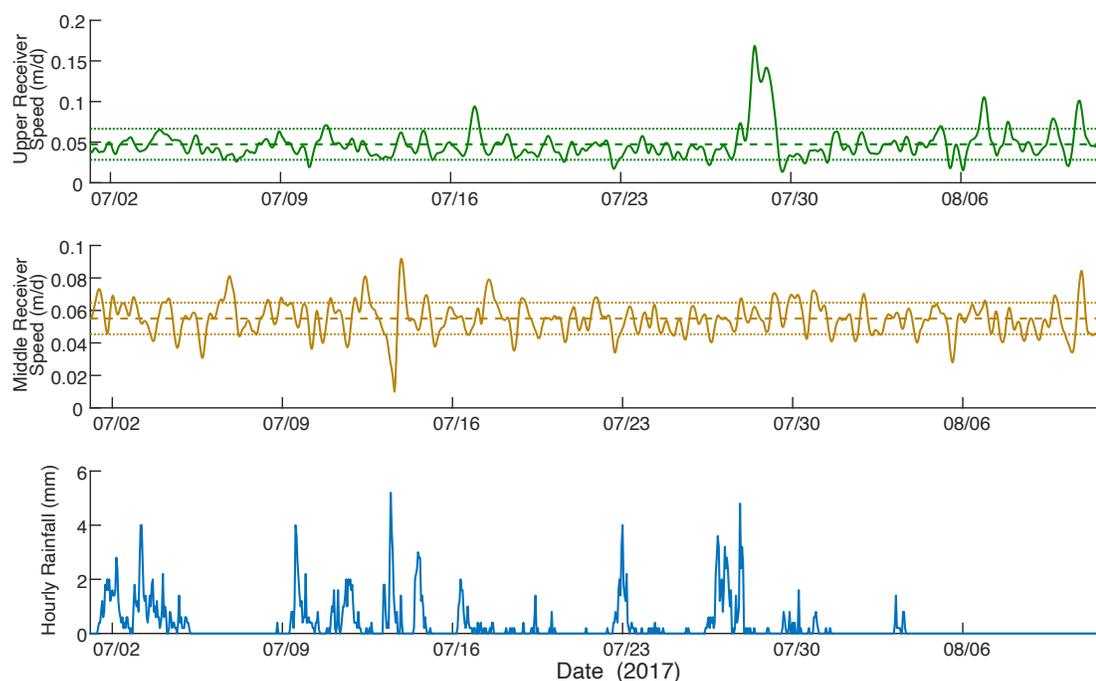
Figure 7. Season-long speed data for the two GPS receivers deployed at Lemon Creek Glacier, as well as rainfall rate. Dashed lines on GPS plots indicate mean speed for each receiver, and dotted lines indicate one standard deviation above and below mean speed for that receiver.
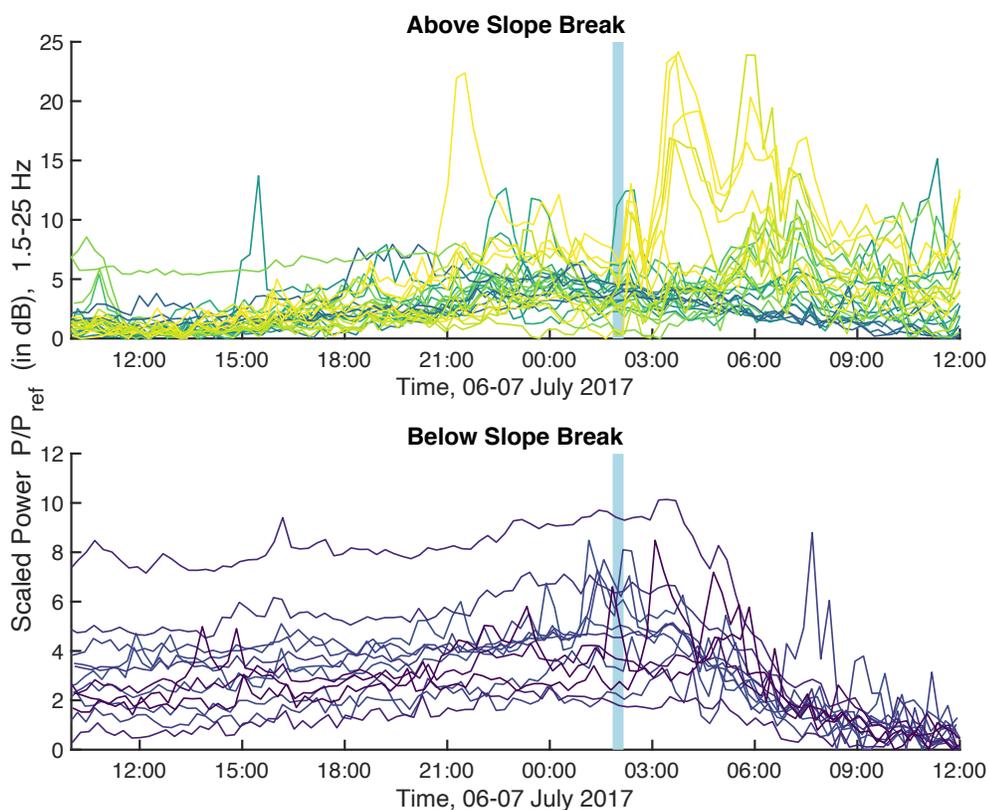
Figure 8. Seismic tremor power over time during the lake drainage for all seismic stations on the glacier. Line color representing the latitude of each seismic station, from yellow in the south (head of the glacier) to violet in the north (toe of the glacier). Upper panel features stations upglacier from the slope break marked in Figure 1, while lower panel features stations downglacier from the slope break. Vertical blue line indicates time of peak water flux.

The scaling relationship between the tremor power and water flux (as presented in Section 2.4) varies spatially over the surface of the glacier and temporally during the lake drainage. Tremor power increases throughout July 6 as water flux increases, and then both decrease after peak outflow is reached on July 7, as shown in two example stations in Figures 6b and Figure 6c. Records from these two stations differ in their relationships between tremor power and water flux. The station near the middle of the glacier (Figure 6b) shows a much higher slope before peak outflow than after peak outflow, while the station low on the glacier

(Figure 6c) shows similar low slopes for both the rise and fall in water flux. The relationships between seismic tremor power and water flux for more stations can be seen in Figure 9.
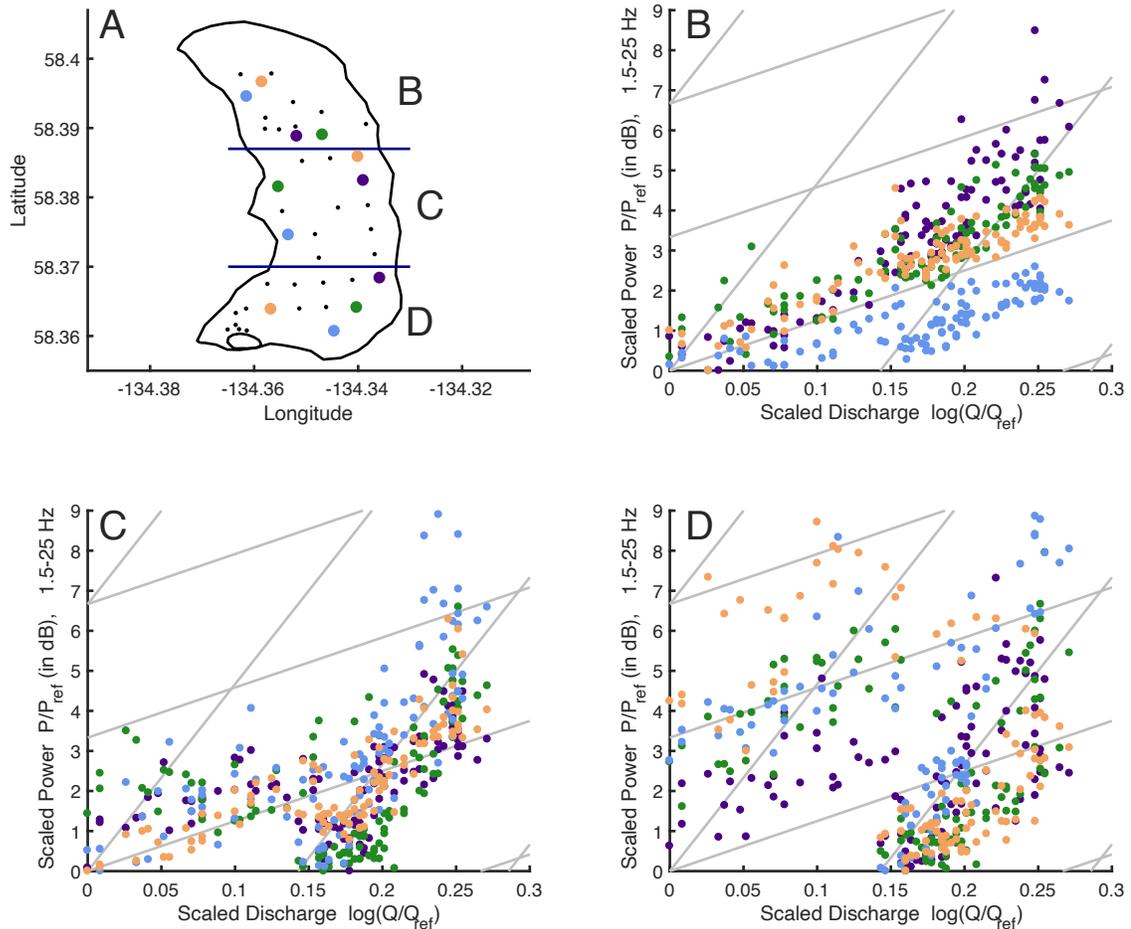
Figure 9. [a]. Map of seismometers (dots) on the surface of Lemon Creek Glacier (black outline). Large colored dots indicate seismometers for which data is shown in [b], [c], and [d]. The line between [b] and [c] regions is the same as the slope break indicated in Figure 1, while the line between [c] and [d] regions is not based on a physical feature, but rather divides the remaining stations approximately evenly. [b, c, d]. Relationship between seismic tremor power and water flux (as in main text figure 3) for seismometers over the course of the lake drainage (same time period as Figure 6 and Figure 8). Color of data points corresponds to color of seismometer icon in panel [a]. Time of each data point is not shown, but follows same patterns as the seismometers in Figure 6. Gray background lines indicate the slopes for the models of a variable pressure gradient system (steep) and a variable hydraulic radius system (shallow), as in Figure 6.
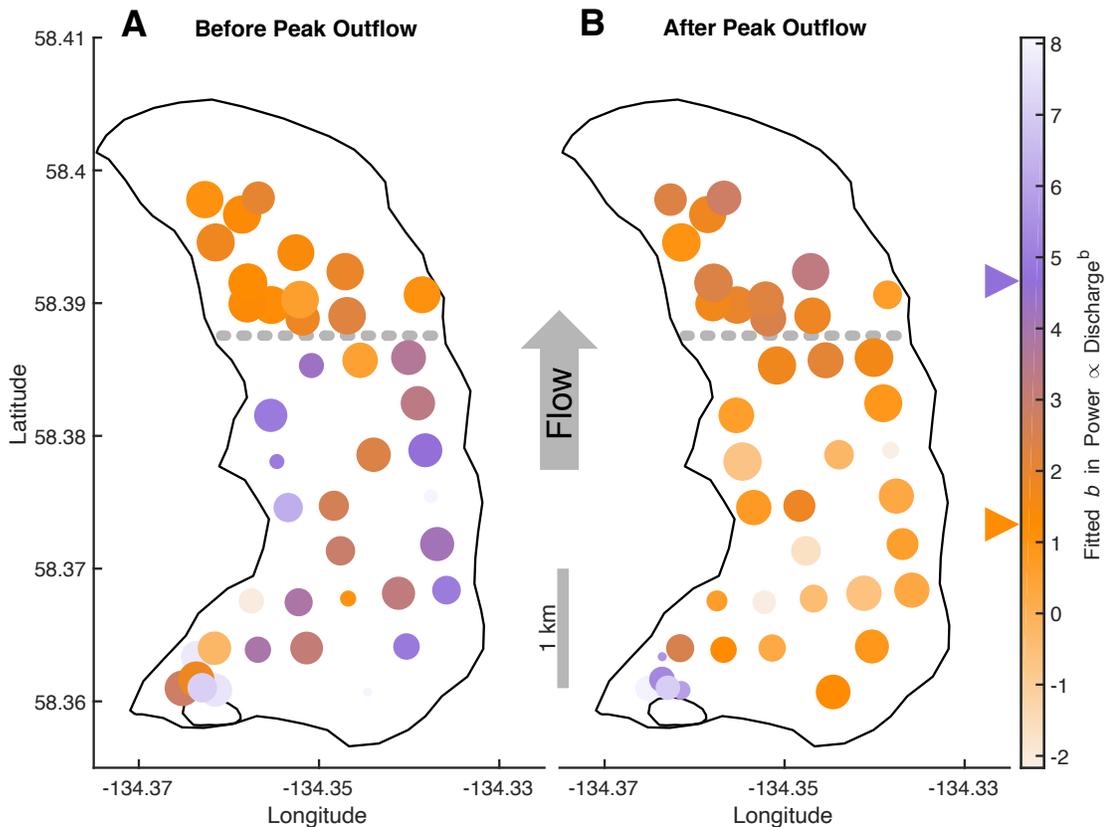
Figure 10. Maps showing fitted exponents b, as in the pressure-flux relation $P \propto Q^b$ for each station, during the water flux increase before the peak of the lake drainage (a) and during the decrease after the peak (b) over the surface of the glacier, outlined in black. Dotted gray line is the latitude of slope break. Arrows on colorbar denote theoretical b values of 5/4 for the variable hydraulic radius and constant pressure gradient case (orange) and 14/3 for the variable pressure gradient and constant hydraulic radius case (purple) as in Gimbert et al., 2014. Marker size is inversely proportional to standard error of the model fit for b (median standard error: 0.297, minimum: 0.083, maximum 1.437).

During the rising limb of the outburst flood on July 6, stations on different parts of the glacier observe different relationships between tremor power and water flux (Figure 10). We start fitting for the exponent b later than the first onset of the lake drainage, because the stream gauge is still receiving rainfall from rapid overland transport from the larger catchment at the initiation of the drainage (see Section 2.2 and Figure 2). Using the fitting method described in Section 2.4 for data from 10:00 July 6 to 01:00 July 7, stations on the lower portion of the glacier, north of the slope break at 58.387°N, observe a median fitted exponent b of 1.391 (interquartile range: 1.151–1.846), while stations on the upper portion of the glacier, south

of the slope break, observe a median fitted exponent *b* of 3.904 (interquartile range: 2.722–5.009). During this time period, prior to peak lake drainage and within the upper portion of the glacier, fitted exponents are greater along the east and west margins than they are near the centerline of the upper glacier. Between the peak water flux of the lake drainage at 03:00 July 7 and the end of elevated water flux from the lake drainage at 12:00 July 7, the relationship between tremor power and water flux is much more uniform across the glacier (Figure 10b), with a median fitted exponent of 1.628 (interquartile range 0.515–2.403). For comparison, as in Section 2.4, the theoretically modeled exponent for changes in power driven by changes in hydraulic radius is 1.250, and the theoretically modeled exponent for filled channels with changes in power driven by changes in hydraulic pressure gradient is 4.667.

Flow speeds at the two GPS stations on Lemon Creek Glacier remained remarkably consistent over the measurement period, including during the period of seismometer deployment (see Figure 7 for full-season GPS speeds). From July 1 to August 13, the uppermost GPS receiver on the glacier had a mean horizontal speed of 0.047 m/day (standard deviation 0.019 m/day) and the GPS receiver on the middle of the glacier had a mean horizontal speed of 0.055 m/day (standard deviation 0.010 m/day). The only notable exception to these consistent speeds is a two-day speedup recorded on the upper GPS receiver on July 28-29, during a period of heavy precipitation, with speed peaking at 0.167 m/day (6.3 standard deviations above the mean). During the drainage of Lake Linda, the upper GPS receiver's speed is slightly lower than the mean, within one standard deviation, around and during the lake drainage event. The middle GPS receiver's speed is higher than normal during the lake drainage, reaching 0.080 m/day (2.5 standard deviations above the mean), but deviations of this magnitude occur at several other times during the deployment. Thus, although the elevated speed at the upper GPS receiver may be a response to the lake drainage, it is difficult to pick out the lake drainage solely from the velocity time series.

4. Discussion

Seismic tremor at frequencies between 1.5 and 25 Hz produced by glaciohydraulic sources is predicted by theory (Gimbert et al., 2014) and detected in other systems (Bartholomaus et al., 2015; Eibl et al., 2020; Lindner et al., 2020; Nanni et al., 2020; Vore et al., 2019). The temporal correlation between water flux through Lemon Creek Glacier and seismic power in these glaciohydraulic tremor frequencies is consistent with the aforementioned literature and leads us to believe that the tremor we report is of dominantly glaciohydraulic origin. The drainage of Lake Linda acts as a natural experiment to support a glaciohydraulic interpretation of the seismic signal, as the tremor amplitude positively correlates with the known water input from the lake directly into the subglacial system. The exception to this relationship is the period of rainfall before the lake drainage on July 3–5 (Figure 5c), when water flux varies much more strongly than tremor amplitude. Relative to the time period containing the drainage of Lake Linda, the weak correlation on July 3–5 is likely due to an overrepresentation in water flux at the stream gauge due to rapid water transport from the non-glacierized portion of the gauge's catchment (approximately equal to the surface area of the glacier). Non-glaciohydraulic explanations of observed seismic tremor, such as earthquake activity, icequake activity, meteorological activity, or human activity are not well supported. No small regional or large global earthquakes are listed in the USGS catalog that would affect ground motion in the frequency range of interest for more than a few seconds at a time, and such short-duration changes are removed as outliers by the median power spectral density process. Local icequakes, while significantly more frequent than earthquakes (small events every few minutes, recorded only at nearby stations), are still infrequent and short-duration enough to be similarly omitted from the median PSD due to the slow velocity of the glacier. See Figure 4 for an example of the median PSD process. In addition, icequakes are typically higher in frequency than the tremor we focus on in this study (Röösli et al., 2014). The tremor amplitude in this frequency range also does not correlate strongly with meteorological factors such as air temperature or wind activity during the lake drainage (Figure 11). Nearby anthropogenic sources of seismic noise, such as the Juneau Icefield Research Program camp's generator, Salmon Creek hydroelectric dam, and mechanical

activity in Juneau would theoretically be preserved through the median PSD computation as continuous signals, but we do not observe significant variation in power on the schedules expected from these activities in our frequency range of interest.
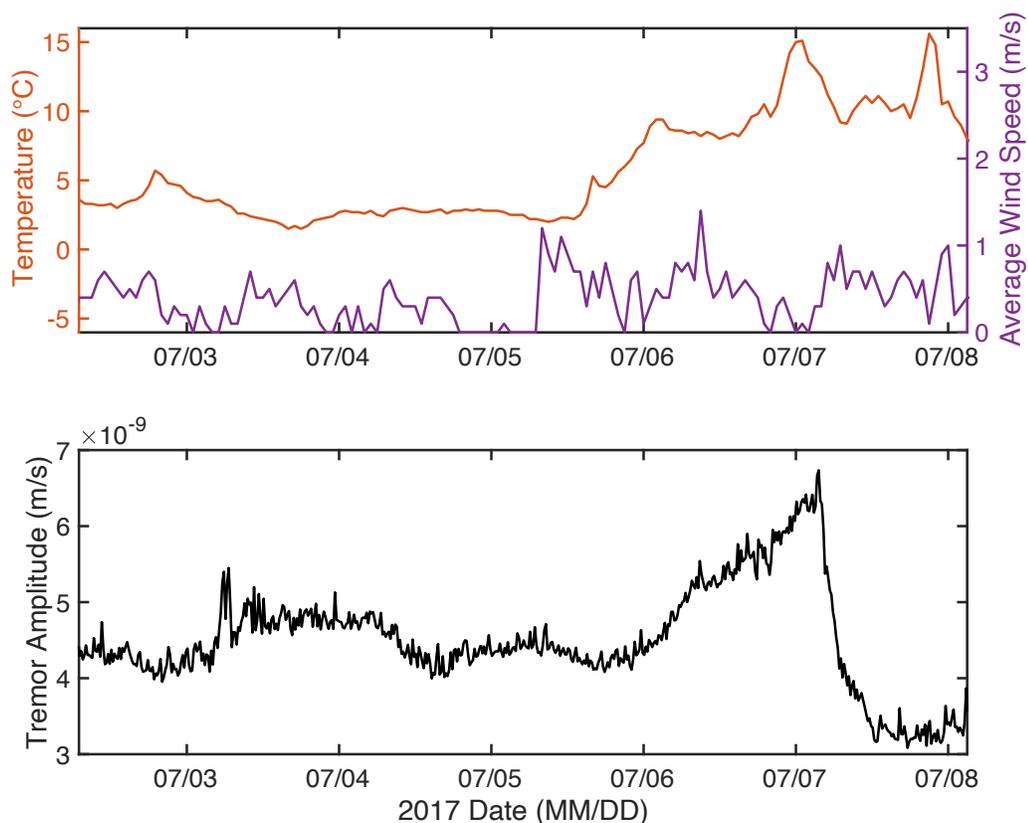
Figure 11. Temperature (upper orange) and average wind speed (upper purple) recorded near Lemon Creek Glacier with median seismic tremor amplitude (lower black) from the seismometer outlined in white in Figure 1 (same station shown in Figure 5) over the time period shown in Figure 5. Temperature was recorded at the Juneau Icefield Research Program Camp 17 on the western margin of the glacier. Wind speed was recorded at the Mt. Roberts Tramway, 7.5 km SSW of the glacier.

In addition to glaciohydraulic tremor generated from water turbulence, as described in Section 2.4, glaciohydraulic tremor can also be generated in subglacial hydrologic systems through bedload saltation of sediment particles (Gimbert et al., 2016; Tsai et al., 2012). We determine that sediment saltation is not likely a significant contributor to the tremor observed at Lemon Creek Glacier by comparing tremor power over time in different portions of the tremor spectrum. The frequency distribution of tremor generated by saltation tends to peak

at higher frequencies than tremor generated from water turbulence in the same system (Gimbert et al., 2014; Tsai et al., 2012). This difference creates changes in slope or hysteresis in power between frequency ranges due to changes in scaling between amplitude at different frequencies (Bakker et al., 2020) or due to depletion in sediment supply (Burtin et al., 2008; Goodling et al., 2018; Roth et al., 2014). We found a consistent relationship with no significant hysteresis over the course of the lake drainage event between seismic power in the 1.5–10 Hz range and seismic power in the 10–20 Hz range (see Figure 12). Although the frequency ranges of sediment-generated tremor and turbulence-generated tremor overlap and cannot be completely separated, this relationship between the tested frequency bands suggests that water turbulence is the dominant source of glaciohydraulic tremor in this system. Without clear significant contribution from sediment, we believe the model of tremor generation described in Section 2.4 is most appropriate.
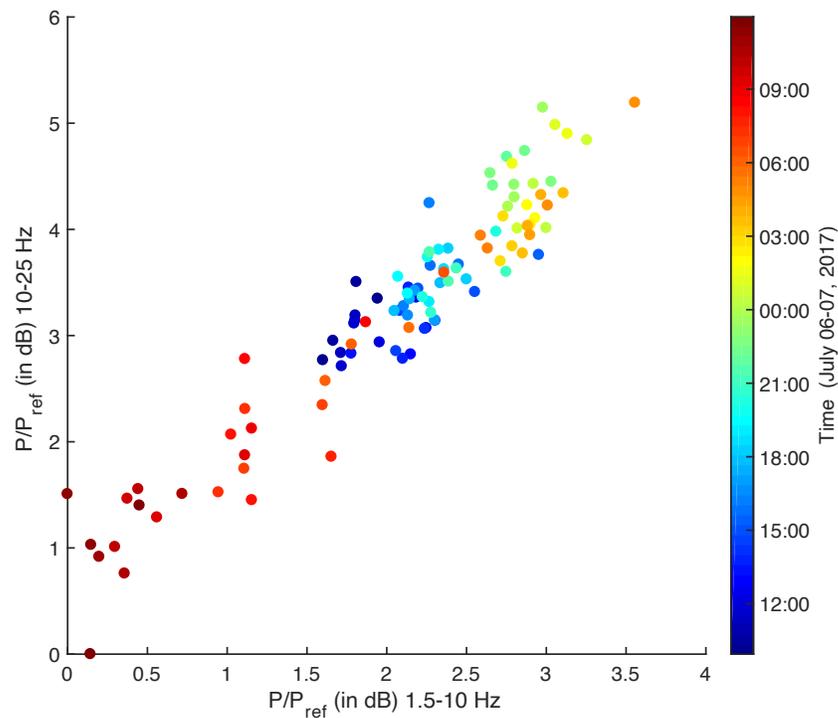
Figure 12. Comparison of seismic power levels in 1.5-10 Hz and 10-25 Hz frequency ranges over the course of the drainage of Lake Linda at one example seismometer in the array (same seismometer as in Figure 6c).

The changing power-law dependence of seismic tremor power on subglacial water flux at each station is consistent with different subglacial pressurization regimes, based on the theoretical relationships described in Section 2.4 from Gimbert et al., 2016. We observe significant variation in this power-law dependence over kilometer length scales, and during time intervals prior to and following peak lake drainage (Figure 10); thus, we interpret that our array of nodes and existing seismological theory allow us to map the spatiotemporal variation in subglacial pressurization at kilometer scales across Lemon Creek Glacier. During increasing discharge from the lake, the fitted exponents b for stations across the glacier reveal two distinct regions of subglacial hydrologic behavior (Figure 10). Stations on the lower portion of the glacier observe tremor power that relates to water flux with an exponent similar to that of a theoretical channel system whose changes in tremor are dominated by changes in hydraulic radius (e.g., water flow through unfilled channels at consistent, presumably atmospheric, pressures). On the upper portion of the glacier, however, stations record tremor power that relates to water flux with higher fitted exponents. Many stations' observations are similar to that of a theoretical channel system whose changes in tremor are dominated by changes in pressure gradient, indicating that the subglacial hydrologic system under only the upper portion of the glacier becomes pressurized in response to the rapid influx of water from the lake. This pressurization is presumably strongest within a distributed system more distal from a central conduit axis, in which increases in discharge result in increases in pressure. This interpretation is supported by the larger *b* values observed near the margins of the upper glacier. The distributed nature of the seismic source and the complex nature of subglacial hydrology mean that any given station is unlikely to contain a perfect record of the idealized end-member models presented in Section 2.4, but we find interpretation at the scales presented here to be reasonable.

For a short period around the time of peak water flux at some stations in the upper portion of the glacier, we observe relationships between tremor power and water flux that are not easily described by either end-member model presented in Section 2.4. For example, in Figure 6b between July 6 22:00 and July 7 02:00, discharge remains nearly constant or increases slightly, while power falls by 1–2 dB. Such behavior can be explained by the co-evolution

of both pressure gradient and hydraulic radius, specifically a simultaneous increase in hydraulic radius and decrease in pressure gradient. Indeed, most models of conduit evolution expect that conduit wall melt increases as a function of pressure gradient (Röethlisberger, 1972; Werder et al., 2013), thus the pattern shown in Figure 6b is expected from the compensation of increasing hydraulic radius maintaining near-steady discharge as the pressure gradient drops. Alternatively, the hydraulic radius could effectively grow through the removal of sediment that potentially obstructs water flow through otherwise efficient conduits. Similar patterns of increasing discharge with falling seismic power are seen in Figure 6b of Gimbert et al., 2016 and interpreted as depressurization.

After peak outflow from the lake has passed and water flux is in decline, stations across the entire surface of the glacier record tremor power that relates to water flux with an exponent near 5/4. These values are predicted for conduits in which changes in water discharge are accommodated by variations in hydraulic radius under a constant pressure gradient, but the different portions of the glacier reach these conditions differently. For the lower portion of the glacier, where the relationship between tremor power and discharge remains consistent for increasing and decreasing discharge (e.g., Figure 6c), subglacial conditions are likely unchanged over the course of the lake drainage. We expect water flow through unfilled channels at consistent, presumably atmospheric, pressures in this area. However, in the upper portion of the glacier, the relationship between tremor power and discharge shows hysteresis, and reflects a regime change in tremor production (e.g., Figure 6b). At these upper glacier sites, we observe higher power levels during the falling limb of the event (when slopes are around 5/4) than during the rising limb (when slopes are around 14/3). If the existing pressurized channels were to simply depressurize and carry remaining water as a partially-empty channel, the post-peak power levels would be lower than pre-peak. The counterintuitively higher post-peak power levels we observe could be expected if the channel's cross-sectional area became significantly smaller than during the rising limb of the event while maintaining a high pressure gradient (Gimbert et al., 2016). Such channel shrinkage with higher than atmospheric pressure can occur by creep closure, but even at the maximum ice thickness of the glacier (approximately 350 m, Veitch et al., 2021) channel

creep closure would take at least four hours from peak water flux (Anderson et al., 2004), and power is already observed as higher than rising-limb levels before this time. Another potential explanation for a change in channel geometry is through movement of sediment. Though we do not expect a large amount of continuously-mobile sediment due to the apparent lack of saltation-generated seismic tremor, some sediment at the beds of subglacial channels is nevertheless reasonable to anticipate. If the high water flux around the peak of the outflow is able to bring new sediment into a channel or redistribute sediment within a channel, that new geometry may be able to generate higher power than on the rising limb of the event as water level falls in the channel. Yet another factor that could drive higher power levels is a change in roughness of the channel walls, with smoother walls generating higher-power tremor through increased flow velocity (Gimbert et al., 2016; Roth et al., 2017). By this mechanism, the observed power levels could be explained by small-scale frictional melt or sediment motion around the peak water flux creating smoother channel walls. More than one of these factors could also contribute in combination to generate the observed tremor behavior on the upper portion of the glacier after pressurization.

The pressurization of at least some portion of Lemon Creek Glacier's subglacial channels during a lake drainage is expected. As water input from the lake rises rapidly, the water flux completely fills existing subglacial channels that earlier in the melt season had only carried smaller, less variable fluxes of rain and meltwater. Thus, lake drainage leads to pressurization and channel growth. As flux from the lake declines after peak lake drainage, the diminishing water ceases to fill now-enlarged channels and the system depressurizes. The geographic boundary between the upper glacier where pressurization is observed and the lower glacier where no pressurization is observed coincides with the glacier's slope break, over which the surface slope more than doubles from 3° to 7° and glacier thickness decreases from 300 m to less than 200 m (Pelto et al., 2013; Thiel et al., 1957; Veitch et al., 2021). A lack of subglacial pressurization below this slope break may occur because of changes in the character of the glacier that lead to increased efficiency of drainage. First, drainage efficiency in the lower portion of the glacier may be high due to increased channel size. Channels below the slope break may be too large to fill completely during lake drainage, because channels

grow larger near glacier termini due to the confluence of tributary channels. Those large channels, created during periods of exceptionally high subglacial water flux (e.g., heavy rain or high melt), can persist over long time scales under thinner ice due to the reduced pressure of closure (Röthlisberger, 1972). Second, drainage efficiency below the slope break may also be high due to an increase in the frequency and extent of basal and englacial crevassing from the thinner and faster-flowing ice (Fountain et al., 2005). Third, efficient drainage below the slope break could also be fostered by rapid growth of channels. The growth rate of channel cross-sectional area over time correlates with the hydraulic potential gradient, which increases with bed slope (Werder et al., 2013). Lemon Creek Glacier has low and even reverse bed slopes just above the slope break, but is likely to have bed slopes more similar to the surface slope below the slope break, where ice is thin (Pelto et al., 2013; Thiel et al., 1957; Veitch et al., 2021). This steeper gradient potentially leads to more rapid channel expansion below the slope break that could allow the system to drain efficiently without pressurization.

Observational and modeling studies commonly indicate that subglacial hydrologic pressurization necessarily triggers an increase in glacier flow velocity (Bartholomew et al., 2010; Gagliardini et al., 2007; Iken & Bindschadler, 1986; Iken & Truffer, 1997; Schoof, 2010), but no remarkable speedup is observed on Lemon Creek Glacier during the drainage of Lake Linda. The speed recorded at the middle GPS receiver during the lake drainage is higher than average (2.5 standard deviations above the mean), but deviations of similar magnitude are recorded at several other times during the deployment, and those deviations are dwarfed by a July 28-29 speedup (6.3 standard deviations above the mean) at the upper GPS receiver associated with a heavy, 6 cm, precipitation event over the entire glacier (see Figure 7 for full-season GPS speeds and rainfall). The sparse GPS coverage in this deployment (only two receivers, both above the slope break) and the low temporal resolution (15 s data collection with processing revealing variability at an approximate minimum scale of 6 hours) does limit the level of detail with which we can describe glacier motion in this study. Yet, since both receivers are located in the portion of the glacier where pressurization is indicated seismically and variability is observed on scales smaller than the duration of the

lake drainage's rise in water flux, we feel reasonably confident in using their recorded speeds to characterize whether or not a visible speedup occurred in conjunction with pressurization.

A lack of major velocity change associated with the lake drainage could be used to suggest that pressurization does not occur and our explanation of glaciohydraulic tremor generation is incomplete in describing the observed seismic signal. However, we argue that pressurization without a significant speedup is entirely reasonable at our field site. First, the drainage of Lake Linda provides only a modest additional flux to the glacier (equivalent to 6 cm of water averaged over the glacier area, over three days). Such a flux is comparable to many of the rain events that typically occur at our Southeast Alaska field site (see Figure 7). Previous modeling work suggests that outburst floods have little impact on glacier flow when the flood discharge is small compared to the background water input to the distal, distributed system (Kingslake & Ng, 2013). Additional explanations emerge based again on geometrical reasoning. As discussed earlier, the hydraulic potential gradient is higher below the slope break due to the increased bed and surface slopes. This high potential gradient makes the subglacial drainage system more likely to flow in a channelized, low pressure configuration (Werder et al., 2013), increasing the basal friction in the lower portion of the glacier (Schoof, 2005). In this lower region, basal friction remains high throughout the lake drainage because pressurization is only observed in the seismic data in the upper portion of the glacier. Because of its high basal friction and lack of pressurization, we argue that the portion of glacier below the slope break could remain at a stable flow velocity despite the lake drainage. The upper portion of the glacier may experience basal conditions conducive to a velocity increase due to pressurization from the lake drainage, but buttressing from the more stable lower portion could prevent a significant speedup of the glacier as a result of strong longitudinal coupling to the ice below the slope break (Jansson, 1997). Though in many cases the pressurization-velocity assumption is reliable, this study suggests that whether subglacial pressurization necessarily produces a significant velocity increase is also dependent on more global controls, such as glacier geometry.

5. Conclusions

Here we demonstrate the utility of seismic data in observing the local subglacial pressurization state of a glacier system by using a hydraulic transient event as a natural experiment. By observing the change in seismic tremor power with respect to subglacial water flux, we observe that the increase in water flux from the drainage of Lake Linda appears to pressurize the subglacial hydrologic system in only the upper portion of Lemon Creek Glacier, while the lower portion remains unpressurized throughout the lake drainage event. Thus, our approach provides mapping of the pressurization state at hourly temporal resolution and kilometer-scale spatial resolution through several-hundred-meter thick ice. The distribution of pressurization we observe coincides with a change in the geometry of the glacier, as the division between the two portions occurs at a slope break below which the glacier's geometry is less conducive to pressurization.

By utilizing seismometers for the bulk of our observations, this study provides insight into a subglacial pressurization event that did not lead to a significant velocity change at two GPS receivers above where the pressurization occurred. As pressurization changes are often assumed to result necessarily in major velocity changes, traditional GPS studies would likely have missed this event entirely. Borehole observations could have revealed pressurization in an event like this if the boreholes intersected the subglacial drainage channels, but a seismic array offers similar insights at lower cost and better spatial coverage. Retrieving information about subglacial conditions through seismic data, as in this study, can fill in observational gaps of other glaciological methods, improving our understanding of the dynamic nature of glacier systems.

Data Availability

Seismic and GPS data used in this manuscript are available at
http://dx.doi.org/10.22002/D1.2078.

Weather data are available under the Camp 17 station at http://denali.micro-specialties.com/cgi-bin/uaseaelpDataQuery.cgi.

Discharge data for Lemon Creek are available at
https://waterdata.usgs.gov/ak/nwis/inventory/?site_ no=15052000.

Data processing MATLAB codes are available at http://dx.doi.org/10.22002/D1.9200.

References

Anderson, R. S., Anderson, S. P., MacGregor, K. R., Waddington, E. D., O'Neel, S.,
    Riihimaki, C. A., & Loso, M. G. (2004). Strong feedbacks between hydrology and
    sliding of a small alpine glacier. Journal of Geophysical Research, 109(F3).
    https://doi.org/10.1029/2004JF000120

Aso, N., Tsai, V. C., Schoof, C., Flowers, G. E., Whiteford, A., & Rada, C. (2017).
    Seismologically observed spatiotemporal drainage activity at moulins. Journal of
    Geophysical Research: Solid Earth, 122(11), 9095–9108.
    https://doi.org/10.1002/2017JB014578

Bakker, M., Gimbert, F., Geay, T., Misset, C., Zanker, S., & Recking, A. (2020). Field
    application and validation of a seismic bedload transport model. Journal of Geophysical
    Research: Earth Surface, 125(5), e2019JF005416.
    https://doi.org/10.1029/2019JF005416

Bartholomaus, T. C., Amundson, J. M., Walter, J. I., O'Neel, S., West, M. E., & Larsen, C. F. (2015). Subglacial discharge at tidewater glaciers revealed by seismic tremor. Geophysical Research Letters, 42, 6391–6398. https://doi.org/10.1002/2015GL064590

Bartholomaus, T. C., Anderson, R. S., & Anderson, S. P. (2011). Growth and collapse of the distributed subglacial hydrologic system of Kennicott Glacier, Alaska, USA, and its effects on basal motion. Journal of Glaciology, 57(206), 985–1002. https://doi.org/10.3189/002214311798843269

Bartholomew, I., Nienow, P., Mair, D., Hubbard, A., King, M. A., & Sole, A. (2010). Seasonal evolution of subglacial drainage and acceleration in a Greenland outlet glacier. Nature Geoscience, 3(6), 408–411. https://doi.org/10.1038/ngeo863

Burtin, A., Bollinger, L., Vergne, J., Cattin, R., & Nábělek, J. L. (2008). Spectral analysis of seismic noise induced by rivers: A new tool to monitor spatiotemporal changes in stream hydrodynamics. Journal of Geophysical Research, 113, B05301. https://doi.org/10.1029/2007JB005034

Burtin, A., Cattin, R., Bollinger, L., Vergne, J., Steer, P., Robert, A., et al. (2011). Towards the hydrologic and bed load monitoring from high-frequency seismic noise in a braided river: The "torrent de St Pierre", French Alps. Journal of hydrology, 408(1–2), 43–53. https://doi. org/10.1016/j.jhydrol.2011.07.014

Chen, G. (1998). GPS kinematic positioning for the airborne laser altimetry at Long Valley, California, PhD thesis. Massachusetts Institute of Technology.

Eibl, E. P., Bean, C. J., Einarsson, B., Pàlsson, F., & Vogfjörd, K. S. (2020). Seismic ground vibrations give advanced early-warning of subglacial floods. Nature Communications, 11(1), 1–11. https://doi.org/10.1038/s41467-020-15744-5

Fountain, A. G., Jacobel, R. W., Schlichting, R., & Jansson, P. (2005). Fractures as the main pathways of water flow in temperate glaciers. Nature, 433(7026), 618–621. https://doi.org/10.1038/nature03296

Gagliardini, O., Cohen, D., Råback, P., & Zwinger, T. (2007). Finite-element modeling of subglacial cavities and related friction law. Journal of Geophysical Research, 112(F2). https://doi.org/10.1029/2006JF000576

Gimbert, F., Tsai, V. C., Amundson, J. M., Bartholomaus, T. C., & Walter, J. I. (2016). Subseasonal changes observed in subglacial channel pressure, size, and sediment transport. Geophysical Research Letters, 43, 3786–3794. https://doi.org/10.1002/2016GL068337

Gimbert, F., Tsai, V. C., & Lamb, M. P. (2014). A physical model for seismic noise generation by turbulent flow in rivers. Journal of Geophysical Research: Earth Surface, 119, 2209–2238. https://doi.org/10.1002/2014JF003201

Goodling, P. J., Lekic, V., & Prestegaard, K. (2018). Seismic signature of turbulence during the 2017 Oroville Dam spillway erosion crisis. Earth Surface Dynamics, 6(2), 351–367. https://doi.org/10.5194/esurf-6-351-2018

Gräff, D., Walter, F., & Lipovsky, B. P. (2019). Crack wave resonances within the basal water layer. Annals of Glaciology, 60(79), 158–166. https://doi.org/10.1017/aog.2019.8

Hock, R. (2003). Temperature index melt modelling in mountain areas. Journal of Hydrology, 282(1–4), 104–115. https://doi.org/10.1016/ S0022-1694(03)00257-9

Hubbard, B. P., Sharp, M. J., Willis, I. C., Nielsen, M., & Smart, C. C. (1995). Borehole water-level variations and the structure of the subglacial hydrological system of Haut Glacier d'Arolla, Valais, Switzerland. Journal of Glaciology, 41(139), 572–583. https://doi.org/10.3189/ S0022143000034894

Iken, A., & Bindschadler, R. A. (1986). Combined measurements of subglacial water pressure and surface velocity of Findelengletscher, Switzerland: Conclusions about drainage system and sliding mechanism. Journal of Glaciology, 32(110), 101–119. https://doi.org/10.3189/ S0022143000006936

Iken, A., & Truffer, M. (1997). The relationship between subglacial water pressure and velocity of Findelengletscher, Switzerland, during its advance and retreat. Journal of Glaciology, 43(144), 328–338. https://doi.org/10.3189/S0022143000003282

Jansson, P. (1997). Longitudinal coupling in ice flow across a subglacial ridge. Annals of Glaciology, 24, 169–174. https://doi.org/10.3189/ S026030550001212X

Kingslake, J., & Ng, F. (2013). Modelling the coupling of flood discharge with glacier flow during jökulhlaups. Annals of Glaciology, 54(63), 25–31. https://doi.org/10.3189/2013AoG63A331

Larose, E., Carrière, S., Voisin, C., Bottelin, P., Baillet, L., Guéguen, P., et al. (2015). Environmental seismology: What can we learn on earth surface processes with ambient noise? Journal of Applied Geophysics, 116, 62–74. https://doi.org/10.1016/j.jappgeo.2015.02.001

Lindner, F., Walter, F., Laske, G., & Gimbert, F. (2020). Glaciohydraulic seismic tremors on an Alpine glacier. The Cryosphere, 14(1), 287–308. https://doi.org/10.5194/tc-14-287-2020

Lydersen, C., Assmy, P., Falk-Petersen, S., Kohler, J., Kovacs, K. M., Reigstad, M., et al. (2014). The importance of tidewater glaciers for marine mammals and seabirds in Svalbard, Norway. Journal of Marine Systems, 129, 452–471. https://doi.org/10.1016/j.jmarsys.2013.09.006

McNeil, C. (2016). Surface mass balance reanalysis of Taku and Lemon Creek glaciers, Alaska: 1946-2015Doctoral dissertation. Alaska Pacific University.

Moore, J. C., Pälli, A., Ludwig, F., Blatter, H., Jania, J., Gadek, B., et al. (1999). High-resolution hydrothermal structure of Hansbreen, Spitsbergen, mapped by ground-penetrating radar. Journal of Glaciology, 45(151), 524–532. https://doi.org/10.3189/S0022143000001386

Motyka, R. J., Truffer, M., Kuriger, E. M., & Bucki, A. K. (2006). Rapid erosion of soft sediments by tidewater glacier advance: Taku Glacier, Alaska, USA. Geophysical Research Letters, 33(24). https://doi.org/10.1029/2006GL028467

Nanni, U., Gimbert, F., Roux, P., & Lecointre, A. (2021). Observing the subglacial hydrology network and its dynamics with a dense seismic array. Proceedings of the National Academy of Sciences, 118(28), e2023757118. https://doi.org/10.1073/pnas.2023757118

Nanni, U., Gimbert, F., Vincent, C., Gräff, D., Walter, F., Piard, L., & Moreau, L. (2020). Quantification of seasonal and diurnal dynamics of subglacial channels using seismic observations on an Alpine glacier. The Cryosphere, 14(5), 1475–1496. https://doi.org/10.5194/ tc-14-1475-2020

Pelto, M., Kavanaugh, J., & McNeil, C. (2013). Juneau icefield mass balance program 1946–2011. Earth System Science Data, 5(2), 319–330. https://doi.org/10.5194/essd-5-319-2013

Porter, C., Morin, P., Howat, I., Noh, M.-J., Bates, B., Peterman, K., et al. (2018). ArcticDEM. Harvard dataverse, V1. https://doi.org/10.7910/ DVN/OHHUKH

Post, A., & Mayo, L. R. (1971). Glacier dammed lakes and outburst floods in Alaska (p. 10). US Geological Survey.

Press, W. H., Flannery, B. P., Teukolsky, S. A., & Vetterling, W. T. (1988). Numerical recipes in C: The art of scientific computing (1st ed.), Cambridge Univ. Press.

Röösli, C., Walter, F., Ampuero, J. P., & Kissling, E. (2016). Seismic moulin tremor. Journal of Geophysical Research: Solid Earth, 121(8), 5838–5858. https://doi.org/10.1002/2015JB012786

Röösli, C., Walter, F., Husen, S., Andrews, L. C., Lüthi, M. P., Catania, G. A., & Kissling, E. (2014). Sustained seismic tremors and icequakes detected in the ablation zone of the Greenland ice sheet. Journal of Glaciology, 60(221), 563–575. https://doi.org/10.3189/2014JoG13J210

Roth, D. L., Finnegan, N. J., Brodsky, E. E., Cook, K. L., Stark, C. P., & Wang, H. W. (2014). Migration of a coarse fluvial sediment pulse detected by hysteresis in bedload generated seismic waves. Earth and Planetary Science Letters, 404, 144–153. https://doi.org/10.1016/j.epsl.2014.07.019

Roth, D. L., Finnegan, N. J., Brodsky, E. E., Rickenmann, D., Turowski, J. M., Badoux, A., & Gimbert, F. (2017). Bed load transport and boundary roughness changes as competing causes of hysteresis in the relationship between river discharge and seismic amplitude recorded near a steep mountain stream. Journal of Geophysical Research: Earth Surface, 122, 1182–1200. https://doi.org/10.1002/2016JF004062

Röthlisberger, H. (1972). Water pressure in intra-and subglacial channels. Journal of Glaciology, 11(62), 177–203. https://doi.org/10.3189/ S0022143000022188

Schmandt, B., Aster, R. C., Scherler, D., Tsai, V. C., & Karlstrom, K. (2013). Multiple fluvial processes detected by riverside seismic and infra- sound monitoring of a controlled flood in the Grand Canyon. Geophysical Research Letters, 40, 4858–4863. https://doi.org/10.1002/grl.50953

Schoof, C. (2005). The effect of cavitation on glacier sliding. Proceedings of the Royal Society A: Mathematical, Physical & Engineering Sciences, 461, 609–627. https://doi.org/10.1098/rspa.2004.1350

Schoof, C. (2010). Ice-sheet acceleration driven by melt supply variability. Nature, 468(7325), 803–806. https://doi.org/10.1038/nature09618 Slater, D. A., Nienow, P. W., Cowton, T. R., Goldberg, D. N., & Sole, A. J. (2015). Effect of near-terminus subglacial hydrology on tidewater glacier submarine melt rates. Geophysical Research Letters, 42(8), 2861–2868. https://doi.org/10.1002/2014GL062494

Thiel, E., LaChapelle, E., & Behrendt, J. (1957). The thickness of Lemon Creek Glacier, Alaska, as determined by gravity measurements. Eos, Transactions of the American Geophysical Union, 38(5), 754–749. https://doi.org/10.1029/tr038i005p00745

Thornton, T. F. (2012). Haa Léelk'w has Aaní Saax': Our grandparents' names on the land. Sealaska Heritage Institute and University of Washington Press.

Tsai, V. C., Minchew, B., Lamb, M. P., & Ampuero, J.-P. (2012). A physical model for seismic noise generation from sediment transport in rivers. Geophysical Research Letters, 39, a–n, L02404. https://doi.org/10.1029/2011GL050255

U.S. Geological Survey. (2017). National water information system. https://doi.org/10.5066/F7P55KJN

Veitch, S., Karplus, M., Kaip, G., Gonzalez, L., Amundson, J., & Bartholomaus, T. (2021). Ice thickness estimates of Lemon Creek Glacier, Alaska, from active-source seismic imaging. Journal of Glaciology, 1–9, 824–832. https://doi.org/10.1017/jog.2021.32

Vore, M. E., Bartholomaus, T. C., Winberry, J. P., Walter, J. I., & Amundson, J. M. (2019). Seismic tremor reveals spatial Organization and temporal changes of subglacial water system. Journal of Geophysical Research: Earth Surface, 124(2), 427–446. https://doi.org/10.1029/2018jf004819

Werder, M. A., Hewitt, I. J., Schoof, C. G., & Flowers, G. E. (2013). Modeling channelized and distributed subglacial drainage in two dimensions. Journal of Geophysical Research: Earth Surface, 118(4), 2140–2158. https://doi.org/10.1002/jgrf.20146

Winberry, J. P., Anandakrishnan, S., & Alley, R. B. (2009). Seismic observations of transient subglacial water-flow beneath MacAyeal Ice Stream, West Antarctica. Geophysical Research Letters, 36, L11501. https://doi.org/10.1029/2009GL037730

Chapter 3

SWARM-LIKE BEHAVIOR OF ICEQUAKES ASSOCIATED WITH SURFACE CREVASSING ACTIVITY ON A MOUNTAIN GLACIER

Abstract

Understanding the behavior of glacier surface crevassing is an important yet undervalued piece of our insight toward overall glacier dynamics. One of the best tools to observe surface crevassing processes in action is seismology, as crevasse propagation can produce icequakes with mode I crack opening sources. In this study, we record and locate 7,731 surface icequakes during a 10-day seismic array deployment on Lemon Creek Glacier, an isolated mountain glacier in southeast Alaska. Based on the distribution of Rayleigh wave amplitudes of individual icequakes and the orientation of linear clusters of icequakes, we attribute these events to surface crevasse opening. We observe a variety of spatiotemporal patterns within icequake clusters, indicating crevasse widening and deepening, reactivation on the same crevasse with hours or days of quiescence between, and related activity on closely-spaced parallel crevasses. The magnitude distribution of these icequakes has a b-value significantly higher than that of tectonic earthquakes, suggesting that cryoseismicity associated with surface crevassing activity behaves much more like earthquake swarms than like classic mainshock-aftershock sequences.

1. Introduction

Cryoseismology is a promising yet still underutilized addition to glaciological observation that can build our knowledge of general glacier dynamics and the behavior of particular glaciers. A wide variety of physical processes in glaciers produce seismic signals. Basal

stick-slip (Helmstetter et al. 2015a), surface crevassing (Roux et al. 2010; Mikesell et al. 2012), basal crevassing (Gräff et al. 2019), calving (Qamar 1988; Bartholomaus et al. 2012), subglacial water flow (Winberry et al. 2009; Bartholomaus et al. 2015), moulin activity (Röösli et al. 2014, 2016; Lindner et al. 2020), and more produce seismic signals that can be observed with seismometers deployed on and around glaciers, and this seismic data can be used to understand and observe those processes. Cryoseismology has many advantages as a primary or complementary observational tool for glacier studies: data recording can be continuous in time, many different types of glacier processes are seismic sources, close proximity to seismic sources is not necessarily required, source and structure information can be inferred, deployment and maintenance of stations can be relatively easy, and more.

Though the surface crevassing layer only comprises the upper 20-30 m of a glacier (Vaughan 1993), understanding the behavior of surface crevasses remains a valuable piece of the glacier dynamics puzzle. Surface crevassing reveals ice flow patterns by forming in alignment with the local stress field (Vaughan 1993), affects the thermal development of glaciers (Jarvis & Clark 1964; Pfeffer & Bretherton 1987), and provides pathways for rain and meltwater to enter the englacial and subglacial hydrologic systems (Irvine-Flynn et al. 2011). Understanding and monitoring surface crevassing activity is also vital for properly interpreting short-term changes in velocity recorded by on-ice GPS receivers, because crevasse opening and closing can cause local surface motion that is not representative of overall ice flow. Ice flow velocity changes on the order of hours to days can be associated with subglacial hydrologic activity, surge initiation, calving events, and/or tides (Willis 1995), and accurate observation of these phenomena benefits from deconvolving GPS readings with any potential shallow motion from local surface crevassing. Prior studies of shallow cryoseismicity have observed icequakes that can be associated with surface crevassing activity (Roux et al. 2010; Mikesell et al. 2012) and change in rate after sudden changes in glacier surface conditions like large supraglacial lake drainages (Roux et al. 2010), but further research is needed to characterize surface crevassing icequakes under a variety of conditions in order to determine how cryoseismicity can most effectively be integrated into studies of overall glacier dynamics.

In this study, we observe and characterize surface icequake activity at Lemon Creek Glacier using an array of on-ice seismometers. We find that icequakes consistent with mode I cracking sources occur in linear clusters whose strikes are in agreement with the expected surface crevassing orientations for their locations on the glacier. The spatiotemporal patterns observed in the icequakes indicate both widening and deepening of individual crevasses, as well as activity migrating through multiple parallel crevasses. Most notably, we observe that the magnitude distribution of these icequakes has a higher b-value than is characteristic of tectonic earthquakes. This high b-value is comparable to volcanic earthquake swarms, earthquake swarms related to fluid infiltration, and hydrofracture-driven icequakes.

2. Field Site and Instrumentation

In this study, we collect seismic data in summer 2017 at Lemon Creek Glacier, an isolated mountain glacier at the southern tip of the Juneau Icefield, Alaska, on Tlingit lands (Thornton 2012), shown in Figure 1. This glacier is approximately 6.5 km long, 1.5 km wide, flowing northward at 20-40 m/yr with a 3-7° surface slope (Thiel et al. 1957; Pelto et al. 2013; Veitch et al. 2021). The glacier is approximately 350 m thick at its thickest point (located at approximately the same area as the southern GPS receiver in Figure 1) and has a shallow reverse bed slope over the next ~600 m downglacier, as determined by an active seismic reflection survey in Veitch et al. 2021. The glacier is situated on local gabbro and diorite bedrock (Thiel et al. 1957). Lemon Creek Glacier hosts Lake Linda, an ice-marginal supraglacial lake at the head margin, which drained 570,000 m^3 of melt and rain water through the glacier over the course of approximately 36 hours starting late on 05 July 2017 (Labedz et al. 2022).
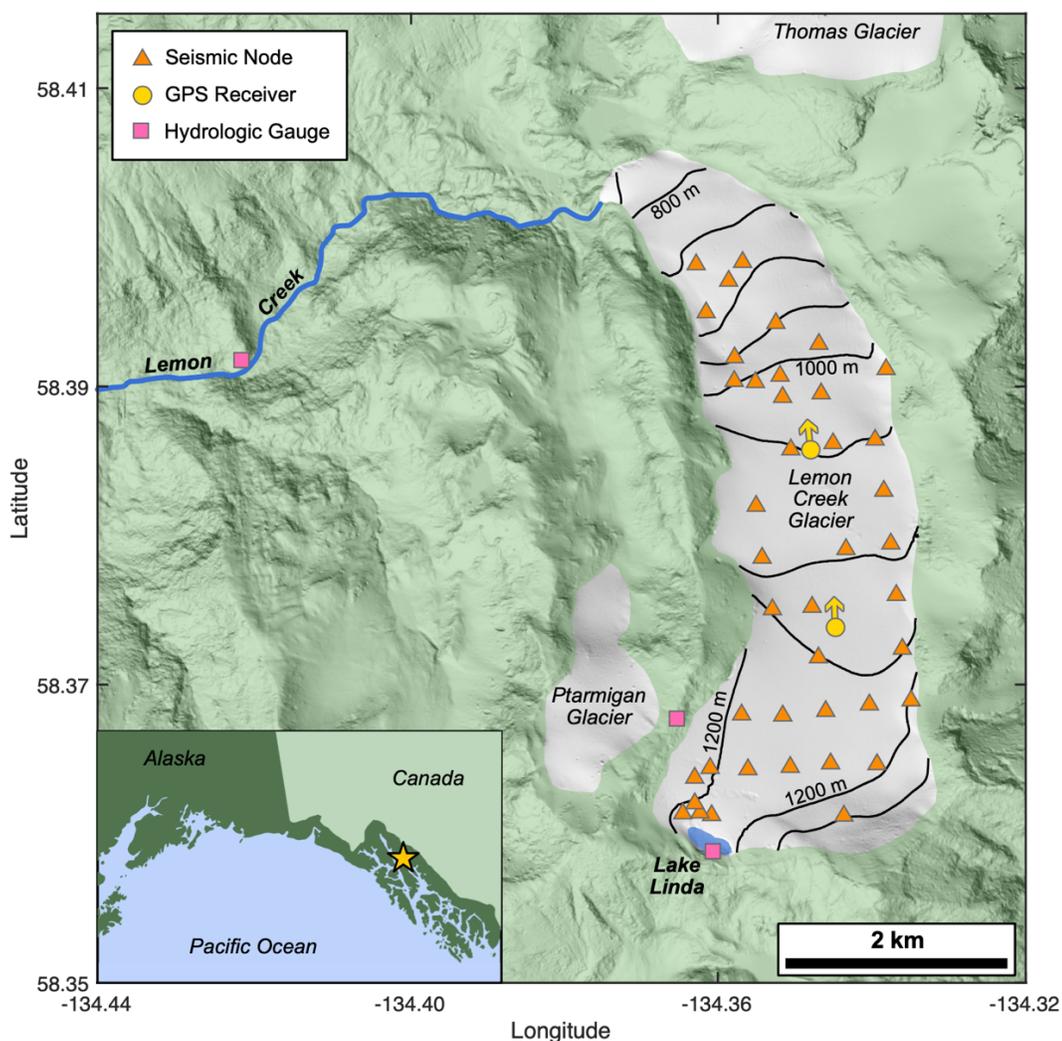
Figure 1. Map of the Lemon Creek Glacier area, showing glacier surfaces (white), Lake Linda and Lemon Creek (blue), geophysical equipment deployed in 2017 (seismometers - orange triangles, GPS receivers - yellow circles, hydrologic gauges - pink squares), and topography of the glacier (black lines, 50 m intervals, 750-1250 m elevation). Hillshade from Arctic DEM by Polar Geospatial Center (Porter et al. 2018). Inset: location of Lemon Creek Glacier in Southeast Alaska.

We use continuous data recording from an array of 42 single-component FairfieldNodal (now Magseis Fairfield) ZLand nodal seismometers, buried in surface snow across the surface of Lemon Creek Glacier from 28 June to 13 July 2017. We originally deployed 55 nodes sampling at 250 Hz in an array spaced 300-400 m apart, however some gaps in array coverage occur in the final data due to malfunctioned sensors. We also deployed two Trimble NetRS GPS receivers atop poles bored approximately 10 m into the ice. Data points every

15 s from these receivers were processed against the UNAVCO Mendenhall AB50 base station (on bedrock 11 km WNW of Lemon Creek Glacier) using the GAMIT-GLOBK processing software track (Chen 1998) and smoothed with a 24-hour running mean. In addition, we observed the hydrology and meteorology of the Lemon Creek Glacier system using several monitoring gauges. A USGS streamflow gauge (USGS 2017) records the water flux of Lemon Creek, which carries the outflow from Lemon Creek Glacier and the nearby Ptarmigan and Thomas Glaciers, each of which is an order of magnitude smaller than Lemon Creek Glacier in surface area (McNeil 2016). To observe the drainage of Lake Linda, we deployed a lake stage gauge in Lake Linda, which recorded water level until it malfunctioned on 05 July, after which we observed the lake stage using time-stamped photographs correlated to a digital elevation model of the empty lake. We monitored rainfall and air temperature on the upper west margin of the glacier, at a Juneau Icefield Research Program camp. The locations of all instrumentation are shown in Figure 1.

3. Surface Icequake Detection, Location, and Characterization

We search for potential seismic wave phase arrivals in the continuously-recorded velocity data from each station using a short-term average to long-term average ratio method (Allen 1978) with STA and LTA window lengths of 0.05 s and 1 s, respectively, and a threshold ratio of 3.5. After each trigger, we impose a 0.05 s reset time before another trigger is allowed to occur if the threshold ratio is reached, in order to prevent immediately-repeating triggers.

To group these individual STA/LTA triggers into potential icequake events, we search for triggers on at least five different stations within a 1 s window. Although two-dimensional location of surface events can be performed with triggers on as few as three stations, we found that using five at minimum reduced the prevalence of non-physical overfitting of spurious triggers in our location process, and we determined that the benefit of higher identification and location quality outweighed the detriment of missing smaller icequakes.

To prevent large events from potentially registering as multiple events, we also impose a 0.5 s delay after each event window before the next trigger can occur.

To locate surface icequakes among the grouped triggers that are potential events, and distinguish them from grouped potential events that contain multiple icequakes or triggers unrelated to surface icequakes, we perform a grid search to locate events in space and time. For this grid search, we assume that the surface of the glacier is a flat plane. Though not perfectly accurate to the form of the glacier (e.g. surface slope increases from 3° to 7° over the along-flow extent of the array), we find it reasonable for these purposes, as most icequakes are detectable only locally, where deviation from a flat plane is small enough that adequate locations can still be determined. For a seismic event at surface location (x, y) and time t, on a flat medium with homogeneous surface wave velocity V, the arrival time d_i of a surface wave at an instrument located at (x_i, y_i) is

$$d_i \; = \; t \; + \; \frac{1}{V} \; \sqrt{(x_i - x)^2 + (y_i - y)^2} \; . \qquad (1)$$

For each grouped potential event, we perform a grid search for variables x, y, t, and V. For each combination of x, y, t, and V, we calculate the theoretical arrival time of a surface wave at each station. We consider the best-fit location to be the combination of x, y, t, and V that minimizes the mean difference between the theoretical arrival time and actual trigger time for each station where a trigger was recorded.

We set the two-dimensional spatial grid for event location (x, y) to be an 800 m by 800 m square centered on the location of the station that recorded the first trigger, with 120 grid points along each axis for a spatial resolution of 6.67 m. We set 50 temporal grid points for t, within the 0.8 seconds before the first trigger for a temporal resolution of 0.016 s. While some studies choose to fix their velocity for icequake detection, we allow velocity to vary within a range around the Rayleigh wave velocity for a snow/firn glacier surface observed in previous studies (Roux et al. 2010; Mikesell et al. 2012), because real features of our system (e.g. variability in snow/firn layer thickness) create variability in velocity. We set 20 velocity grid points between 1000 m/s and 1600 m/s for a velocity resolution of 30 m/s.

For some grouped potential events, we observe multiple triggers on a single station within the grouping time window. More than one trigger can occur when multiple wave phases from the same event are recorded with enough separation in time to independently meet the STA/LTA conditions, when wave phases from multiple events are recorded, or when spurious triggers occur close in time to a real wave phase. To account for these multiply-triggered events, we repeat the grid search for different combinations of arrivals from each station, keeping the combination with the lowest mean error for its best fit as the overall best fit.

This procedure of detecting triggers, grouping potential events, and locating potential events does not always result in a well-located surface icequake. The grouped triggers do not necessarily constitute only the wave arrival triggers from one single surface icequake; they can contain wave arrivals from deep icequakes, wave arrivals from non-icequake phenomena, wave arrivals from multiple events that occur close in time, spurious triggers, or a combination of sources. In order to determine which potential events are most likely to be well-located surface icequakes, we filter the results of the grid search in two ways. First, we set an upper threshold of 0.02 s for the average error value of the best-fit location, slightly larger than the temporal resolution of the grid search. Second, we discard events whose best-fit locations occurred on the outside edge of the spatial grid around the first-triggered station, as we observed that a large portion of events that the grid search located there appeared to be overfitted, even if the result happened to have low error. This strategy for quality filtering almost certainly excludes some real surface icequakes and includes some non-surface-icequake events, but we find these errors to be infrequent enough to provide a generally accurate picture of surface icequake activity when event quantity is too large to feasibly sort by hand.

In order to compare the sizes of detected surface icequakes, we derive a relative surface wave magnitude scale based on the general form of a relationship for magnitude M_S (e.g. Lay and Wallace, 1995, equation 9.30)

$$M_s \ = \ \log_{10}\left(A/_T\right) + f(R) \qquad (2)$$

where A is the maximum ground displacement amplitude of a Rayleigh wave with period T recorded at a station at distance R away from the event epicenter, and f is a correction factor based on the distance that accounts for geometric spreading and attenuation. To simplify the calculation of magnitudes, we standardize the value of T to an average value T_{ave} found by hand-picking the Rayleigh periods of waveforms of arrivals from 50 randomly-selected events. We found a mean period of 0.055 s to use for T_{ave}, with standard deviation of 0.014 s. Using this value across all measurements is mathematically equivalent to adding a constant C to the magnitude instead of dividing A by this constant within the logarithm. To further simplify calculations, we replace the distance correction factor f by the normalization of the maximum displacement amplitude observations to a standard distance. We perform this normalization by calculating for each event the ratios of maximum displacement amplitudes and epicentral distances between each station recording that event and the nearest station to the epicenter (Figure 2). A least-squares fit of these data provides the normalization factor required to calculate the adjusted maximum amplitude values A_{norm} if all stations were at the same distance. Performing the normalization based on real data values corrects for both geometric spreading and attenuation simultaneously. Therefore, our magnitude calculations are performed as

$$M_s = \log_{10}(A_{norm}) + C . \qquad (3)$$
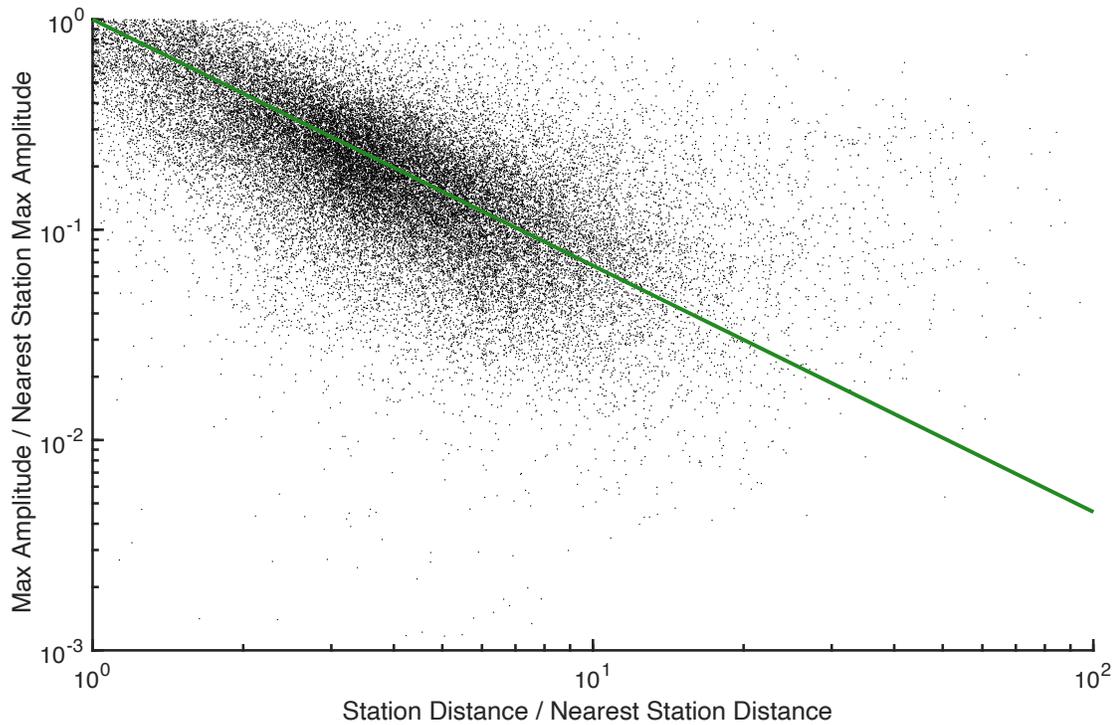
Figure 2. Distance and maximum amplitude ratios for pairs of stations recording the same surface icequake event (black dots) and best-fit relationship used to normalize maximum amplitude values to a standard distance (green line).

For each event, we calculate MS for the amplitude recorded at each station and use the median value among the stations to describe the event as a whole. These magnitude values are consistent internally among the entire data set, but not related in absolute value to other magnitudes such as earthquake moment magnitude. For ease of use, we set the largest event to have a magnitude of 0 by adjusting the added constant C uniformly across all events. In addition, we use the relative magnitude to calculate relative energy release, which scales with the 3/2 power of the maximum amplitude (Vassilou & Kanamori 1982).
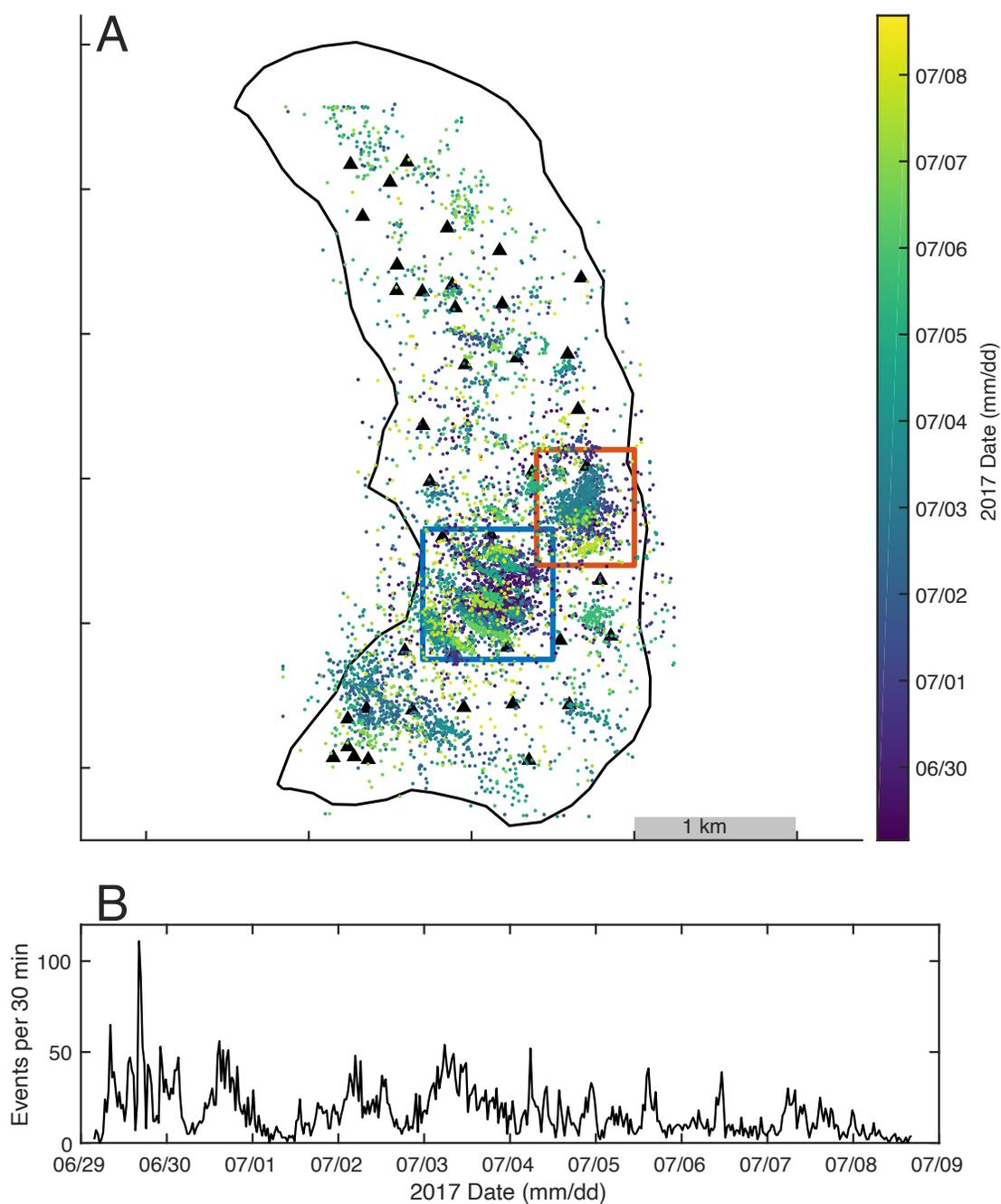
**Figure 3**. A) Map of located surface icequake events on Lemon Creek Glacier, colored by time over the course of the deployment. Black triangles indicate seismic station locations. Blue box outlines the west highlight area (expanded in Figure 4A) and red box outlines the east highlight area (expanded in Figure 4B). Axes tick scale: 1000 m. B) Event rate (per 30 min) over time across the entire surface of the glacier.
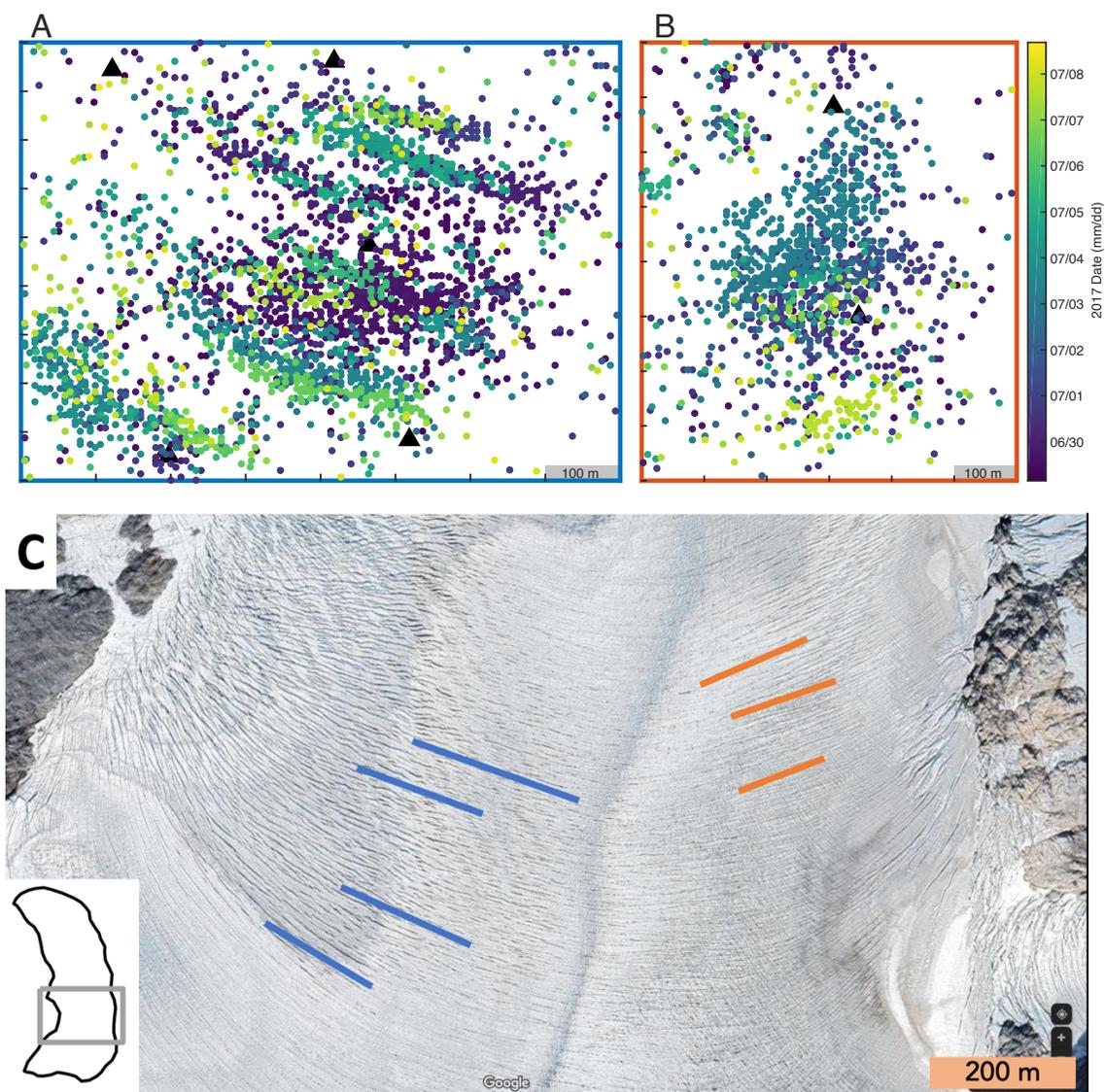
Figure 4. A) Map of the west highlight area, outlined in blue in Figure 3A, with surface icequakes colored by time. Black triangles indicate seismic station locations. Axes tick scale: 100 m. B) Map of the east highlight area, outlined in red in Figure 3A, with surface icequakes colored by time. Black triangles indicate seismic station locations. Axes tick scale: 100 m. C) 2019 satellite image (Maxar Technologies, 2022) of a portion (see inset) of Lemon Creek Glacier. Added lines indicate examples of surface crevasse strikes in the approximate locations of the highlight regions shown in A and B.

4. Results

Using the event detection, location, and quality filtering process described in the previous section, we found high-quality locations for 7,731 unique surface icequake events from 29 June to 09 July 2017 when seismic stations were active. These events can be seen in Figures 3 and 4. During the first and last day of this period, spatial coverage of the network is limited because not all stations were simultaneously active during deployment and pickup activities. Surface icequakes appear across the glacier throughout the deployment period. Some events occur in relative spatiotemporal isolation, while others appear in clear clusters of activity. The most obvious clusters of events occur in linear configurations, primarily the NW-SE striking features shown in Figure 4A and the NE-SW striking features shown in Figure 4B. Waveforms from three icequake events can be seen in Figure 5. Wave velocities from all events have a mean of 1275 m/s and a standard deviation of 161 m/s.

Cryoseismicity over time and magnitude is shown in Figure 6 for the entire glacier and for the two regions outlined in Figure 4. Event magnitudes have a median one-sigma error of 0.14 based on the distribution of maximum amplitudes recorded among all stations detecting each event. Clear mainshock-aftershock patterns are not visible; rather, clusters of events appear with no obvious mainshock. Some clusters feature relatively abrupt starts or stops, while others remain diffuse in time. The Gutenberg-Richter plot in Figure 7 suggests that events at low magnitude are incompletely cataloged due to low signal-to-noise ratios, while events with higher magnitude may be described with the Gutenberg-Richter law

$$\log_{10}(N) = a - bM \ . \qquad (4)$$

where N is the number of events above magnitude M, and a and b are constants. The best-fit b value from a linear least-squares fit over several example ranges are shown in Figure 7.
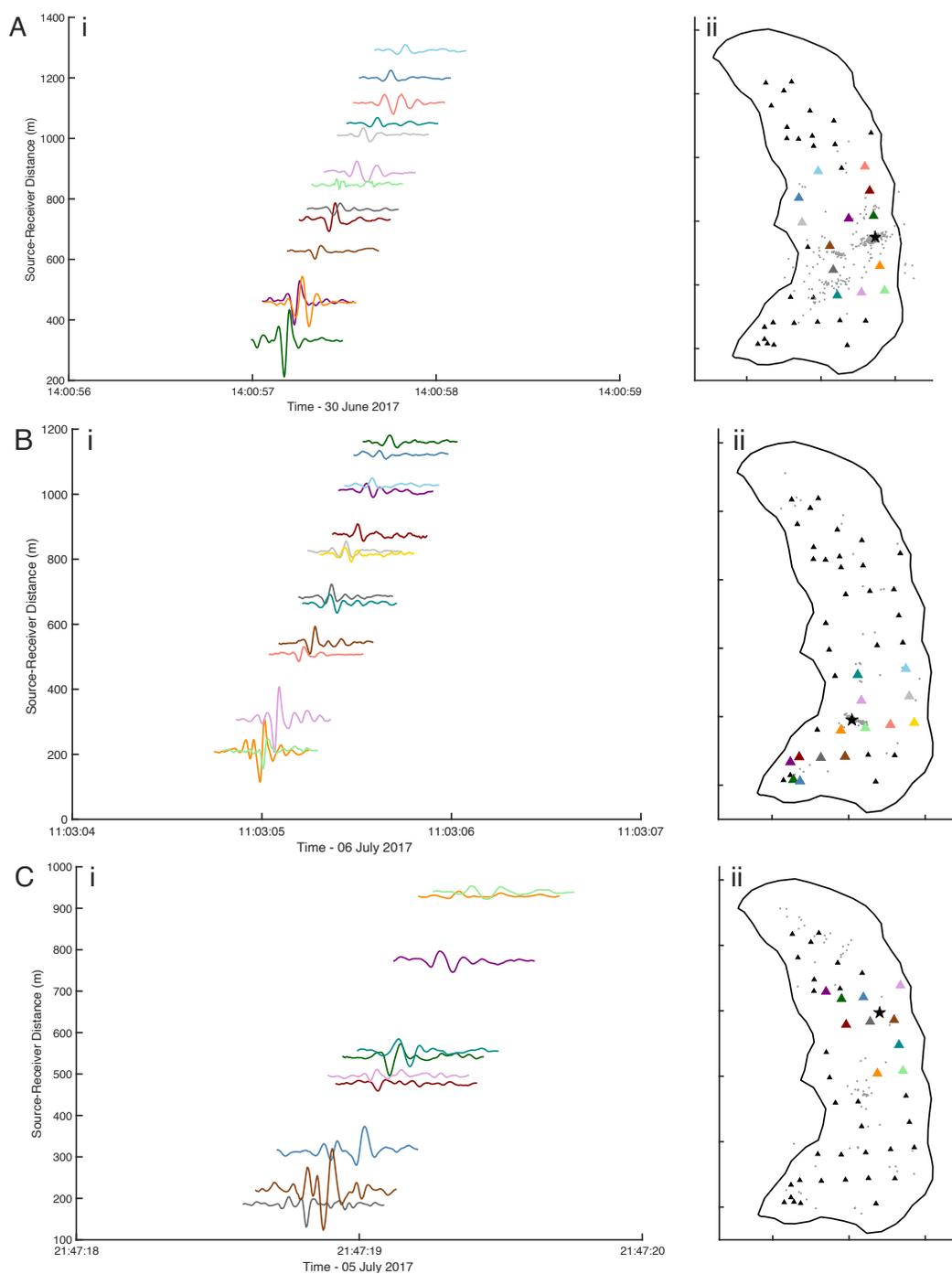
Figure 5. Ai, Bi, Ci) Record section of displacement data from all detecting seismic stations for three example surface icequakes. Vertical scale of data is normalized relative to the maximum displacement recorded at any station. Aii, Bii, Cii) Map showing location of event (black star), locations of stations recording the event (large triangles, color corresponding to record section), locations of stations not recording the event (small black triangles), and all events located within two hours before or after the example event (gray dots).
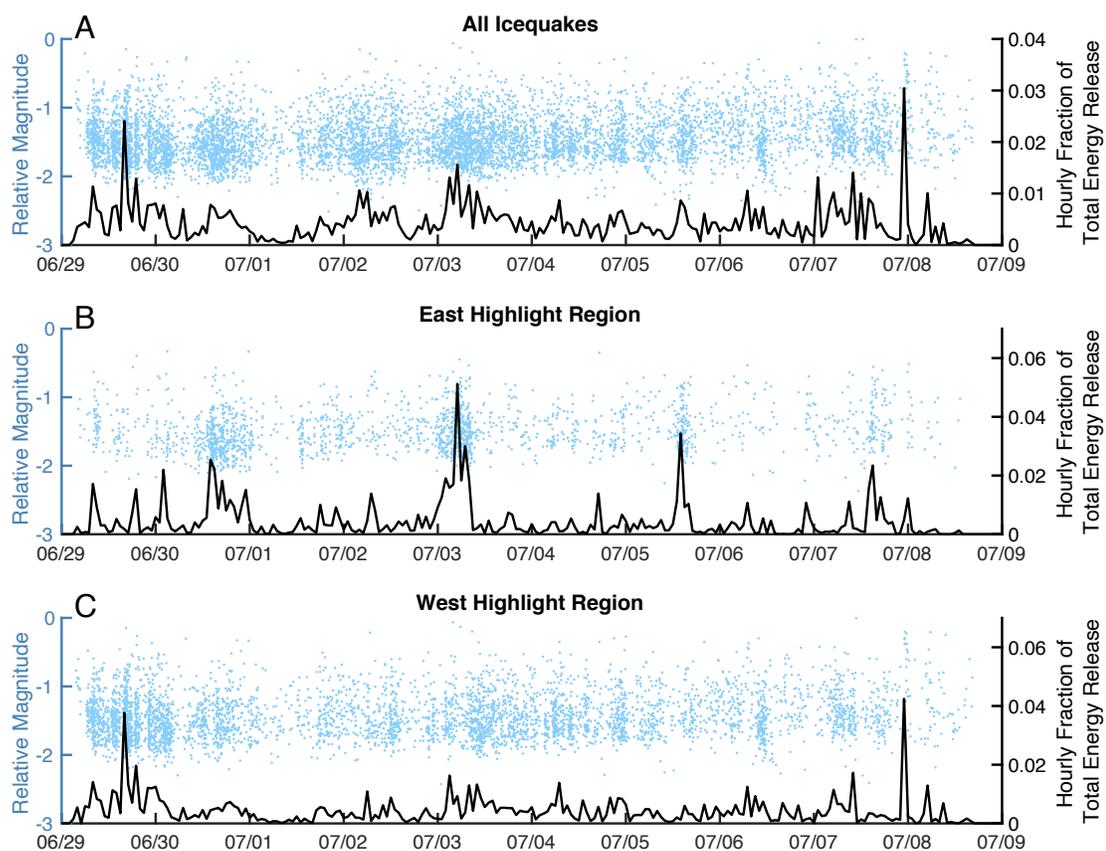
Figure 6. Relative magnitude and time (blue points) and hourly fraction of total energy release (black lines) of surface icequakes recorded at Lemon Creek Glacier during the 2017 deployment over the entire glacier (A), in the east highlight region, outlined in red in Figure 3A (B), and in the west highlight region, outlined in blue in Figure 3A (C).
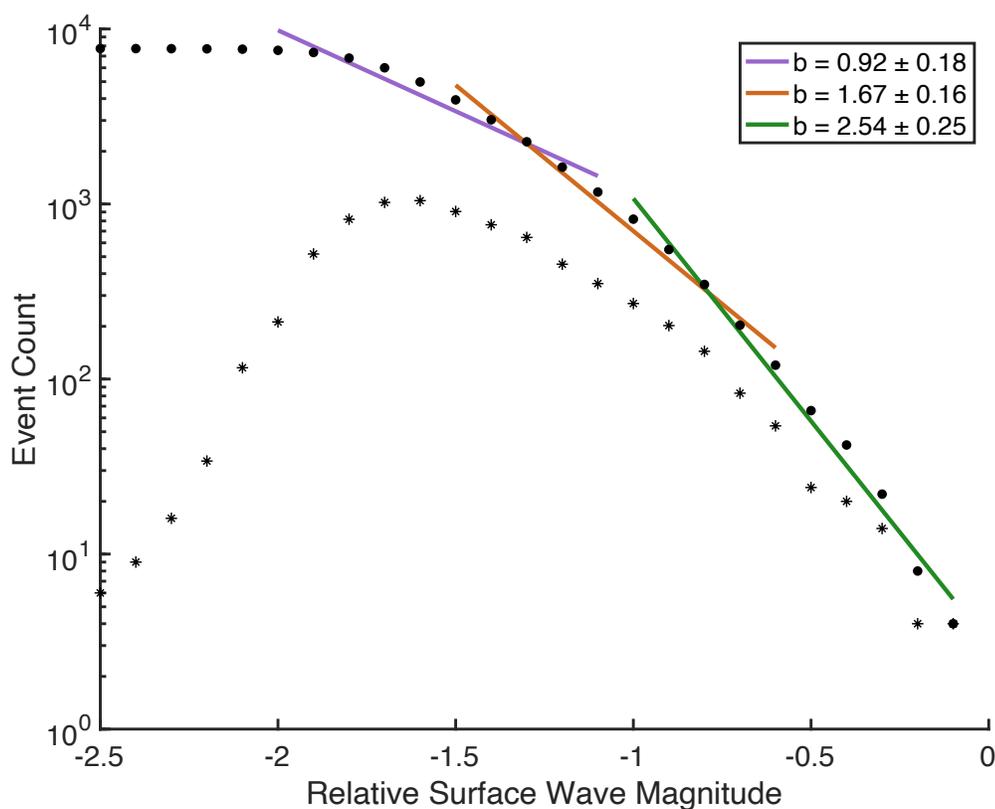
Figure 7. Gutenberg-Richter plot of all surface icequakes recorded at Lemon Creek Glacier during the 2017 deployment. Dots indicate cumulative counts of all events above the points' corresponding magnitude. Stars indicate non-cumulative counts of events by magnitude. Lines show best-fit b-values for cumulative event counts in magnitude ranges -2.0 to -1.0 (violet), -1.5 to -0.5 (orange), and -1.0 to 0 (green).

In Figure 8, we compare the cryoseismicity to several other observations of the glacier's condition: horizontal speed of the two on-ice GPS receivers, precipitation rate, water flux at the outlet stream, and air temperature. During times of low rainfall in this part of the melt season, water flux at the outlet stream acts as a reliable proxy for the throughput of the subglacial hydrologic system of Lemon Creek Glacier (Labedz et al. 2022). Notable events in these data include rainfall on 01-05 July, the drainage of Lake Linda starting late on 05 July and peaking at the start of 07 July, deviation between the two GPS receivers on 01-03 and 06 July, and warm weather from 05 July onward. Icequakes occur in isolation and in clusters throughout the 10-day period of this study, without obvious correlation to any one of these data categories.
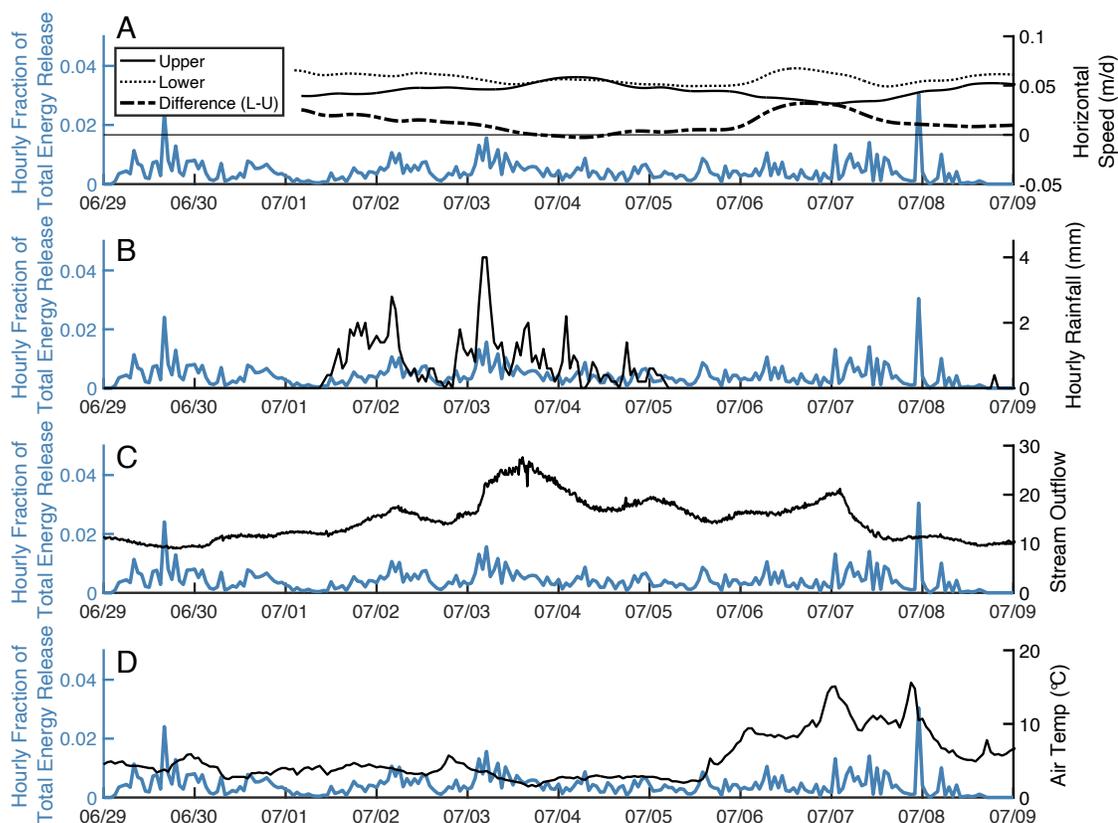
Figure 8. Hourly fraction of total energy release of surface icequakes recorded at Lemon Creek Glacier during the 2017 deployment over the entire glacier (blue line), compared with environmental and motion data from the glacier: A) Along-flow horizontal speed recorded by two GPS receivers (upper/southern - solid line, lower/northern - dotted line) with 24-hour smoothing and their difference (dashed line). B) Hourly rainfall recorded at the west margin of the glacier. C) Water flux recorded at the USGS stream gauge at Lemon Creek. D) Air temperature recorded at the west margin of the glacier.

Within the individual linear clusters visible in Figures 3 and 4, we observe a variety of spatiotemporal patterns in cryoseismicity; three examples are shown in Figure 9. Some clusters show clear spatial migration over time along their axis, like the one shown in Figure 9a. When clear migration is visible, the icequake fronts advance outward at rates of 0.02-0.05 m/s (1-3 m per minute). Many clusters show repeated activity along the same axis, sometimes in rapid succession over just a few hours, such as in Figure 9b, and sometimes

with longer gaps of several days between activity. Some clusters also showed activity along multiple parallel linear axes, migrating between lines on the scale of hours, such as in Figure 9c. Many clusters show more than one of these properties simultaneously, such as repeated activity along the same axis with propagating icequake fronts in each burst of activity. Individual clusters show magnitude distributions similar to that of the entire catalog, with a lack of clear mainshock-aftershock patterns.
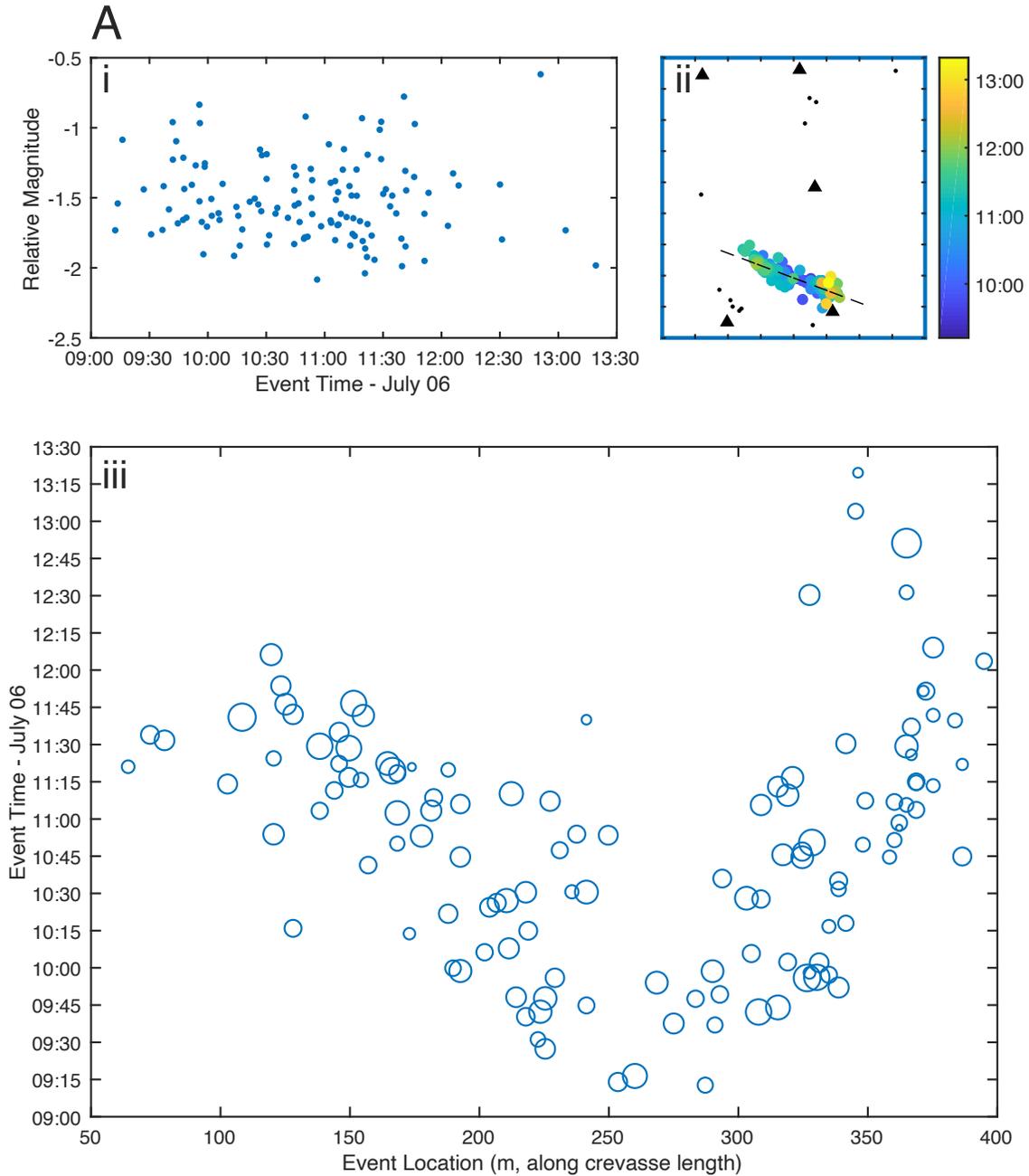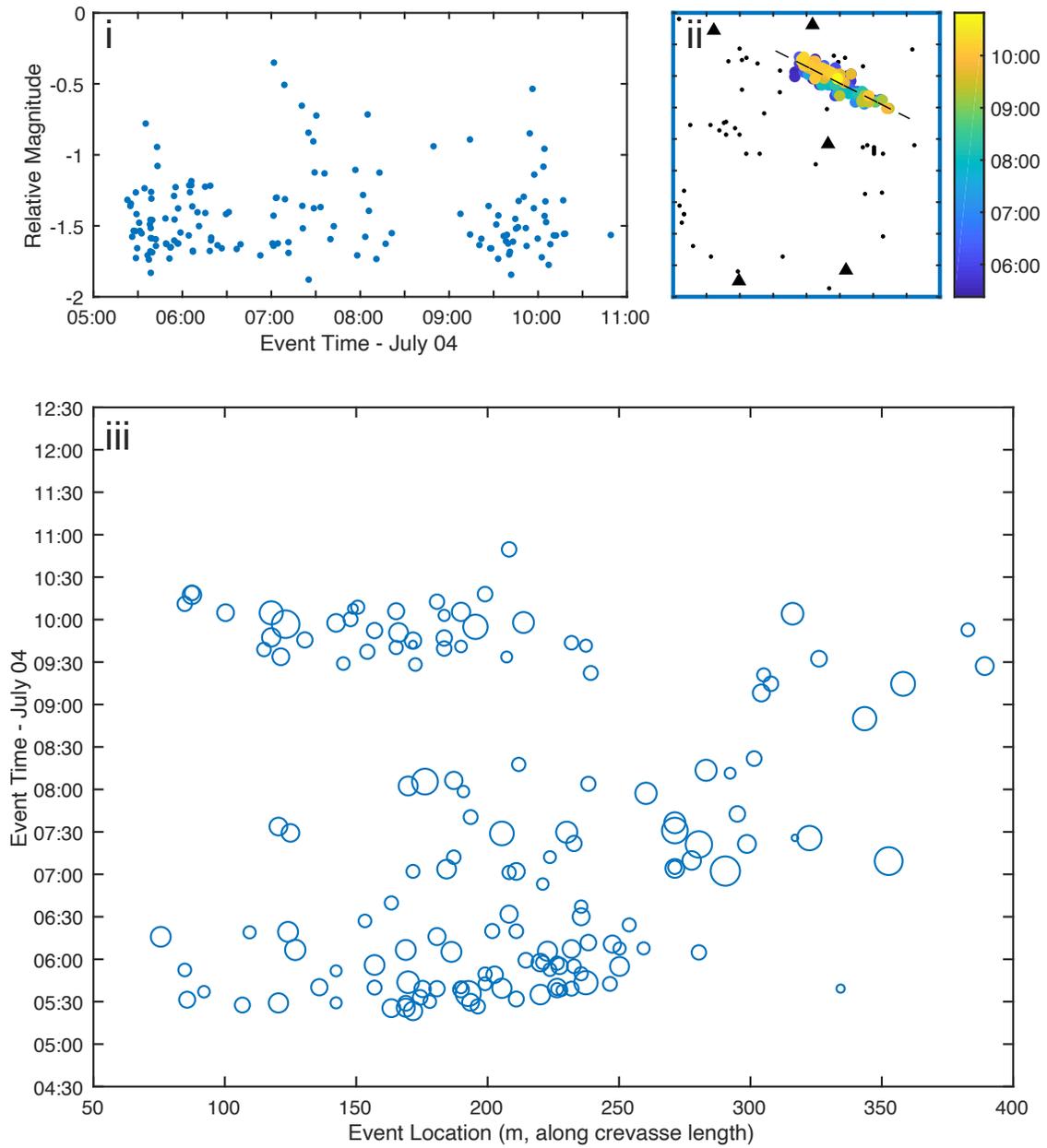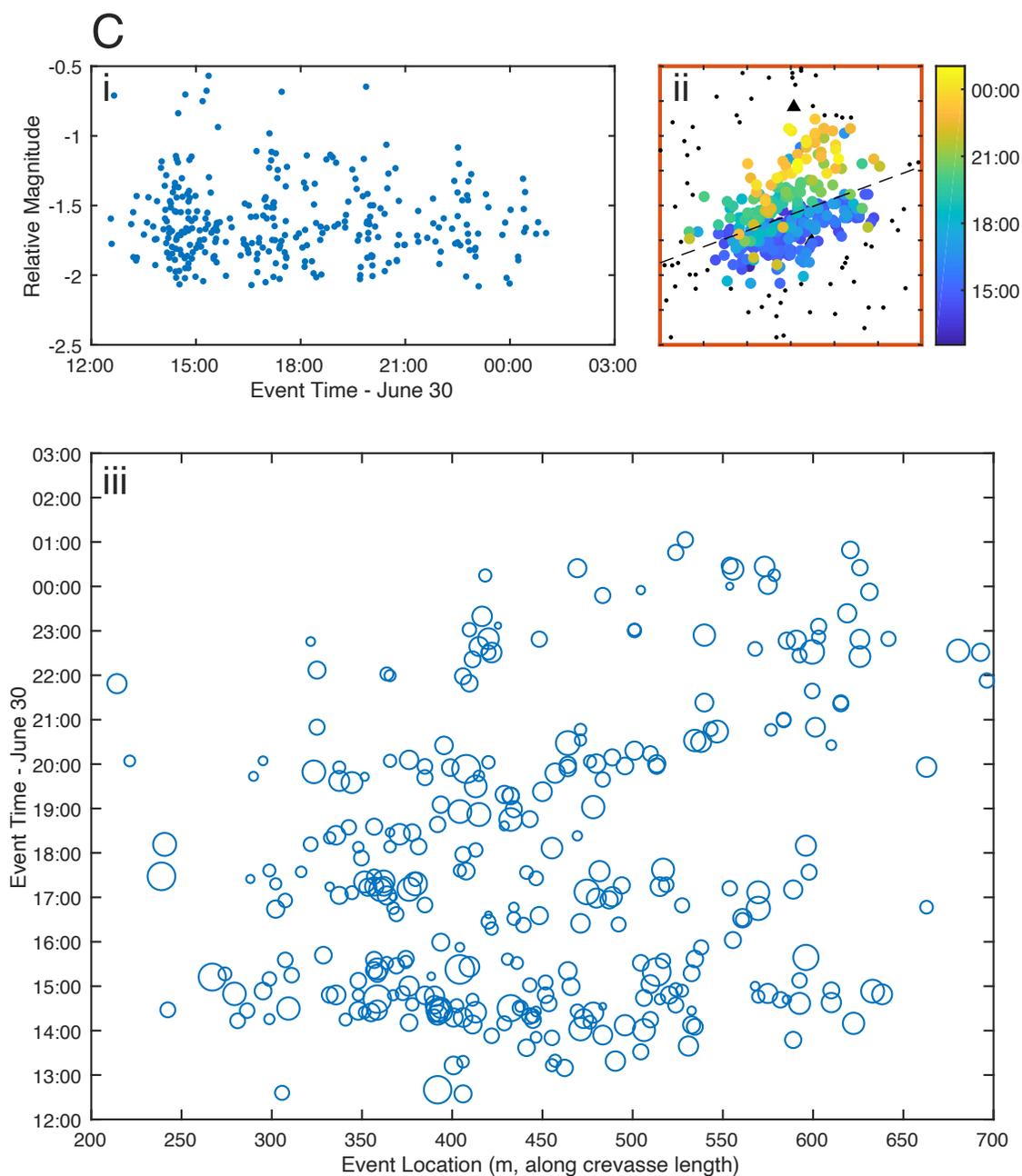
Figure 9. Ai, Bi, Ci) Relative magnitude and time of surface icequakes recorded in three example linear clusters. Aii, Bii, Cii) Map of west highlight region (Aii, Bii) or east highlight region (Cii) showing locations of surface icequakes in linear cluster (large dots, colored by event time), fitted axis of linear cluster (dashed black line), locations of surface icequakes outside of linear cluster (small black dots), and seismic station locations (black triangles). Axes tick scale: 100 m. Aiii, Biii, Ciii) Locations of icequakes in their linear cluster, projected onto the fitted cluster axis, over time. Circle size is proportional to relative event magnitude.

5. Discussion

In order to identify the source mechanisms of the surface icequakes, we observe the properties of the emitted seismic waves, through the velocities fit through a grid search, and the individual waveforms detected by the STA/LTA algorithm. The velocity range allowed by the grid search contains previously observed values of Rayleigh wave velocity for a snow/firn glacier surface, and the best-fit values for events with high-quality locations had a mean of 1275 m/s and standard deviation of 162 m/s. This velocity is lower than some previously observed values (e.g., approximately 1650 m/s in both Roux et al. 2010 and Mikesell et al. 2012), but slower speeds are not surprising given the presence of significant surface snow at our field site at the time of the deployment. When we computed the grid search model for a wider range of velocities, including P and S wave velocities for ice (approximately 3800 m/s and 1940 m/s, respectively, from Kohnen 1974) events with high-quality locations were still most often found using the Rayleigh wave velocity found in the constrained grid search, indicating that Rayleigh waves dominate the wave phases detected by the STA/LTA algorithm. Inspection of waveforms produced by larger-magnitude events revealed some cases of a P-wave arriving before the Rayleigh wave, occasionally with high enough amplitude and a long enough separation to be separately detected by the STA/LTA algorithm, but the resulting event location was still convergent with the subsequent Rayleigh wave phases, sorted with the multiple-pick procedure outlined above. Even for events large enough to produce a clear P wave, clearly-distinguishable S waves are not observed before the arrival of the Rayleigh wave. The observed Rayleigh waves have an average period of 0.055 s (standard deviation 0.014 s), and duration of the Rayleigh wave phase is consistent across observed magnitudes (average of 0.19 s and standard deviation 0.05 s from hand-picked durations of the closest-recording station from each of 50 randomly-selected icequakes across a range of magnitudes), indicating that the rupture duration is significantly shorter than the Rayleigh wave period.
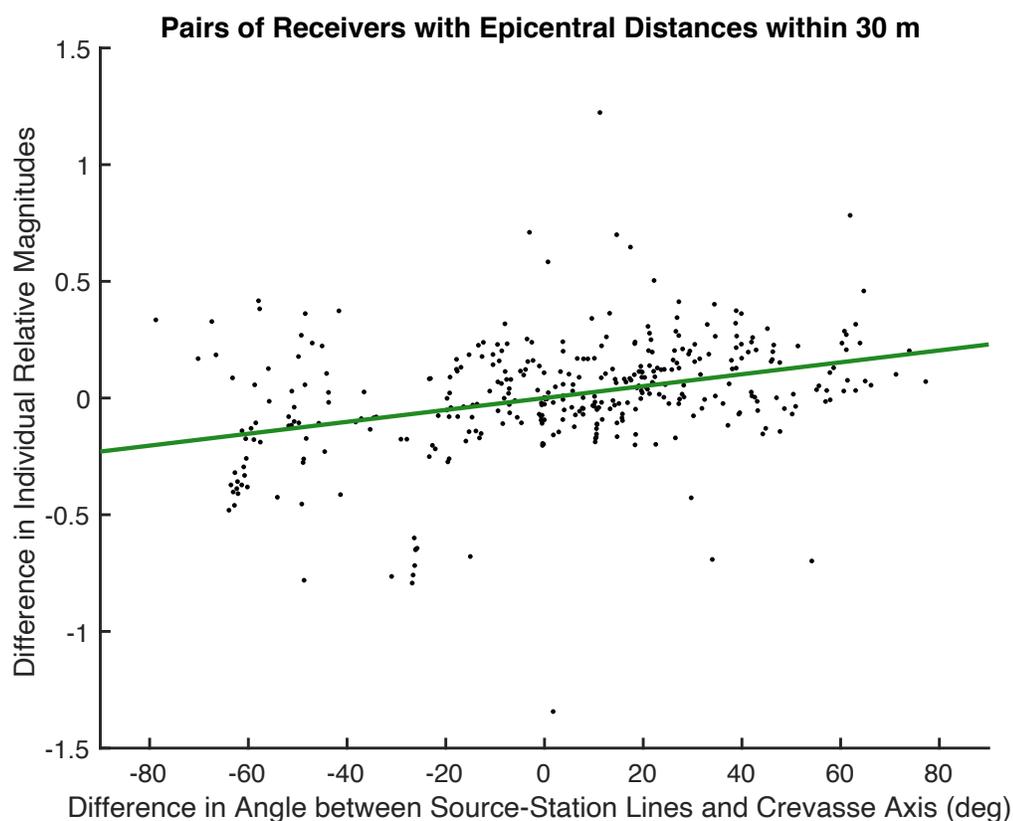
Figure 10. Differences in relative magnitude (black dots) calculated for pairs of stations recording the same event within the linear cluster of events shown in Figure 4a at epicentral distances with a difference less than 30 m, plotted against the difference between the absolute acute angle between their source-station lines and the axis of the linear cluster, with a linear least-squares fit (green line).

The lack of clear S wave phases and the radial distribution of Rayleigh wave polarizations and amplitudes is consistent with that of mode I crack opening (Gupta 1966). Polarization of the Rayleigh wave is consistent regardless of angle around the event, and for events in linear clusters, amplitude of the Rayleigh wave is highest for stations perpendicular to the cluster axis (presumably also the mode I crack axis) and lower for stations along the cluster axis line. To demonstrate, among the linear cluster of events shown in Figure 4a, Figure 10 shows the difference in magnitude calculated from pairs of stations recording the same event with epicentral distances within 30 m of each other, but with different absolute acute angles between their source-station line and the axis of the linear cluster. Based on a linear least-squares fit of these data, a station perpendicular to the cluster axis would record a magnitude

0.23 ± 0.03 higher for the same event than a station parallel to the crevasse axis, consistent in scale with the previously-mentioned intra-event magnitude error value of 0.14 based on the variation in amplitude among recording stations.

Mode I crack activity is expected on the surface of this system; surface crevassing is common on glaciers and observed in high-resolution satellite imagery of the surface of Lemon Creek Glacier late in the 2019 melt season when surface snow was fully depleted (Maxar Technologies 2022). Indeed, the linear clusters of icequakes observed in this study have axes orientations in the expected directions of surface crevasses based on the stress field at the surface of the glacier (Nye 1952) and observed in the satellite imagery, as shown in Figure 4c. In many cases, even events not associated with a cluster of icequakes show amplitude distributions consistent with crack axes in the expected orientations of surface crevassing. For example, the event shown in Figure 5c shows stations to the NE and SW of the event record lower peak amplitudes than stations to the NW and SE, similar to the event in Figure 5a, which is part of a cluster of the same expected orientation.

While we refer to these events as "surface" icequakes, mode I crack activity associated with crevassing is not necessarily taking place truly at zero depth in the glacier. The surface crevassing layer comprises the upper 20-30 m of brittle material (hard ice or well-compressed firn), and individual crevasses can occasionally temporarily extend deeper, but tend to quickly re-seal under pressure of closure from the weight of the ice (Vaughan 1993). In addition, surface snow and poorly-compressed firn lie above the brittle ice where fracture occurs; early in the melt season, this layer can be up to a few 10s of meters in the accumulation zone at the top of Lemon Creek Glacier (McNeil 2016). Our method of detection and location using Rayleigh waves does not return event depth information, but rather returns the surface projection of an event. For the scales of our system, where event depths are a few 10s of meters and station spacing is on the order of a few 100s of meters, we consider these surface projections to be accurate enough to meet the goals of this study.

An individual surface crevasse can extend via ice fracture in two ways: the crevasse can become wider at a given depth, extending outward along its axis, or become deeper,

extending downward into the ice. From the spatiotemporal patterns of icequake activity, we infer that both processes apparently occur in this system, sometimes simultaneously. We interpret the cluster shown in Figure 9a as an example of a widening crevasse; the crack tip on each side of the crevasse propagates outward in each direction at approximately 0.02 m/s (1.2 m per minute), as shown by the advancing fronts of icequakes. We interpret clusters where icequakes occur repeatedly at the same surface locations without clear propagating fronts of icequakes (such as those in Figures 9b and 9c) to be crevasses expanding primarily through deepening into the ice. Some events showed characteristics of both, an outward-propagating icequake front with events continuing to occur behind it, indicating simultaneous widening and deepening of the crevasse. Importantly, these icequakes alone do not entirely capture the evolution of crevasse shape and size. Firstly, smaller icequakes than can be reliably detectable with our instruments and methods also contribute to crevasse growth. Secondly, crevasse-opening fractures may not be completely described by simple mode I crack opening; they could also have mode II or III shearing components that contribute to cryoseismic wave generation in some capacity, but not strongly enough to create reliably-detectable S waves with our instruments and methods. Thirdly and perhaps most importantly, crevasse closure also occurs regularly on the surface of glaciers, and often occurs aseismically through slow creep closure (Weertman 1983).

Surface crevassing activity can be modulated in part by changes in glacier motion changing the stress distribution of ice at the surface (Nye 1952), or by changes in environmental factors like temperature and precipitation changing the amount of water available to drive hydrofracturing (Irvine-Flynn et al. 2011). As shown in Figure 8, over the period of our seismic deployment, the two GPS receivers record relatively constant velocity, even during a period of increased subglacial water flux due to a lake drainage (Labedz et al. 2022). The small increases, decreases, and deviations between the GPS receiver velocities do not show a strong correlation with cryoseismicity, however many clusters of icequakes occur on time scales much shorter than variability is observed in our processed GPS data, indicating that different GPS processing procedures that optimize for shorter-term velocity changes may be more useful for comparison with surface cryoseismicity. Regarding meteorological

observations (rainfall and temperature), cryoseismic energy release appears somewhat correlated to rainfall during the period where rain is occurring, and the period of active crevassing in the eastern highlighted region on 03 July shown in Figure 4 occurs at the same time as the highest rainfall rates, suggesting that hydrofracture-driven crevasse growth could be occurring. In addition, a small cluster of high-magnitude events in the western highlighted region shortly after the local midday temperature peak at the turn of UTC 08 July. However, we cannot clearly and causally link the crevassing to rain- or melt-driven hydrofracture with such a limited period of data collection; though some correlations appear, crevassing activity also occurs at times without rainfall or increased surface melt from exceptionally warm weather, and periods of rainfall and warm weather occur without significantly higher-than-average crevassing activity.

One of the main limitations of this study is the relatively short deployment time of the array due to the battery life of the nodal seismometers. Over the ten days of data collection, we observe extensive crevassing activity in two regions of the glacier (highlighted in Figure 4), but only sporadic activity elsewhere. A longer period of data collection in future studies would allow for improved understanding of how surface crevassing events behave and relate to each other over space and time, and how crevassing activity is correlated with environmental variables like meteorology and overall glacier activity like flow speed.

One of the most notable features of the cryoseismicity at Lemon Creek Glacier is the distribution of magnitudes, shown in Figure 7, and the lack of clear mainshock-aftershock patterns within clusters of events, as shown in Figure 9. In earthquake seismology, the magnitudes of tectonic earthquakes in a seismically active region can generally be considered to follow a Gutenberg-Richter distribution with a b-value of approximately 1.0, as can the magnitudes of aftershocks in a single earthquake sequence (Gutenberg & Richter 1944; Shaw 1993). It can be difficult to declare a single definitive b-value for a system with a deployment like this one for two reasons: 1. the short duration of deployment means that the largest yet most infrequent events may be underobserved, and 2. the noise levels in the environment limit the sampling completeness of the smallest events. To demonstrate the approximate

distribution of magnitudes, we fit for b over multiple example magnitude ranges: -2.0 to -1.0, -1.5 to -0.5, and -1.0 to 0, all shown in Figure 7. The lowest magnitude range, clearly affected by low signal-to-noise incompleteness has a b-value of 0.92 ± 0.18, closest of the three to the standard tectonic value. The other two example ranges are distinctly higher than 1.0, with the middle showing $b = 1.67 \pm 0.16$ and the highest (which could potentially be affected by underobservation of rare large events) showing $b = 2.54 \pm 0.25$. Based on these fits and the clear influence of incomplete cataloging at low magnitudes, we feel confident in declaring that the overall b-value for this system is clearly differentiable as higher than the standard tectonic behavior of $b = 1.0$. That a discrepancy occurs is not surprising, given the differing physics between the mode I cracking icequakes observed here and the slipping motion of earthquakes. In an earthquake sequence, subsequent earthquakes can occur with slip on the same area of the fault as prior events, because the two sides of the fault remain in contact. In a sequence of mode I cracking icequakes in a growing crevasse, however, the ruptured area does not remain in contact and therefore cannot immediately rupture again. Surface crevasses can heal over time due to pressure of closure from the weight and flow of the ice, or from the freezing of liquid water within the crevasse, but these healing processes occur over hours to days, slower than many icequake sequences observed here.

Higher b-values can be observed for earthquakes in the cases of swarms, where no outstanding principal event occurs, rather than classic mainshock-aftershock sequences. One cause of high b-values in earthquake swarms is reduced effective stress in the faults involved (Wyss 1973). Changes in effective stress can be caused by the movement of fluids in and around fault zones, which is known to occur in some earthquake swarms, particularly those in areas with induced seismic activity like several European geothermal sites that showed an average b-value of 1.94 (Grünthal 2014; Ross et al. 2020). Icequakes associated with crevasse expansion could be considered as an extreme edge case of this process, where effective stress is reduced to zero by the separation of crevasse walls. Another feature associated with high b-values in earthquake swarms is a heterogeneous stress system associated with highly fractured crust that limits fault length (Mogi 1963), which is applicable to the surface glaciers, where crevassing can occur extensively across the surface.

Perhaps the most notable parallel case to our system is earthquake swarms associated with active volcanism, which can have elevated b-values due to both of these features. In volcanic systems such as Long Valley, Yellowstone, Kilauea, Pinatubo, and Etna, b-values of 1.5-2.0 are regularly observed in earthquake swarms, and *b* can be as high as 3.0 for swarms occurring at depths such that earthquakes are adjacent to magma bodies, where rock can be highly fractured and magma can infiltrate those fractures (McNutt 2005). High b-values have also been observed in other cryoseismic activity, such as intermediate-depth icequakes in alpine glaciers (Helmstetter et al. 2015b) and basal icequakes in Rutford ice streams that showed a b-value of at least 3.3 (Kufner et al. 2021), both of which suspected hydraulic fracturing as the main icequake driver. A b-value of 1.5 was also observed in surface events at a large, actively-propagating rift in the Ross Ice Shelf (Olinger et al. 2019; Olsen et al. 2021). Like icequakes associated with normal surface crevassing, both hydrofracturing and rift-associated crevassing occur with separation between the sides of the fracture surface, reducing the effective stress to zero and preventing re-rupture, suggesting that this property of icequakes may be a driver in elevating b-values.

6. Conclusions

In this study, we have located 7,731 surface icequakes over a 10-day period using an array of on-ice seismometers at Lemon Creek Glacier. These icequakes are largely consistent with mode I cracking sources and their spatiotemporal distribution in linear clusters indicate surface crevassing activity as their source. We observed a variety of spatiotemporal patterns of icequakes within clusters, suggesting both widening and deepening of individual crevasses, reactivation of individual crevasses in bursts of cryoseismicity spaced hours to days apart, and simultaneous or migrating activity in multiple close parallel crevasses. The magnitude distribution of the observed icequakes has a b-value that is significantly higher than is characteristic of tectonic earthquakes. Such a high b-value is comparable to volcanic earthquake swarms, earthquakes swarms related to fluid infiltration, and hydrofracture-driven icequakes, potentially reflective of similarities between their mechanisms.

Understanding that cryoseismicity from surface crevassing occurs in swarm-like distributions in time and magnitude (rather than like classic mainshock-aftershock distributions) is useful for future investigations of glaciers that apply seismometer observations. A seismic array as dense as this one is impractical for many studies, but sparse arrays limit the ability to detect small icequakes, so understanding the distribution of magnitude allows for improved extrapolations to lower magnitude and therefore better characterization of relevant crevassing activity. Future studies with dense arrays would further improve knowledge of how surface crevassing activity in a given region of a glacier starts and stops, how crevassing activity might migrate from region to region, and how crevassing activity and its associated icequakes relate to environmental variables and glacier flow variability (e.g. changes in b-value or rate of energy release associated with changes like surges or hydrologic events).

<u>References</u>

Allen, R. V. (1978). Automatic earthquake recognition and timing from single traces. Bulletin of the seismological society of America, 68(5), 1521-1532. https://doi.org/10.1785/BSSA0680051521

Bartholomaus, T. C., Larsen, C. F., O'Neel, S., & West, M. E. (2012). Calving seismicity from iceberg–sea surface interactions. Journal of Geophysical Research: Earth Surface, 117(F4). https://doi.org/10.1029/2012JF002513

Bartholomaus, T. C., Amundson, J. M., Walter, J. I., O'Neel, S., West, M. E., & Larsen, C. F. (2015). Subglacial discharge at tidewater glaciers revealed by seismic tremor. Geophysical Research Letters, 42, 6391–6398. https://doi.org/10.1002/2015GL064590

Chen, G. (1998). GPS kinematic positioning for the airborne laser altimetry at Long Valley, California, PhD thesis. Massachusetts Institute of Technology

Gräff, D., Walter, F., & Lipovsky, B. P. (2019). Crack wave resonances within the basal water layer. Annals of Glaciology, 60(79), 158–166. https://doi.org/10.1017/aog.2019.8

Grünthal, G. (2014). Induced seismicity related to geothermal projects versus natural tectonic earthquakes and other types of induced seismic events in Central Europe. Geothermics, 52, 22-35. https://doi.org/10.1016/j.geothermics.2013.09.009

Gutenberg, B., & Richter, C. F. (1944). Frequency of earthquakes in California. Bulletin of the Seismological Society of America, 34(4), 185-188. https://doi.org/10.1785/BSSA0340040185

Gupta, I. N. (1966). Use of reciprocity theorem for obtaining Rayleigh wave radiation patterns. Bulletin of the Seismological Society of America, 56(4), 925-936. https://doi.org/10.1785/BSSA0560040925

Helmstetter, A., Nicolas, B., Comon, P., & Gay, M. (2015a). Basal icequakes recorded beneath an Alpine glacier (Glacier d'Argentière, Mont Blanc, France): Evidence for stick-slip motion?. Journal of Geophysical Research: Earth Surface, 120(3), 379-401. https://doi.org/10.1002/2014JF003288

Helmstetter, A., Moreau, L., Nicolas, B., Comon, P., & Gay, M. (2015b). Intermediate-depth icequakes and harmonic tremor in an Alpine glacier (Glacier d'Argentière, France): Evidence for hydraulic fracturing?. Journal of Geophysical Research: Earth Surface, 120(3), 402-416. https://doi.org/10.1002/2014JF003289

Irvine-Fynn, T. D., Hodson, A. J., Moorman, B. J., Vatne, G., & Hubbard, A. L. (2011). Polythermal glacier hydrology: a review. Reviews of Geophysics, 49(4). https://doi.org/10.1029/2010RG000350

Jarvis, G. T., & Clarke, G. K. (1974). Thermal effects of crevassing on Steele glacier, Yukon Territory, Canada. Journal of Glaciology, 13(68), 243-254. https://doi.org/10.3189/S0022143000023054

Kohnen, H. (1974). The temperature dependence of seismic waves in ice. Journal of
    Glaciology, 13(67), 144-147. https://doi.org/10.3189/S0022143000023467

Kufner, S. K., Brisbourne, A. M., Smith, A. M., Hudson, T. S., Murray, T., Schlegel, R., ...
    & Lee, I. (2021). Not all icequakes are created equal: Basal icequakes suggest diverse
    bed deformation mechanisms at Rutford Ice Stream, West Antarctica. Journal of
    Geophysical Research: Earth Surface, 126(3), e2020JF006001.
    https://doi.org/10.1029/2020JF006001

Labedz, C. R., Bartholomaus, T. C., Amundson, J. M., Gimbert, F., Karplus, M. S., Tsai,
    V. C., & Veitch, S. A. (2022). Seismic mapping of subglacial hydrology reveals
    previously undetected pressurization event. Journal of Geophysical Research: Earth
    Surface, 127(3), e2021JF006406. https://doi.org/10.1029/2021JF006406

Lindner, F., Walter, F., Laske, G., & Gimbert, F. (2020). Glaciohydraulic seismic tremors
    on an Alpine glacier. The Cryosphere, 14(1), 287–308. https://doi.org/10.5194/tc-14-
    287-2020

Maxar Technologies, © 2022, satellite imagery of Lemon Creek Glacier, accessed via
    Google Maps on 16 April 2022.

McNeil, C. (2016). Surface mass balance reanalysis of Taku and Lemon Creek glaciers,
    Alaska: 1946-2015. Doctoral dissertation, Alaska Pacific University.

McNutt, S. R. (2005). Volcanic seismology. Annu. Rev. Earth Planet. Sci., 32, 461-491.
    https://doi.org/10.1146/annurev.earth.33.092203.122459

Mikesell, T. D., van Wijk, K., Haney, M. M., Bradford, J. H., Marshall, H. P., & Harper, J.
    T. (2012). Monitoring glacier surface seismicity in time and space using Rayleigh
    waves. Journal of Geophysical Research: Earth Surface, 117(F2).
    https://doi.org/10.1029/2011JF002259

Mogi, K. (1963). Some discussions on aftershocks, foreshocks and earthquake swarms-
the fracture of a semi-infinite body caused by an inner stress origin and its relation the
earthquake phenomena. Bull. Earthq. Res. Inst., 41, 615-658.

Nye, J. F. (1952). The mechanics of glacier flow. Journal of Glaciology, 2(12), 82-93.
https://doi.org/10.3189/S0022143000033967

Olinger, S. D., Lipovsky, B. P., Wiens, D. A., Aster, R. C., Bromirski, P. D., Chen, Z., ... &
Stephen, R. A. (2019). Tidal and thermal stresses drive seismicity along a major Ross
Ice Shelf rift. Geophysical Research Letters, 46(12), 6644-6652.
https://doi.org/10.1029/2019GL082842

Olsen, K. G., Hurford, T. A., Schmerr, N. C., Huang, M. H., Brunt, K. M., Zipparo, S., ...
& Aster, R. C. (2021). Projected Seismic Activity at the Tiger Stripe Fractures on
Enceladus, Saturn, From an Analog Study of Tidally Modulated Icequakes Within the
Ross Ice Shelf, Antarctica. Journal of Geophysical Research: Planets, 126(6),
e2021JE006862. https://doi.org/10.1029/2021JE006862

Pelto, M., Kavanaugh, J., & McNeil, C. (2013). Juneau icefield mass balance program
1946–2011. Earth System Science Data, 5(2), 319–330. https://doi.org/10.5194/essd-5-
319-2013

Pfeffer, W. T., & Bretherton, C. S. (1987). The effect of crevasses on the solar heating of a
glacier surface. IAHS Publ, 170, 191-205.

Porter, C., Morin, P., Howat, I., Noh, M.-J., Bates, B., Peterman, K., Keesey, S., Schlenk,
M., Gardiner, J., Tomko, K., Willis, M., Kelleher, C., Cloutier, M., Husby, E., Foga, S.,
Nakamura, H., Platson, M., Wethington, M., Williamson, C., Bauer, G., Enos, J.,
Arnold, G., Kramer, W., Becker, P., Doshi, A., D'Souza, C., Cummens, P., Laurier, F.,
Bojesen, M. (2018). ArcticDEM. Harvard Dataverse, V1, Accessed 2021-04-23.
https://doi.org/10.7910/DVN/OHHUKH

Qamar, A. (1988). Calving icebergs: A source of low-frequency seismic signals from Columbia Glacier, Alaska. Journal of Geophysical Research: Solid Earth, 93(B6), 6615-6623. https://doi.org/10.1029/JB093iB06p06615

Röösli, C., Walter, F., Ampuero, J. P., & Kissling, E. (2016). Seismic moulin tremor. Journal of Geophysical Research: Solid Earth, 121(8), 5838–5858. https://doi.org/10.1002/2015JB012786

Röösli, C., Walter, F., Husen, S., Andrews, L. C., Lüthi, M. P., Catania, G. A., & Kissling, E. (2014). Sustained seismic tremors and icequakes detected in the ablation zone of the Greenland ice sheet. Journal of Glaciology, 60(221), 563–575. https://doi.org/10.3189/2014JoG13J210

Ross, Z. E., Cochran, E. S., Trugman, D. T., & Smith, J. D. (2020). 3D fault architecture controls the dynamism of earthquake swarms. Science, 368(6497), 1357-1361. https://doi.org/10.1126/science.abb0779

Roux, P. F., Walter, F., Riesen, P., Sugiyama, S., & Funk, M. (2010). Observation of surface seismic activity changes of an Alpine glacier during a glacier-dammed lake outburst. Journal of Geophysical Research: Earth Surface, 115(F3). https://doi.org/10.1029/2009JF001535

Shaw, B. E. (1993). Generalized Omori law for aftershocks and foreshocks from a simple dynamics. Geophysical research letters, 20(10), 907-910. https://doi.org/10.1029/93GL01058

Thiel, E., LaChapelle, E., & Behrendt, J. (1957). The thickness of Lemon Creek Glacier, Alaska, as determined by gravity measurements. Eos, Transactions of the American Geophysical Union, 38(5), 754–749. https://doi.org/10.1029/tr038i005p00745

Thornton, T. F. (2012). Haa Léelk'w has Aaní Saax': Our grandparents' names on the land. Sealaska Heritage Institute and University of Washington Press.

U.S. Geological Survey. 2017. National Water Information System, access online 2017 at https://waterdata.usgs.gov/ak/nwis/inventory/?site_no=15052000 . https://doi.org/10.5066/F7P55KJN

Vassiliou, M. S., & Kanamori, H. (1982). The energy release in earthquakes. Bulletin of the Seismological Society of America, 72(2), 371-387. https://doi.org/10.1785/BSSA0720020371

Vaughan, D. G. (1993). Relating the occurrence of crevasses to surface strain rates. Journal of Glaciology, 39(132), 255-266. https://doi.org/10.3189/S0022143000015926

Veitch, S., Karplus, M., Kaip, G., Gonzalez, L., Amundson, J., & Bartholomaus, T. (2021). Ice thickness estimates of Lemon Creek Glacier, Alaska, from active-source seismic imaging. Journal of Glaciology, 1–9, 824–832. https://doi.org/10.1017/jog.2021.32

Weertman, J. (1983). Creep deformation of ice. Annual Review of Earth and Planetary Sciences, 11(1), 215-240.

Willis, I. C. (1995). Intra-annual variations in glacier motion: a review. Progress in Physical Geography, 19(1), 61-106. https://doi.org/10.1177/030913339501900104

Winberry, J. P., Anandakrishnan, S., & Alley, R. B. (2009). Seismic observations of transient subglacial water-flow beneath MacAyeal Ice Stream, West Antarctica. Geophysical Research Letters, 36, L11501. https://doi.org/10.1029/2009GL037730

Wyss, M. (1973). Towards a physical understanding of the earthquake frequency distribution. Geophys. JR Astron. Soc, 31(4), 341-359.

C h a p t e r   4

CORRELATED CHANGES IN COMMUNITY ACTIVITY AND URBAN SEISMIC NOISE IN LOS ANGELES ON SHORT AND LONG TIME SCALES

Contains data previously published as part of this publication, on which C.R.L. was a co-author, processed data for some cities, and provided contributions to manuscript editing: Lecocq, T., Hicks, S. P., Van Noten, K., Van Wijk, K., Koelemeijer, P., De Plaen, R. S., ... & Xiao, H. (2020). Global quieting of high-frequency seismic noise due to COVID-19 pandemic lockdown measures. Science, 369(6509), 1338-1343. https://doi.org/10.1126/science.abd2438

Abstract

Human activity such as transit and industry generates high-frequency vibrations that can couple with the solid earth to create anthropogenic seismic noise. The amplitude of this seismic noise varies in tandem with community activity, following day/night and weekday/weekend cycles, particularly in dense urban areas. Breaking from standard cycles for holidays, special events, or emergency situations also creates an observable change in seismic noise levels. In this study, we observe urban seismic noise levels at a seismometer in Los Angeles, California. We find that unwanted transient signals like earthquakes can be addressed statistically when generating power spectra in order to most accurately reflect only continuous signals in seismic data. We use seismic noise to observe two deviations from standard community activity. First, on the scale of a few hours, we observe a sustained drop in noise levels during the 2022 Super Bowl as many people watched the game rather than participate in normal activities. Second, on the scale of weeks to months, we observe a significant and prolonged drop in noise levels during COVID-related lockdowns in 2020. Seismic noise levels during 2020 do not correlate well with policy measures intended to be

prescriptive of community behavior, but do correlate well with the Google COVID-19 Community Mobility Reports, which are reflective of actual community behavior based on smartphone location durations. Understanding how anthropogenic seismic noise behaves is vital for seismic studies such as hazard mapping that involve urban areas, and understanding what level of detail anthropogenic seismic noise can reflect human behavior is vital for public support of collecting and sharing seismic data.

1. Introduction

Seismometers can detect ground motion from far more than just earthquakes. Though often designed for recording earthquake-generated seismic waves, seismometers can detect ground motion from any source, provided it is within the frequency and amplitude parameters of the instrument. The growing field of environmental seismology delves into seismic signals sourced from a wide variety of earth surface processes, such as ocean waves (e.g. Cessaro 1994), landslides (e.g. Suriñach et al. 2005), rivers (e.g. Gimbert et al. 2014), glaciers (e.g. Podolskiy & Walter 2016), and more (Larose et al. 2015). Human activity is also an earth surface process that creates seismic energy through transit, industry, crowds, and any other motions that couple with the solid earth (e.g. Riahi & Gerstoft 2015; Díaz et al. 2017; Denton et al. 2018). Anthropogenic activity can appear seismically in discrete events such as mining blasts, or as spatially and temporally continuous signals such as the vibrations from many cars along a highway. Changes in high-frequency background seismic noise levels around human settlements have long been observed to follow day/night and weekday/weekend/holiday schedules due to changes in anthropogenic activity, with the strongest correlations observed in dense urban areas (Groos & Ritter 2009; Boese et al. 2015; Green et al. 2017). Seismometer network coverage of urban areas that face potential danger from earthquakes is vital for developing accurate hazard maps and safe building standards, but high background noise levels can obscure some transient seismic wave signals that are of interest to these aims, highlighting the importance of accurate characterization of the anthropogenic seismic noise field.

Understanding the detail with which seismic recordings reflect human activity is also a matter of national security and open data policy, as indicated by conversations surrounding the media coverage of Lecocq et al. 2020. Availability of seismic data from around the globe allows the field of seismology to progress in understanding earth structure, processes, and hazards, and allows governments to monitor for unauthorized weapons testing that may foreshadow conflicts. If it is found that seismometer data can be processed to return too much detail about nearby human activity, some local communities and authorities could become concerned about allowing data to be collected or widely shared, hampering scientific progress and security monitoring. The seismic noise environment in urban and remote areas is generally composed of a wide range of simultaneous signals that are difficult to deconvolve into detailed individual activities (Larose et al. 2015; Díaz et al. 2017), but analyzing the detail with which urban data reflects community behavior is still valuable in evaluating concerns about or reactions to the idea of potential seismometer-based surveillance.

In this study, we examine the urban seismic noise field at a seismometer in Los Angeles, California, USA and its connection to two examples of changes in human activity, one on the time scale of a few hours (the 2022 Super Bowl game) and one on the time scale of many weeks (lockdowns in 2020 due to COVID-19). We examine the processing of seismic noise data with the median power spectral density method, which can remove the impact of large transient events such as earthquakes on power spectra without prior knowledge of when such events occur. We find that even short-term changes in human activity can be visible in seismic noise levels, but that large, long-term changes create the clearest signal that can be best correlated with other measures of human activity.
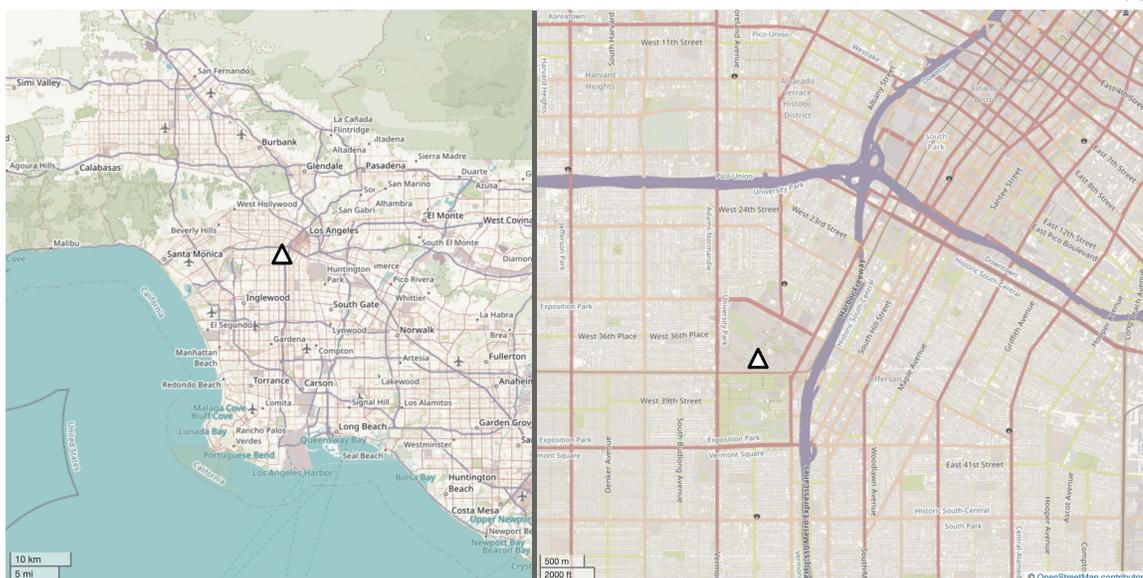
Figure 1. Location of station CI.USC (white triangle) at large in the Los Angeles area (left) and in detail on the USC campus (right). Purple lines indicate freeways, and red and orange lines indicate major surface streets. Map base copyright OpenStreetMap Contributors, 2022.

2. Seismic Signal Processing

To observe the urban seismic noise environment of Los Angeles, we use data from seismic station CI.USC of the California Integrated Seismic Network, located on the campus of the University of Southern California, just outside of downtown Los Angeles (Figure 1). The campus area has heavy pedestrian and bicycle traffic and is surrounded with many busy surface streets, and the station is within one kilometer of the CA 110 freeway and the Expo line of the Los Angeles Metro rail. We use vertical channel velocity data from an STS-2 40 Hz Streckeisen sensor (SCEDC 2022), which has a flat instrument response across our frequency range of interest.

One common obstacle in seismic noise analysis is the presence of unwanted transient events such as earthquakes that can contaminate the continuous signals of interest. This issue can be addressed by cutting out segments of data with known unwanted discrete events through comparison to earthquake catalogs, but this strategy can also unnecessarily remove desired

noise data or leave in unwanted transient signals from non-earthquake events or earthquakes too small to be reliably cataloged. A preferable option for many circumstances is to statistically remove events through methods like median power spectral density, as used for glaciohydraulic tremor analysis in Bartholomaus et al. 2015. In this method, the median power spectral density for a segment of data is constructed by dividing that segment into smaller time windows, taking the individual power spectral density of those time windows, and selecting the median power value among all the windows' spectra at each frequency value. As long as transient events do not significantly contaminate the power spectra for more than half of the individual windows, they will be sorted out by the median power spectral density process, leaving only the continuous signals in the final spectrum for the data segment. Calculation of the multiple single power spectral densities to build a median power spectral density is more computationally expensive by a factor equal to the number of short windows chosen than simply calculating one power spectral density for the data segment, but the statistical removal of transient events can be worth the trade-off when analysis of true background noise is required. Like single power spectral density data, median power spectral density can then be averaged or integrated over a frequency range to create a representative measure for seismic noise power in that range. In this study, we take the median power value of the median power spectra from 5-15 Hz to represent seismic noise in this range as a signal value for comparison over time. This frequency range has been previously observed to contain a strong anthropogenic seismic signal in urban areas without significant contamination from common non-anthropogenic continuous noise sources, such as ocean microseism (Larose et al. 2015; Díaz et al. 2017).

A comparison of 5-15 Hz median noise power time series constructed from five-window median power spectral density method and single power spectral densities is shown in Figure 2. The clearest difference between the two methods is visible around the time of an M 3.6 earthquake that took place at 11:41 pm local time on 21 January 2020 in the San Fernando Valley, 36.5 km northwest of station CI.USC. This event is most dramatically visible in the data with the highest temporal resolution; the time series with 30-minute data segments has an approximately 6 dB difference between the single power spectral density where the event

is included and the median power spectral density where the event is statistically removed. The impact of weak transient events can lessen when the data segments are much longer than the event duration; for four-hour data segments, the period containing the earthquake is only approximately 1 dB higher in single power spectral density than in median power spectral density.
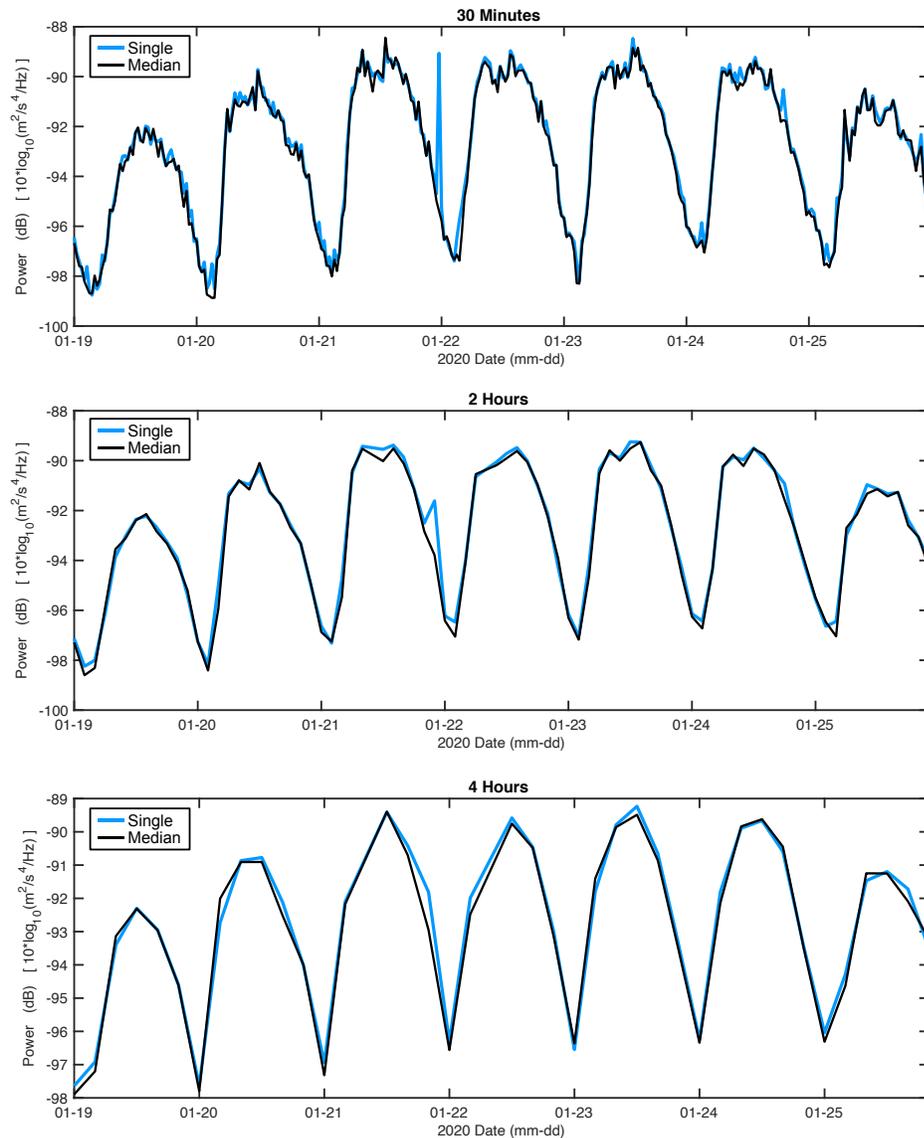

Figure 2. Comparison of 5-15 Hz power time series from single power spectral densities (blue) and five-window median power spectral densities (black) for 30-minute data segments (top), two-hour data segments (middle), and four-hour data segments (bottom) over the course of a week (Sunday-Saturday) in January 2020.

3. Normal Urban Seismic Noise Features

Figure 2 shows the most common patterns visible in anthropogenic urban seismic noise data. Noise levels are much lower at nighttime than they are during the day, as fewer people are driving, taking mass transit, operating equipment, or generally moving around during the night. Daytime peaks are notably lower on weekends and holidays (Monday, 20 January 2020 was Martin Luther King Jr. Day, a federal holiday when many workplaces are closed) than on standard weekdays. Weekdays also often show a bimodal peak in analysis with high temporal resolution, such as the time series with 30-minute data segments in Figure 2, corresponding to the busiest commuting times in the morning and late afternoon/early evening, when more people are driving and more public transit is in operation than during the early morning, midday, or late evening.

4. Super Bowl Sunday: A Short-Term Change in Urban Seismic Noise

Though we think of most urban noise level changes as operating on diurnal or multi-day scales, anomalies of only a few hours in community behavior can also be reflected in seismic noise levels. Since urban noise levels are well-correlated with transit activity, a good target time with which to observe short-term changes would be a period where a significant portion of the local population temporarily and synchronously abstained from traveling within the area. An example of such an event is the annual Super Bowl football game, which is broadcast live each year and is consistently one of the most-watched television programs annually. Super Bowl LVI was played from 15:30-19:00 Pacific Standard Time on 13 February 2022, and had an estimated U.S. viewership of 112.3 million viewers (Young 2022). This number is approximately one-third of the U.S. population, but proportional viewership in the Los Angeles area may have been higher than the nationwide average, given that the game took place in Los Angeles and one of the competing teams was the Los Angeles Rams.
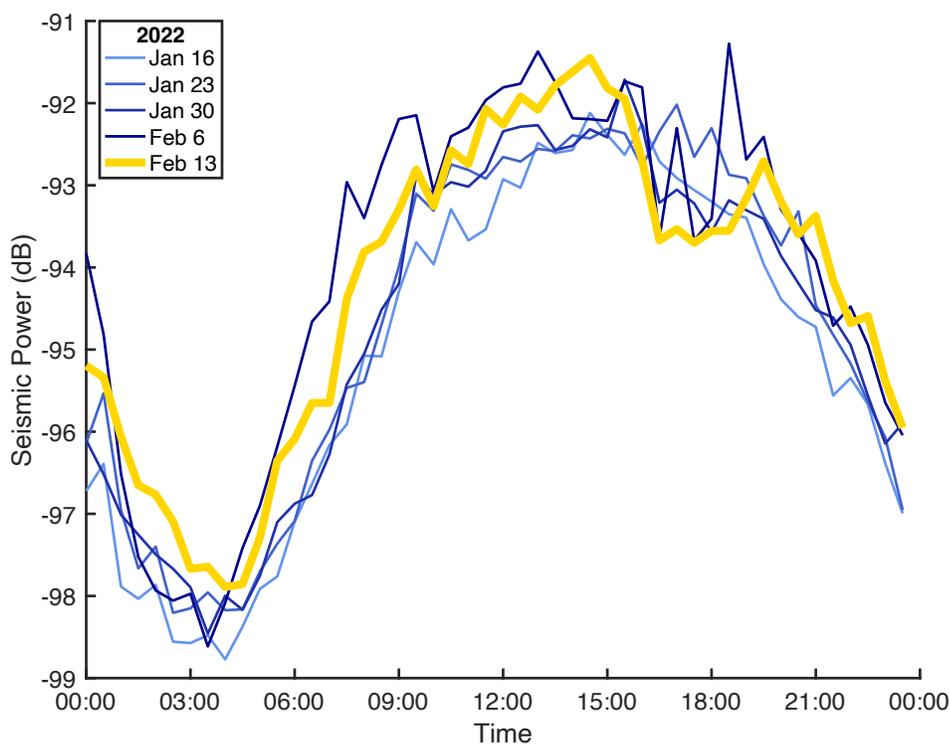
Figure 3. 5-15 Hz power time series from ten-window median power spectral densities of 30 minute data segments for five consecutive Sundays in early 2022. Super Bowl LVI was played and aired on television from 15:30-19:00 on February 13 (yellow).

Figure 3 shows the 5-15 Hz power time series from ten-window median power spectral densities of 30 minute data segments for Super Bowl Sunday and the four Sundays before it. For most of the day of the game, seismic noise levels are well within the normal range demonstrated by the previous Sundays. During the time of the game, however, a drop of 1-1.5 dB occurs as people stay at their homes, parties, or public viewing events to watch, rather than participating in normal activities that might require transit around the area. The amplitude of this drop is within the range of variability seen in previous Sundays, but the sustained nature of the drop over a 3.5 hour period is unique to the game day. A seismometer very near to the location of the game might have recorded an increase in seismic noise due to crowd activity in the stadium, as has been observed at other sporting events (Denton et al. 2018), but SoFi Stadium was located 8.7 km southwest of station CI.USC, rendering its noise less significant than nearer sources such as the freeway.
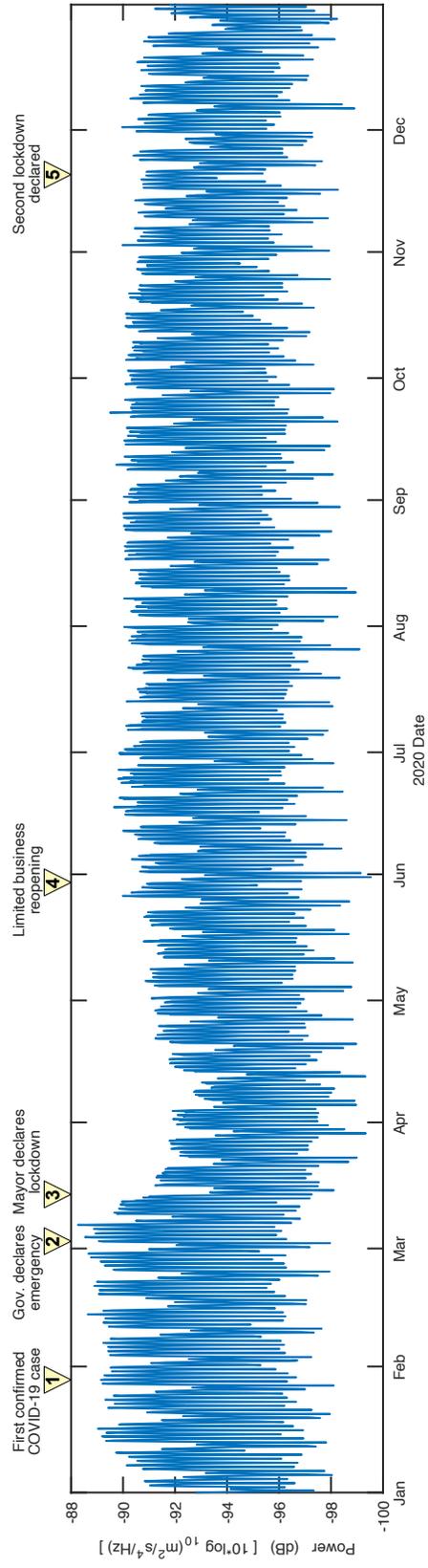
Figure 4. 5-15 Hz power time series from three-window median power spectral densities of four hour data segments for all of 2020. Numbered triangles and their labels indicate notable events in the progression of COVID-related lockdowns in the Los Angeles area, with a key of exact dates in Table 1.

5. COVID-19 Lockdowns: A Long-Term Change in Urban Seismic Noise

Significant, long-term changes in community activity can completely change the character of an area's anthropogenic seismic noise environment, but such events are very rare. The most widespread and notable case of such an event in recent history is the COVID-19 pandemic, which resulted in lockdowns in many countries around the world in early 2020. These precautionary lockdown measures caused a corresponding drop in anthropogenic seismic levels in urban areas around the globe (Lecocq et al. 2020). In this study, we focus on the data from CI.USC in Los Angeles (which is included in Lecocq et al. 2020) for the entire year of 2020. Figure 4 shows the 5-15 Hz power time series from three-window median power spectral densities of four hour data segments over the course of the year.

The progression seismic noise levels correlates with some of the policy-related events shown on Figure 4 and keyed in Table 1. Lockdowns, including remote work for most non-essential workers and remote schooling for most students, for some began voluntarily by individuals and companies shortly after the California governor's declaration of a state of emergency in early March, leading to a mild decrease in urban seismic noise levels. Lockdowns became much more complete and widespread after the Los Angeles mayor's issuance of the "Safer At Home" shelter-in-place order, leading to a sharper drop in noise power. Even during the height of lockdowns, weekdays still had higher ambient seismic power levels than weekends. The lowest recorded daytime peak power was 12 April (Easter Sunday), with a daytime high that was approximately 5 dB lower than average weekday highs in early 2020 before lockdowns began. Noise levels rose again through June, reaching a "new normal" of weekday highs approximately 1.5 dB lower than those in early 2020. Limited reopening of on-site operation of restaurants, salons, and many other non-essential businesses in late June

did not correlate with a significant change in noise levels. A second "Safer At Home" order was issued for Los Angeles in November, but unlike the first one, significant reductions in seismic noise levels were not observed. Widely-observed holidays like Thanksgiving on 26 November and Christmas on 25 December saw significantly reduced noise levels, as is common for these dates in any year.

Table 1. Notable events in the progression of COVID-related lockdowns in the Los Angeles area, as indicated on Figure 4.

#	Date	Event
1	26 Jan	First confirmed COVID-19 cast in the LA area
2	04 Mar	California governor declares state of emergency
3	19 Mar	LA mayor issues "Safer At Home" order
4	28 Jun	Limited reopening of restaurants, salons, etc.
5	21 Nov	Second "Safer At Home" order issued

Policy changes surrounding COVID-19 related lockdowns show limited correlation with urban seismic noise levels because policy changes incompletely describe the actual activity of people in the Los Angeles area. To get a better representation of true community activity during 2020, we turn to the Google COVID-19 Community Mobility Reports (Google LLC 2022), which used anonymized data from mobile phone apps such as Google Maps to track the time users spent in different categories of places daily from 15 February 2020 onward, compared to the baseline calculated from 03 January to 06 February 2020. The time spent in places categorized as "workplaces" and "residential" by users in Los Angeles County is shown in Figure 5, compared with the daily peak seismic noise power values selected from the time series data shown in Figure 4. Correlation of the percent change in activity to the daily peak power values from March 15 onward are shown in Figure 6. The bimodal nature of the correlation is due to differences between weekdays (lower right cluster for workplaces and upper right cluster for residential in Figure 6) and weekends (upper left for workplaces and lower left for residential). The clear positive correlation between workplace activity and

seismic noise levels and the negative correlation between residential activity and seismic noise levels are consistent with the interpretation of commuter transit and industrial activity as strong sources of urban seismic noise in Los Angeles. The Community Mobility Reports data is much more predictive of seismic noise levels than sparse policy changes, because it reflects the choices of individuals and sub-communities (such as schools and companies) within a policy structure, rather than the policy structure alone. The mobility data reflects more subtle features of the seismic noise data, such as the timing and rate of initial entry into lockdown, and the small variations in activity after the "new normal" was reached in June.
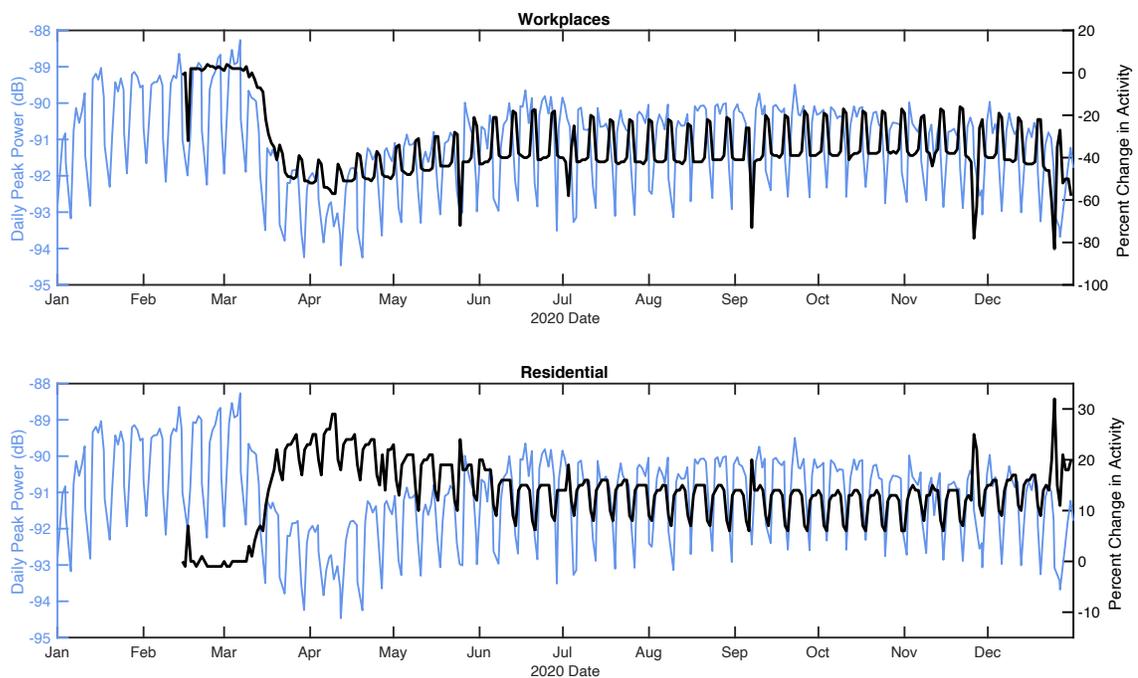

Figure 5. Daily peak values of the 5-15 Hz power time series shown in Figure 4 (blue) and percent change in location duration activity from the early 2020 baseline (black) for workplace locations (top) and residential locations (bottom) from the Google COVID-19 Community Mobility Reports for Los Angeles County (Google LLC 2022).
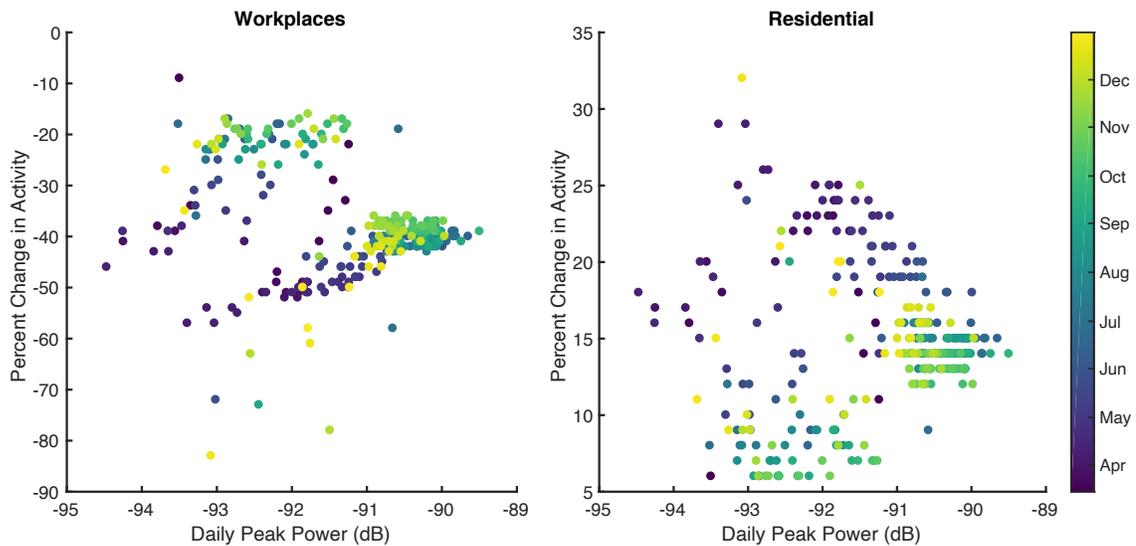
Figure 6. Percent change in location duration activity for workplace locations (left) and residential locations (right) from the Google COVID-19 Community Mobility Reports for Los Angeles County (Google LLC 2022) compared to daily peak values of the 5-15 Hz power time series shown in Figure 4, from March 15 onwards.

6. Conclusions

In this study, we observe the behavior of anthropogenic urban seismic noise over time in Los Angeles, California. We find that data processing methods like performing median power spectral density calculations rather than single power spectral density calculations increase the computational cost of urban seismic noise analysis, but can reduce the influence of unwanted transient events such as earthquakes on the final data product. Using median power spectral density processing, we find that human activity is well-reflected in observed seismic noise levels in normal repeated cycles of day to night and weekday to weekend, as well as deviations from standard patterns, consistent with past studies of urban seismic noise patterns (e.g. Díaz et al. 2017). Large changes in human activity on the scale of weeks to months are easily visible in seismic data, as exemplified by data from 2020 during COVID-related lockdowns. Like other cities observed in Lecocq et al. 2020, the noise level changes in Los Angeles correlate very well with observations of community activity in Google's COVID-19 Community Mobility Reports, but not as well with measures like policy changes that are

intended to be prescriptive rather than descriptive of community behavior. Changes in urban seismic noise levels can also be seen for much shorter-duration deviations from normal activity, as exemplified by the 2022 Super Bowl, when a sustained drop in noise levels occurred in Los Angeles throughout the game's broadcast, a complement to past observations of elevated seismic noise amplitudes in the very near vicinity of sporting events (e.g. Denton et al. 2018).

References

Bartholomaus, T. C., Amundson, J. M., Walter, J. I., O'Neel, S., West, M. E., & Larsen, C. F. (2015). Sublacial discharge at tidewater glaciers revealed by seismic tremor. Geophysical Research Letters, 42, 6391–6398. https://doi.org/10.1002/2015GL064590

Boese, C. M., Wotherspoon, L., Alvarez, M., & Malin, P. (2015). Analysis of anthropogenic and natural noise from multilevel borehole seismometers in an urban environment, Auckland, New Zealand. Bulletin of the seismological Society of America, 105(1), 285-299. https://doi.org/10.1785/0120130288

Cessaro, R. K. (1994). Sources of primary and secondary microseisms. Bulletin of the Seismological Society of America, 84(1), 142-148. https://doi.org/10.1785/BSSA0840010142

Denton, P., Fishwick, S., Lane, V., & Daly, D. (2018). Football quakes as a tool for student engagement. Seismological Research Letters, 89(5), 1902-1907. https://doi.org/10.1785/0220180078

Díaz, J., Ruiz, M., Sánchez-Pastor, P. S., & Romero, P. (2017). Urban seismology: On the origin of earth vibrations within a city. Scientific reports, 7(1), 1-11.

Gimbert, F., Tsai, V. C., & Lamb, M. P. (2014). A physical model for seismic noise generation by turbulent flow in rivers. Journal of Geophysical Research: Earth Surface, 119, 2209–2238. https://doi.org/10.1002/2014JF003201

Google LLC (2022). COVID-19 Community Mobility Reports: Los Angeles County, California, USA. Last accessed 2022-04-26. https://www.google.com/covid19/mobility/

Green, D. N., Bastow, I. D., Dashwood, B., & Nippress, S. E. (2017). Characterizing broadband seismic noise in Central London. Seismological Research Letters, 88(1), 113-124. https://doi.org/10.1785/0220160128

Groos, J. C., & Ritter, J. R. R. (2009). Time domain classification and quantification of seismic noise in an urban environment. Geophysical Journal International, 179(2), 1213-1231. https://doi.org/10.1111/j.1365-246X.2009.04343.x

Larose, E., Carrière, S., Voisin, C., Bottelin, P., Baillet, L., Guéguen, P., ... & Massey, C. (2015). Environmental seismology: What can we learn on earth surface processes with ambient noise?. Journal of Applied Geophysics, 116, 62-74. https://doi.org/10.1016/j.jappgeo.2015.02.001

Lecocq, T., Hicks, S. P., Van Noten, K., Van Wijk, K., Koelemeijer, P., De Plaen, R. S., ... & Xiao, H. (2020). Global quieting of high-frequency seismic noise due to COVID-19 pandemic lockdown measures. Science, 369(6509), 1338-1343. https://doi.org/10.1126/science.abd2438

OpenStreetMap Contributors (2022). OpenStreetMap. Last accessed 2022-04-26. https://www.openstreetmap.org/#map=10/33.9644/-118.2232

Podolskiy, E. A., & Walter, F. (2016). Cryoseismology. Reviews of geophysics, 54(4), 708-758. https://doi.org/10.1002/2016RG000526

Riahi, N., & Gerstoft, P. (2015). The seismic traffic footprint: Tracking trains, aircraft, and cars seismically. Geophysical Research Letters, 42(8), 2674-2681. https://doi.org/10.1002/2015GL063558

Southern California Earthquake Data Center. (2022). Seismic data for CI.USC.--.BHZ. https://dx.doi.org/10.7909/C3WD3xH1

Suriñach, E., Vilajosana, I., Khazaradze, G., Biescas, B., Furdada, G., & Vilaplana, J. M. (2005). Seismic detection and characterization of landslides and other mass movements. Natural Hazards and Earth System Sciences, 5(6), 791-798. https://doi.org/10.5194/nhess-5-791-2005

Young, J. (2022). Super Bowl 2022 attracted more than 112 million viewers, but failed to top record. CNBC Sports. https://www.cnbc.com/2022/02/15/super-bowl-2022-ratings-.html

C h a p t e r   5

CONCLUSIONS AND FUTURE PROSPECTS

In this thesis, I present two studies in cryoseismology. First, in Chapter 2, I observe seismic tremor generated by the turbulent flow of water in subglacial channels at Lemon Creek Glacier. Comparing the relationships between seismic tremor power and hydrologic throughput, I observe a spatially-limited pressurization event during the drainage of an ice-marginal lake. Integrating these different geophysical methods provided unique insight to the connection between subglacial hydrology and glacier motion in this system: that partial pressurization can occur without a corresponding obvious change in glacier velocity thanks to controls like glacier geometry. Studies like this highlight the importance of input from diverse data sets when using or challenging assumptions about the dynamic connections between the facets of glacier systems.

Second, in Chapter 3, I observed surface crevassing processes through spatiotemporal patterns in discrete icequake events at Lemon Creek Glacier. These icequakes indicate mode I crack opening sources, and show individual surface crevasses propagating lengthwise, reactivating after periods of quiescence, and affecting the behavior of neighboring crevasses. The icequakes observed at the surface of the glacier showed a magnitude distribution with a high b-value, more similar to earthquake swarms rather than classic tectonic earthquakes. Studies like these that characterize the cryoseismic environment can help future studies extrapolate event occurrence from sparser (and therefore often more practical) seismic arrays and look for changes in cryoseismicity that could be indicative of dynamic changes within the glacier

In addition to the cryoseismology studies, in Chapter 4 I presented an analysis of anthropogenic seismic noise in Los Angeles, and the statistical environmental seismology tools that can facilitate its accurate and efficient observation. This urban noise is a topic

which garnered public interest in 2020 through social media and traditional reporting, bringing community education and interest to environmental seismology.

Reliable field observations of glacier processes are vital for building a fundamental scientific understanding of the cryosphere and for preparing communities for changes in geohazards and water resources due to modern anthropogenic climate change. Cryoseismology has entered the playing field of glacier observations, but still needs development to maximize its value and practicality as a reliable geophysical tool. I see the future of cryoseismology not just as a trail of scientific curiosity for seismologists, but also as a practical and widely-used tool for glaciologists and communities. For glaciologists, I envision cryoseismology used as widely as other geophysical methods such as GPS, altimetry, or ice-penetrating radar, with results that are shown to be reliable for how we describe individual glaciers and applicable to how we model glaciers as a whole. For communities, I see seismometers deployed with other geophysical equipment in glaciated mountain ranges around the world, managed by local communities to provide real-time warning of flood hazards and forecasts of water availability. In order to reach these goals, our cryoseismology community needs to further integrate seismic observations with other data types to improve ground-truthing and applicability of seismic studies, implement more short- and long-term seismic deployments in rapidly-changing glaciated areas to test and optimize passive monitoring in real-world scenarios, and open more connections with communities proximal to glaciers so that we can support each other in building knowledge and meeting needs.

Practical and convenient seismology for the purposes of glaciologists and communities will be widely benefitted by advances in nodal seismometer technology that have already occurred since this study was conducted and will continue into the future. These two cryoseismology studies used early-generation vertical-component nodes with less than two weeks of battery life, but new nodal units in 2022 collect three-component motion data at higher sampling rates (as well as other geophysical information such as GPS location and electromagnetic field data) with battery durations of several months, while retaining the waterproofing, self-containment, and portability that make them ideal for glacier surface

work. Investment in equipment by research institutions could allow for more studies like these that bring further light into the dynamic relationships between subglacial hydrology and broader glacial motion or glacier environmental conditions and surface crevassing in ice, both in general to improve theoretical understanding of glacier behavior and specifically for individual glacier systems that are of interest to communities nearby. Using seismology has already expanded the available time scales for geophysical observation of glaciers, and as seismology expands via improved sensor technology, all of the fields that it intersects with can also expand further.